2018

Mitochondrial dynamics: regulation of insulin secretion and novel quantification methods

BOSTON UNIVERSITY

SCHOOL OF MEDICINE

Dissertation

MITOCHONDRIAL DYNAMICS: REGULATION OF INSULIN SECRETION AND NOVEL QUANTIFICATION METHODS

by

NATHANAEL ALAN MILLER

B.S., Otterbein University, Ohio, 2012

Submitted in partial fulfillment of the

requirements for the degree of

Doctor of Philosophy

2018

Approved by

First Reader_____

Orian Shirihai, M.D., Ph.D.
Professor of Medicine

Second Reader_____

Marc Liesa-Roig, Ph.D.
Assistant Professor of Medicine

Third Reader_____

Susan Fried, Ph.D.
Professor of Medicine

DEDICATION

This work is dedicated to my wife, Holly Nicole Miller. If not for her encouragement and unwavering belief in me, I would have never realized my potential and none of this work would have been possible.

ACKNOWLEDGMENTS

I would like to thank my mentor, Orian Shirihai for his kind guidance, endless patience, contagious passion, and love for discovery. Without his open door and acute mind, I would have floundered. Marc Liesa taught me the importance of rigor and attention to detail, and his mental index of PubMed was invaluable in discussion. Susan Fried gave me the chance to start this journey and provided valuable guidance at its outset. Marcus Oliveira provided immeasurable encouragement and discussion, both personal and professional. Jude Deeney was invaluable in technical discussions. Tamar Aprahamian provided valuable feedback and considerations that otherwise would have been overlooked.

My fellow “littermates” Nour Alsabeeh and Ilan Benador proved to be invaluable friends with unique perspectives that taught me more than they know. Our time and discussions in and out of the lab proved fruitful and enriching. Eleni Ritou always found a way to make sure the lab ran smoothly. In reality, the entire team in Orian’s lab, Marc’s lab, and collaborators enabled both a productive and enjoyable time spent doing this work. I thank every one of them for their feedback, friendship, and advice.

My parents instilled in me a love of knowledge, and without that basis I would never have loved science enough to pursue this journey. Thank you.

MITOCHONDRIAL MORPHOLOGY: CONTROL OF INSULIN SECRETION AND NOVEL QUANTIFICATION METHODS

NATHANAEL ALAN MILLER

Boston University School of Medicine, 2018

Major Professor: Orian Shirihai, M.D., Ph.D., Professor of Medicine

ABSTRACT

The recent surge in Type 2 Diabetes (T2D) has renewed interest in the study of cellular metabolism – which mitochondria tightly control. Previous work has shown mitochondrial dysfunction plays a critical role in the development of metabolic diseases, such as T2D. The pancreatic β-cell synthesizes and secretes insulin *in vivo* in response to diverse fuel signals such as glucose, fatty acids, and amino acids; failure or loss of β-cell mass is a hallmark of T2D. Pancreatic β-cell mitochondria are dynamic organelles living a life of fusion, fission, and movement collectively called mitochondrial dynamics. Mitochondrial fusion is impaired in obesity and models of obesity, while basal secretion of insulin is elevated. Previous studies demonstrate that hyperinsulinemia alone is sufficient to induce insulin resistance, yet the relationship between mitochondrial morphology and basal insulin secretion has not yet been studied. Here, we investigated the link between loss of mitochondrial fusion and insulin secretion at basal glucose concentrations

by reducing the expression of mitofusin 2 (Mfn2), which controls mitochondrial morphology and metabolism. We found that forced mitochondrial fragmentation caused increased insulin secretion at basal glucose concentrations. In addition, fragmentation of mitochondria enhanced the secretory response of islets to palmitate at nonstimulatory glucose concentrations and increased fatty acid uptake and oxidation in a cell model of pancreatic β-cells. We developed unique solutions to challenges posed by the measurement of mitochondrial dynamics via confocal microscopy by using novel image analysis techniques, including a novel method of mitochondrial segmentation. This technique also revealed novel biology of brown adipose tissue mitochondria dependent on their localization within the cell. Our findings demonstrate that changes to mitochondrial dynamics in the β-cell can lead to increased insulin secretion at basal glucose concentrations. These data support the possibility that hyperinsulinemia and the downstream outcome of insulin resistance can be initiated by altered mitochondrial function in the β-cell independently of other tissues. By uncovering a new process that governs basal insulin secretion, we provide novel targets for regulation, such as mitochondrial morphology or fatty acid induced insulin secretion that may present new approaches to treatment of diabetes.

TABLE OF CONTENTS

LIST OF TABLES

LIST OF FIGURES

LIST OF ABBREVIATIONS

ABHD6 .....α/β Hydrolase Domain-6

ACC.....Acetyl-CoA Carboxylase

ATGL ..... Adipose Triglyceride Lipase

BAT .....Brown Adipose Tissue

cAMP ..... Cyclic Adenosine Monophosphate

CPT1 ..... Carnitine Palmitoyl Transferase I

DAG..... Diacylglycerol

Drp1.....Dynamin Related Protein 1

DZ.....Diazoxide

ER .....Endoplasmic Reticulum

ETC .....Electron Transport Chain

FA..... Fatty Acid

FAO ..... Fatty Acid Oxidation

FCCP.....Carbonyl Cyanide P-trifluoromethoxyphenylhydrazone

FFA.....Free Fatty Acid

Fis1..... Mitochondrial Fission Protein 1

G3P .....Glycerol 3 Phosphate

GK .....Glucokinase

GL.....Glycerolipid

GLT ..... Glucolipotoxicity

GPR40.....G-protein coupled receptor 40

GSIS ..... Glucose-Stimulated Insulin Secretion

HI ..... Hyperinsulinemia

HSL ..... Hormone Sensitive Lipase

IR ..... Insulin Resistance

K_{ATP} ..... ATP-sensitive K^+ channel

KREBS ..... Krebs-ringer Bicarbonate Buffer

LC ..... Long-Chain

MAG ..... Monoacylglycerol

Mff ..... Mitochondrial fission factor

Mfn1 ..... Mitofusin 1

Mfn2 ..... Mitofusin 2

MGL ..... Monoacylglycerol Lipase

MOI ..... Multiplicity of infection

NAC ..... N-acetylcysteine

OPA1 ..... Optic Atrophy 1

PINK1 ..... PTEN-induced putative kinase protein 1

PKA ..... Protein Kinase A

PKC ..... Protein Kinase C

Px ..... Pixels

ROI ..... Region of Interest

ROS ..... Reactive Oxygen Species

SNARE .. Soluble N-ethylmaleimide-sensitive Factor Attachment Protein Receptor

T2D..... Type 2 Diabetes

TAG..... Triacylglycerol

VDCC..... Voltage-Dependent Ca^{2+} Channel

CHAPTER ONE: General Introduction

The prevalence of obesity and T2D is increasing at an alarming rate nationally and worldwide, even among young patients (Geiss et al., 2014; Imperatore et al., 2012). The financial burden of T2D is increasing accordingly, and an effective cure remains elusive, except in the case of bariatric surgery (Nannipieri et al., 2011, 2013). T2D is a metabolic disease at its core; the affected patient is unable to properly respond to and metabolize nutrient challenges, such as ingestion glucose. Systemically, T2D is characterized by uncontrolled glycemia resulting from either loss of insulin secretion capacity or loss of tissue response to insulin signals in the bloodstream.

Development of T2D

Insulin is one of the signals of plenty; its primary functions are suppression of glucose production in the liver (Perry et al., 2015; Titchenell, Lazar, & Birnbaum, 2017) and regulation of energy storage in muscle and adipose (Jensen, Caruso, Heiling, & Miles, 1989; Nicholls et al., 2010; Scherer et al., 2012). These roles are impeded when the insulin responsive tissues cease responding to normal levels of insulin and place increased demand on pancreatic β-cells. A main focus of this work centers on an alternative hypothesis suggesting that hyperinsulinemia causes insulin resistance (Corkey, 2012).

Insulin was first isolated in 1922 by Banting and Best (Karamitsos, 2011) and is now known to control circulating and stored nutrient regulation, particularly glucose. Glucose metabolism is aerobic or anaerobic, with aerobic oxidation

requiring mitochondrial involvement. Glucose is largely consumed by the brain, which requires a ~5mM concentration of glucose in the blood (Wasserman, 2009), demonstrating the need for such tight regulation. Glucose is also consumed by muscle, either through oxidation or storage as glycogen. Muscle uptake of glucose is strongly activated by insulin, and loss of insulin sensitivity plays a major role in the hyperinsulinemia observed in prediabetic and obese subjects (Kahn, 2003). An additional arm of insulin resistance occurs in the liver, where insulin is unable to suppress gluconeogenesis (Perry et al., 2015; Titchenell et al., 2017) upon development of insulin resistance. Insulin resistance occurs in multiple tissues and is difficult to tease apart from the coincident compensatory increased insulin secretion from β-cells.

One hypothesis suggests insulin resistance precedes compensatory hyperinsulinemia. According to this model, overworking of β-cells leads to eventual exhaustion and failure (C J Nolan et al., 2006). However, an alternative hypothesis suggests hyperinsulinemia is the primary defect, which leads to downstream insulin resistance. This hypothesis is supported by several lines of evidence: rhesus monkeys become hyperinsulinemic before insulin resistance is evident (Hansen & Bodkin, 1990); high-fat fed rats become hyperinsulinemic before insulin resistance is evident (Bonen et al., 2015); and mice with genetically impaired insulin production are protected from high-fat diet effects compared to their wild-type controls (Mehran et al., 2012), demonstrating a need for hyperinsulinemia in the progression to diabetes

Hyperinsulinemia as an initiating factor

Over 40 years ago, Olefsky *et al.* demonstrated that hypertriglyceridemia and hyperinsulinemia precede insulin resistance in humans (Olefsky, Crapo, Ginsberg, & Reaven, 1975). In fact, genetic prevention of hyperinsulinemia in high-fat diet fed mice prevents weight gain and insulin resistance (Mehran et al., 2012). Conversely, rats and humans administered exogenous insulin develop insulin resistance after forced hyperinsulinemia (Del Prato et al., 1994; Destefano, Stern, & Castonguay, 1991).

Hyperinsulinemia is conceivably due to either increased entry into circulation or reduced clearance therefrom. Insulin production occurs specifically in the pancreatic β-cells and is tightly regulated in both production and storage. Not only does glucose stimulate secretion of existing insulin, but it also stimulates further production via transcription of preproinsulin mRNA which is translated as proinsulin, which is subsequently cleaved into two co-secreted peptides packaged in secretory granules: insulin and c-peptide (reviewed in Fu, Gilbert, & Liu, 2013). Insulin synthesis is perturbed by several stimuli; adipocyte signaling by leptin and FFA both reduce preproinsulin mRNA production (Bollheimer, Skelly, Chester, McGarry, & Rhodes, 1998; Pallett, Morton, Cawthorne, & Emilsson, 1997; Seufert et al., 1999), in spite of FFA's acute stimulatory effects on insulin secretion. Increased β-cell mass could also contribute to increased insulin in circulation in the obese state. In both rodents and humans, β-cell mass increases in response to obesity (Butler et al., 2003; Dalbøge et al., 2013; Jetton et al., 2005; Mezza et

al., 2014; Steil et al., 2001) with a corresponding increase in insulin secretion (Polonsky, Given, Hirsch, et al., 1988; Polonsky, Given, & Van Cauter, 1988).

Insulin clearance is primarily accomplished by hepatocytes, where 50-70% of insulin is cleared on the first pass through the portal vein (Duckworth & Kitabchi, 1981). Hepatic insulin clearance is reduced in obesity and inversely correlates with hepatic lipid accumulation (Kotronen, Vehkavaara, Seppälä-Lindroos, Bergholm, & Yki-Järvinen, 2007; Kotronen, Westerbacka, Bergholm, Pietiläinen, & Yki-Järvinen, 2007). Lipid perfusion alone is sufficient to significantly lower insulin clearance in rats (Svedberg, Strömblad, Wirth, Smith, & Björntorp, 1991) and dogs (Yoshii et al., 2006), suggesting a close link between excess lipid exposure and impaired hepatic insulin clearance. Conversely, obese human children and adolescents exhibited increased hepatic insulin clearance upon weight loss (Escobar et al., 1999).

Insulin Secretion regulation and dysregulation by different nutrients

Insulin secretion is a tightly regulated process arising from a characteristically nutrient-sensing cell. Insulin secretion follows a general pattern in two phases: first phase insulin secretion exhibits a brief drop in insulin exocytosis from β-cells, followed by a rapid peak of insulin release on the scale of minutes; second phase insulin secretion follows with a gradual decline in insulin release on the scale of minutes to hours. Loss of first phase is one of the first hallmarks of early diabetes, and is generally coincident with an increased second phase insulin secretion (Perley & Kipnis, 1967). The two pathways have distinct but

complementary mechanisms. First phase insulin secretion is stimulated by the rapid conversion of glucose to ATP in the β-cells, which triggers ATP-sensitive potassium channels (K_{ATP} channels), whose closure depolarizes the cell membrane. Voltage dependent calcium channels (VDCCs) then open, permitting calcium entry to stimulate insulin granule exocytosis through SNARE-mediated exocytosis (reviewed in V Poitout & Robertson, 1996). Second phase insulin secretion is dependent on initial triggering and can enhance it. However, regulation of second-phase insulin secretion remains a challenge to study, and so far several factors have been shown to regulate second-phase, including FFA (C J Nolan et al., 2006), lipid accumulation (Erion, Berdan, Burritt, Corkey, & Deeney, 2015), incretins such as GLP-1 (Drucker & Nauck, 2006) and GIP via raising cAMP levels , and ROS (Pi et al., 2007), among others.

FA, specifically, play an important role in insulin secretion. The presence of endogenous or exogenous FFA are necessary for GSIS, possibly via GPR40, a FFA receptor on the plasma membrane (El-Azzouny, Evans, Treutelaar, Kennedy, & Burant, 2014; Itoh et al., 2003; Latour et al., 2007). However, a chronic excess of exogenous FFA inhibits insulin secretion, an effect compounded by excess glucose in the condition of GLT (reviewed in Vincent Poitout et al., 2010). FFA act through several mechanisms to influence insulin secretion. Glucose metabolism produces malonyl-CoA via ACC, which inhibits CPT-1, the main rate-limiting step in mitochondrial β-oxidation. FA-CoA which is spared from oxidation can be incorporated into complex lipid molecules such as DAGs and phospholipids

capable of stimulating insulin exocytosis, a key component of the LC-CoA hypothesis (M Prentki & Corkey, 1996; Roduit et al., 2004).

FA esterification (Roduit et al., 2004) and lipolysis (Christopher J Nolan, Madiraju, Delghingaro-augusto, Peyot, & Prentki, 2006) are both activated by products of glucose metabolism; inhibition of these processes abrogates the FFA enhancement of glucose stimulated insulin secretion. Collectively, this futile cycle has been called Glycerolipid/Fatty Acid (GL/FA) cycling, and β-cells express the necessary enzymes for this process. FA esterification is initiated by the formation of lysophosphatidic acid condensed from long-chain CoA (LC-CoA) and G3P. This product is then esterified with another LC-CoA via acylglycerol-3-phosphate acyltransferase to form phosphatidic acid. TAG is formed by the final esterification of a final LC-CoA with phosphatidic acid via DAG acyltransferase. Conversely, in the process of lipolysis, TAG is broken down by ATGL to yield DAG, which is subsequently hydrolyzed by HSL to MAG. MAG can be hydrolyzed to its final remaining FFA and glycerol via MAG lipase (MGL) or α/β hydrolase domain-6 (ABHD6). Because β-cells do not express glycerol kinase, they cannot recycle the resultant glycerol; it is therefore released from the cell (MacDonald & Marshall, 2000).

The consequences of GL/FA cycling include increased intracellular concentrations of the above intermediates. While TAG has not been shown to affect insulin secretion, DAGs can bind the exocytotic protein Munc13-1 to stimulate exocytosis, and heterozygous Munc13-1 knockout mice demonstrate

impaired insulin secretion in response to glucose (Kwan et al., 2006). Further evidence for the role of DAG interaction with Munc13-1 includes a mutant form of the protein incapable of binding DAG, which similarly impairs glucose stimulated insulin secretion (Kwan et al., 2006). The lipolytic product of DAG, MAG also stimulates insulin secretion in a ROS dependent manner (Zhao et al., 2014).

Over 40 years ago, Olefsky and colleagues observed a stark increase (30%) in circulating triglyceride and insulin response to glucose after a hypercaloric diet in humans (Olefsky et al., 1975) preceding insulin resistance. Subsequent studies have shown increased low-density and decreased high-density lipoproteins (Opie & Walfish, 1963; Vijayaraghavan, 2010) possibly due to insulin not effectively inhibiting hepatic lipolysis (Jensen et al., 1989). The role of FFAs in insulin secretion, particularly palmitate, is a primary focus of this work, and forced fragmentation of mitochondria through loss of Mfn2 sensitized β-cells to FFA induced insulin secretion at nonstimulatory levels of glucose, suggesting an interplay between mitochondrial morphology and insulin secretion regulation.

Within the pancreatic islets of Langerhans reside β-cells, among other cell types such as α-cells and δ-cells. β-cells are characteristically sensitive to their nutrient environment and express GLUT2, a high-K_m plasma membrane glucose transporter (reviewed in Thorens, 2015) and glucokinase, a high-K_m glucose phosphorylating enzyme, which both enable β-cells to respond quickly to changes in circulating glucose concentrations. The pyruvate derived from glucose is almost exclusively metabolized in mitochondria, further demonstrating the tight link

between β-cell glucose metabolism and nutrient sensing (Schuit et al., 1997). In addition, β-cells respond to fatty acids which can elicit insulin secretion independently of elevated glucose, through receptors such as GPR40 (El-Azzouny et al., 2014; Christopher J Nolan et al., 2006). As a result of this sensitivity, β-cells are also prone to damage from excess nutrient conditions, particularly elevated glucose and FFA (Molina et al., 2009; Vincent Poitout et al., 2010; Wikstrom et al., 2007), a condition exploited by researchers to mimic the obese state using glucolipotoxicity (GLT; Y. Zhou & Grill, 1994).

Mitochondria are responsible for oxidative phosphorylation, beta oxidation, and nutrient signaling to the rest of the cell. To facilitate and regulate these functions, mitochondria fuse and fission during the process of mitochondrial dynamics (Molina et al., 2009; Stiles & Shirihai, 2012). Mitochondrial dynamics influences the quality control of mitochondria (Y. Chen & Dorn, 2013; Twig et al., 2008) and overall network health as a result via the PINK/Parkin system (Y. Chen & Dorn, 2013; Narendra et al., 2010; Pickrell & Youle, 2015; Yun et al., 2014; Ziviani, Tao, & Whitworth, 2010). Mitochondrial fusion and fission are controlled by specific proteins: fusion requires Mfn1 and/or Mfn2 for fusion of the outer mitochondrial membrane, and OPA1 for fusion of the inner mitochondrial membrane; fission utilizes Drp1, Fis1, and Mff (reviewed in Liesa & Shirihai, 2013). Together, these processes regulate mitochondrial morphology and function, both of which can be examined by long-utilized tools such as microscopy and respirometry.

Because mitochondrial dynamics determine mitochondrial morphology and quality control, measuring morphology is a snap shot of the process of mitochondrial dynamics. Our lab and others have previously published a link between mitochondrial morphology and nutrient availability suggesting a possible functional role for morphology as opposed to morphology being a passive outcome of dynamics (Anello et al., 2005; Twig et al., 2008; Wikstrom et al., 2007). This link is observed in cellular subpopulations of mitochondria, as brown adipose tissue (BAT) mitochondria near lipid droplets are more elongated and express more ATP synthase (Benador et al., 2018) and inhibition of mitochondrial fusion inhibits BAT thermogenesis (Mahdaviani et al., 2017). Similarly, mitochondrial morphology proteins such as Mfn2 exert effects beyond morphological regulation: a fusion-deficient truncated form of Mfn2 is able to regulate metabolism in skeletal muscle (Pich et al., 2005).

Regulation of mitochondrial dynamics and quality control

Mitochondrial fusion is regulated by fusion proteins: mitofusins 1 and 2 (Mfn1 and Mfn2) fuse the outer mitochondrial membrane, and Optic Atrophy 1 (OPA1) fuses the inner mitochondrial membrane. Conversely, mitochondrial fission factor (Mff) and Dynamin Related Protein 1 (Drp1) are responsible for mitochondrial fission. These proteins tightly regulate mitochondrial dynamics and morphology via hydrolysis of GTP to power their activities (Sesaki & Jensen, 1999; Shaw & Nunnari, 2002; Yaffe, 1999). Critically, mitochondrial morphology and dynamics control mitochondrial degradation via autophagy or mitophagy (Dagda

et al., 2009; Twig et al., 2008), probably by influencing mitochondrial membrane potential and PINK1-mediated phosphorylation of Mfn2 (Y. Chen & Dorn, 2013; Pickrell & Youle, 2015; Song, Mihara, Chen, Scorrano, & Ii, 2015; Yun et al., 2014). PINK1, which is normally degraded in polarized mitochondria, is stabilized on depolarized mitochondria (Narendra et al., 2010) due to inhibition of its protease. Stabilized PINK1 phosphorylates Mfn2, which is targeted by Parkin. Parkin ubiquitinates Mfn2, whose ubiquitination designates mitochondria destined for removal by mitophagy.

The selective elimination of defective mitochondria, or mitophagy, is a critical housekeeping process within a cell; Parkin is named for the disease that results from defective parkin: Parkinson's disease (Y. Chen & Dorn, 2013). Our lab has previously published the critical importance of mitochondrial quality control and network maintenance for maintaining cell health in the excess nutrient environment (Molina et al., 2009; Twig et al., 2008; Wikstrom et al., 2007). Mfn2 is also the target of ubiquitination by a second, redundant pro-mitophagy ubiquitin ligase, MUL1, whose loss exacerbates the Parkin-null phenotype (Yun et al., 2014). This is a tightly regulated process, where deubiquitinases such as ubiquitin carboxyl-terminal hydrolase L1 (UCH-L1) act in opposition to the ubiquintation of Mfn2 and other proteins (Costes et al., 2011; Costes, Gurlo, Rivera, & Butler, 2014). Mitophagy is well-controlled but can fail at any of the above steps. While the above mechanisms describe the targeting of defective mitochondria to the mitophagic process, functional mitophagy also requires proper lysosomal function, which has

been shown to be impaired in excess nutrient conditions (Trudeau et al., 2016), a situation rectified by re-acidifying the lysosomes.

This concept of constant mitochondrial fusion, fission, degradation, and regulation has led to the concept of a mitochondrial lifecycle, such that mitochondria live and die by dynamics.

Measurement of mitochondrial shape and function

Mitochondria are significantly smaller than the cells they reside in, with a diameter around 1 μm and a length from 1 μm to >10 μm as part of a frequently overlapping network. As a result, direct quantification of their function and shape poses a unique challenge. The most common approach to measure mitochondrial function is via cellular oxygen consumption because mitochondria consume a vast majority of the oxygen in a cell (Liesa & Shirihai, 2013). Oxygen consumption has been measured since the early days of cell biology (Chance & Williams, 1956) and still provides one of the most direct measures of mitochondrial function and health. Oxygen consumption measurement can be performed on pieces of tissue, spheroids of cells, monolayers of cells, perforated versions of the aforementioned samples (via detergents, etc.), and on isolated mitochondria. Each of these preparations provide slightly different information. For example, a monolayer of cells still must transport substrates and treatments across a plasma membrane, whereas perforated cells or isolated mitochondria bypass cellular substrate transport machinery.

Measurements of oxygen consumption are usually performed in the presence of specific substrates providing electrons to Complex I and/or to Complex II, such as glucose or succinate, respectively. Such granular approaches provide a tool to tease apart the specific contributions of each fuel and/or complex to the oxygen consumption of the sample. Additional compounds provide tools to inhibit or activate specific complexes and transporters, such as oligomycin, which inhibits Complex V (ATP synthase), Etomoxir, which inhibits CPT-1, or FCCP, which strongly uncouples mitochondria. Uncoupled respiration is frequently used to measure the reserve capacity of mitochondria within a cell, e.g. the maximal respiration capacity. Uncoupled respiration (also known as proton leak) is named as such because coupled respiration is defined as oxygen consumption utilized for ATP synthesis (e.g. oxidative phosphorylation). The concept of proton leak is an important metric of the efficiency of mitochondria: how well they convert fuel to ATP. Measuring leak can provide valuable information on the integrity of the inner mitochondrial membrane or activity of distinct proteins such as the BAT-specific uncoupling protein 1 (UCP-1) (Wikstrom et al., 2014; Zingaretti et al., 2009).

Yet another approach to characterize mitochondria is metabolomics. Metabolomics is the fusion of historical methods such as radiolabeling or isotopomer labeling with new technology such as advanced chromatography and mass spectroscopy and high-throughput data handling (Sauer, 2006). Inspired by genomics and proteomics approaches, metabolomics collects vast information about isotopomer enrichment and uses modern computing power to model and

derive the meaning and biological basis of labeling patterns (Buescher et al., 2015). By combining this approach with oxygen consumption and the fuel dependency measurements derived therefrom, metabolomics enables specific dissection of steady-state concentrations and flux through various metabolic pathways, including the TCA cycle (Buescher et al., 2015; Sauer, 2006; Young, 2013) and fatty acid metabolism (Argus, Yu, Wang, Williams, & Bensinger, 2017).

Powerful computers have enabled the processing of data in new and previously impossible ways. Yet another advance provided by the march of technological progress is advanced light microscopy and image analysis. Light microscopy has advanced in recent years by discovery of novel ways to overcome the refraction limit set forth by physical laws inherent to the wavelength of incident light. Structured illumination microscopy (SIM) uses a Fourier transform of interference patterns from the sample; Stimulated emission depletion (STED) microscopy uses a donut-shaped laser beam to quench the airy disk of the fluorophore of interest and localize its point source; and stochastic localization microscopy such as the Zeiss Airyscan uses powerful computers to deconvolve the point spread function of a fluorophore (Weisshart, 2014). Modern computing power has greatly enhanced the resolution of light microscopy beyond the theoretical refraction limit of ~250nm (Abbe, 1873) to ~120nm and even less in some cases. The resultant super-resolution images can be analyzed and quantified faster and more accurately than ever before as a result of modern computing power. Not only does each of the above techniques provide many

gigabytes to terabytes of data per experiment, but modern analysis programs such as ImageJ and its plugin-rich fork FIJI (Schindelin et al., 2012) enable rapid automated analysis of these large data sets, often times enabled by resource-intensive machine learning algorithms for segmentation and quantification of image objects (Arganda-Carreras et al., 2017). Image analysis programs also contain tools for generating macros – sets of repetitive instructions to be repeated on every image for analysis. Macros enable rapid, repeatable, and unbiased analysis of large image data sets.

Goals of the thesis

The mechanism of regulation of basal insulin secretion remains elusive and is a central focus of this work. Mitochondrial fragmentation and fatty acid metabolism present several potential druggable control points, promising novel treatments for obesity and diabetes, for instance modulating activity of CPT1, the rate-limiting step of mitochondrial β-oxidation. A broad, nontargeted approach investigating the metabolic consequences of knockdown of Mfn2 provides a basis from which future studies can be conducted in immortalized cell models in addition to examining mechanisms of the metabolic changes incurred in this model. Measurement of many mitochondrial parameters, particularly via microscopy, poses several unique challenges for repeatable, unbiased quantification. Providing the basis for this type of analysis is beneficial for the scientific community at large – easily accessible and customizable mitochondrial analysis tools are rare.

1) Aim 1 (Chapter Two) will determine the role of mitochondrial fragmentation in basal insulin secretion and examine mechanisms for the palmitate-induced increase in non-glucose-stimulated insulin secretion.
2) Aim 2 (Chapter Three) will investigate the role of Mfn2 downregulation in an immortalized cell line utilizing high-throughput approaches to elucidate the metabolic effects of mitochondrial morphology on metabolic parameters, such as fuel preference and respirometry.
3) Aim 3 (Chapter) Four will describe novel image segmentation methods and image analysis methods designed to increase repeatability and throughput of measurement of subcellular structures in high-resolution micrographs.

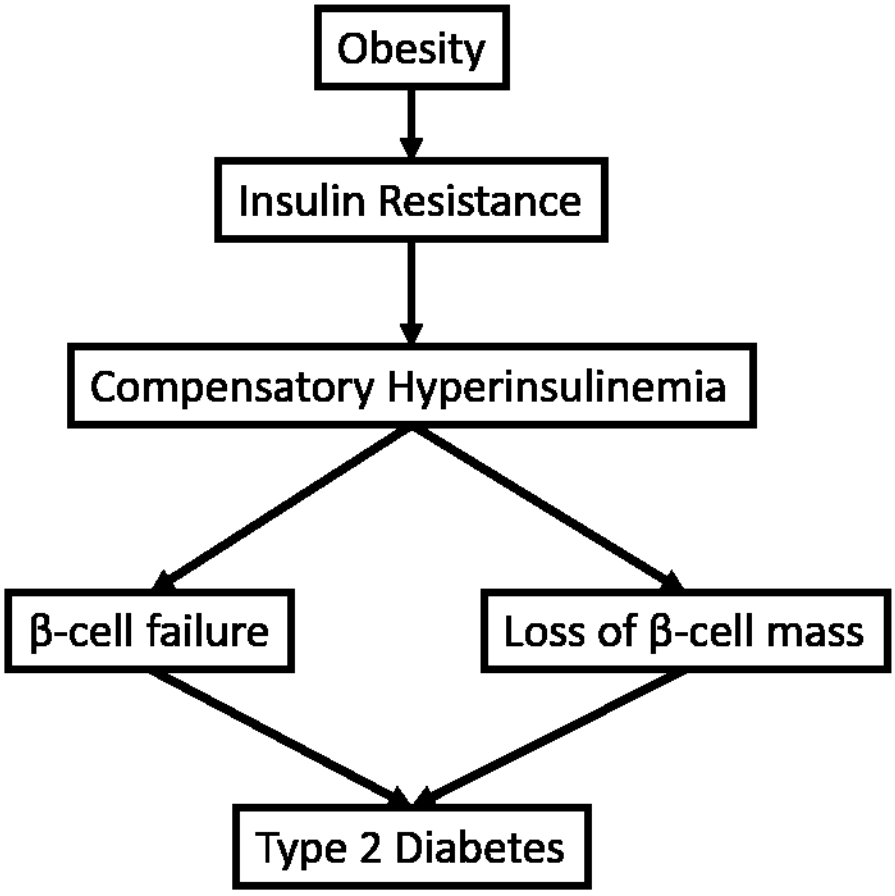

Figure 1.1. Conventional model for the progression of T2D development.

Obesity is associated with Insulin resistance, which leads to compensatory hypersecretion of insulin through several mechanisms, including β-cell hypertrophy and exocytosis of insulin. This overworking of β-cells leads to cellular damage and loss of β-cell mass. The loss of insulin secretion capacity induces T2D and uncontrolled glycemia.

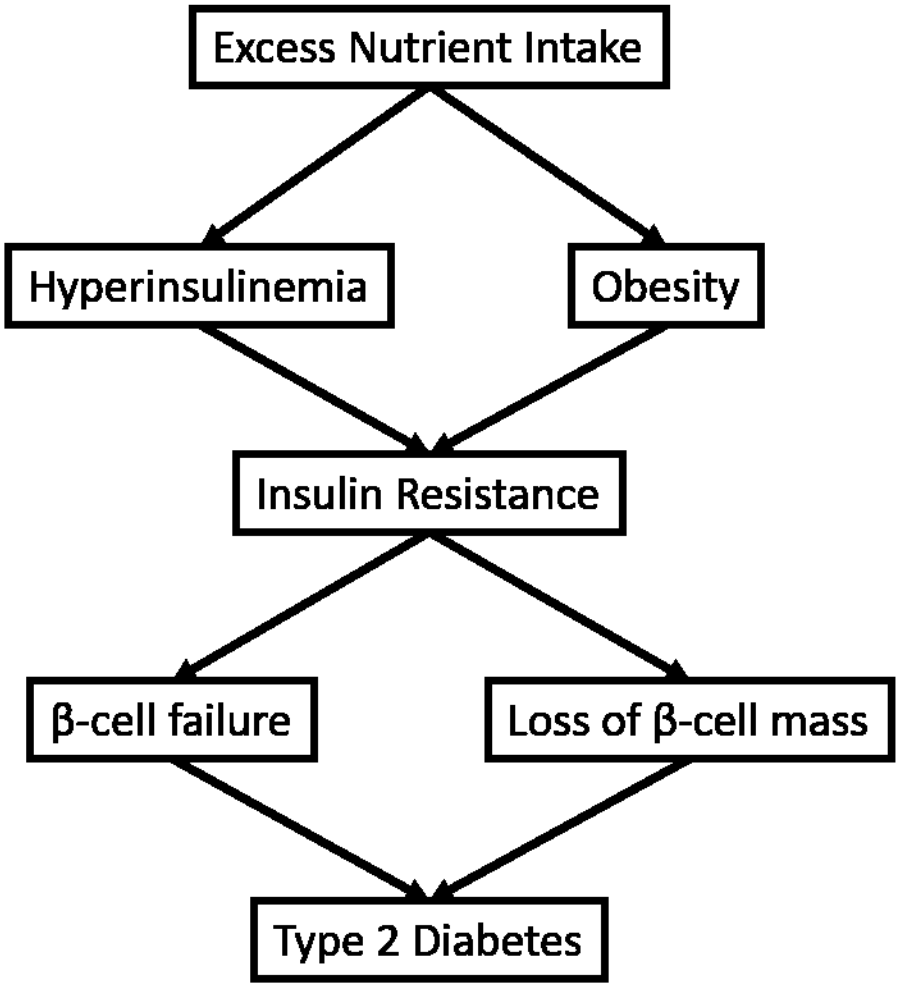

Figure 2.1. Alternative model for T2D progression with a focus on HI.

Excess nutrient intake induces hypersecretion of insulin in obese subjects by several mechanisms, including increased exocytosis via FFA/GL cycling, The excess insulin induces insulin resistance in peripheral tissues contributing to a vicious cycle of hypersinulinemia and insulin resistance, eventually leading to β-cell failure and loss of β-cell mass, followed by development of overt T2D.

CHAPTER TWO: Mitofusin 2 Expression Controls Fuel Preference and Lipid-Induced Insulin Secretion in Pancreatic β-Cells

Nathanael Miller[1,2], Anthony J. A. Molina[2], Linsey Stiles[1,2], Samuel B. Sereda[2], Jakob D. Wikstrom[2], David Chan[3], Barbara E. Corkey[2], Marc Liesa[1,2], and Orian S. Shirihai[1,2]

Affiliations

1. Division of Endocrinology, Department of Medicine, David Geffen School of Medicine at UCLA, Los Angeles, CA, USA

2. Obesity Research Center, Department of Medicine, Boston University School of Medicine, Boston, MA, USA

3. Howard Hughes Medical Institute and Division of Biology, California Institute of Technology, Pasadena, CA. USA

Keywords: beta cell (β-cell); type 2 diabetes; hyperinsulinemia; insulin secretion; metabolism; lipid; Mfn2; mitochondria; dynamics

ABSTRACT

There are two competing hypotheses to explain the development of T2D: insulin resistance initiating hyperinsulinemia or the inverse thereof. The mechanisms governing basal insulin secretion are not known, but alterations therein are well known to be associated with obesity and diabetes. Pancreatic islets from obese type 2 diabetic (T2D) subjects are characterized by decreased glucose stimulated insulin secretion (GSIS) and increased basal nonstimulated secretion. In this study, we identify Mitofusin 2 (Mfn2) is reduced in obese high fat diet mice and zucker rats. β-cell specific Mfn2 deletion elevated nonstimulated insulin secretion, in addition to recapitulating other features of obese prediabetic β-cells, such as enhanced fatty acid oxidation and disturbed second-phase GSIS oscillations. Mfn2-deficient β-cells demonstrate increased fatty acid uptake and preferentially secrete insulin in response to fatty acids, specifically palmitate at nonstimulatory glucose concentrations. We have found that Mfn2 bridges obesity and diabetes by inducing hyperinsulinemia in response to increased fatty acid sensitivity in the pancreatic beta cell.

INTRODUCTION

Hyperinsulinemia is generally thought to be a compensatory mechanism by the pancreatic β-cell in order to preserve glucose homeostasis in the face of insulin resistance. However, an alternative hypothesis stipulates that

hyperinsulinemia may be an initiating factor in the progression of glucose intolerance (Czech, 2017). Over 40 years ago, Olefsky *et al.* demonstrated that hypertriglyceridemia and hyperinsulinemia precede insulin resistance in humans (Olefsky et al., 1975). In fact, genetic prevention of hyperinsulinism via heterozygous ablation of the insulin gene in high-fat diet fed mice prevented weight gain and insulin resistance (Mehran et al., 2012). Conversely, rats and humans administered insulin via minipumps develop hyperinsulinemia followed by insulin resistance (Del Prato et al., 1994; Destefano et al., 1991). It remains a challenge to study this alternative hypothesis of T2D due to the limited understanding of the factors regulating basal insulin secretion. Unlike glucose-stimulated insulin secretion (GSIS), the mechanisms regulating basal insulin secretion are currently not known. To our knowledge, no study has attempted to determine the specific role of mitochondria and mitochondrial morphology in the changes of basal secretion that result from obesity, regardless of the central role of mitochondria in metabolism. The pancreatic β-cell mitochondria are integrators of diverse fuel signals, such as carbohydrate, protein, and fat, positioning them at the intersection of metabolism and nutrient regulation.

Mitochondria are highly dynamic organelles whose morphology is regulated by continuous cycles of fusion and fission, collectively termed mitochondrial dynamics (Frank, 2006; Skulachev, 2001). Mediators of mitochondrial fusion include Optic Atrophy 1 (OPA1) and mitofusins 1 (Mfn1) and 2 (Mfn2); fission is mediated by dynamin related protein 1 (Drp1), mitochondrial fission protein 1

(Fis1), and mitochondrial fission factor (Mff). Mitochondrial networking contributes to mitochondrial quality control mechanisms, allowing for the buffering of mitochondrial reactive oxygen species (ROS) and calcium overload (Frieden et al., 2004; Szabadkai et al., 2004), as well as the selective removal of dysfunctional mitochondrial units by mitophagy (Twig et al., 2008).

Mfn2 expression is decreased in different tissues by diet induced obesity and contributes to tissue dysfunction (Bach et al., 2003; Le Blanc et al., 2012; Pich et al., 2005; Sorianello et al., 2012). Changes in mitochondrial morphology have been reported in the β-cells isolated from Type 2 Diabetic patients, Zucker Diabetic Fatty rats, and in diet induced obesity (Anello et al., 2005; Bindokas et al., 2003; Fex et al., 2007; Higa et al., 1999). Previously, we found that fragmentation due to extended exposure to high levels of nutrients stems from nutrient-induced inhibition of mitochondrial fusion, rather than an increase in mitochondrial fission (Molina et al., 2009). In order to investigate the time-dependence of these phenomena, we utilized Zucker fatty rats and Zucker diabetic fatty rats at 12 weeks of age, prior to the onset of overt diabetes in the Zucker diabetic fatty rats around 14 weeks of age. These experiments revealed that fragmentation of mitochondria preceded overt diabetes. Furthermore, Cerqueira *et al.* reported that calorie restricted animals, which have increased life spans and lower incidence of diabetes, displayed an increase in Mfn2 expression in both adipose tissue and skeletal muscle. Additionally, serum from calorie restricted animals increased Mfn2 expression in INS-1 cells (Cerqueira et al., 2016; Cerqueira, Cunha, Laurindo, &

Kowaltowski, 2012). However, whether Mfn2 plays an important role in β-cell nutrient sensing and secretory function is unknown. As a result, we investigated the consequences of manipulation of mitochondrial morphology via modulation of Mfn2 expression in primary tissue.

Mfn2 has been implicated in the regulation of mitochondrial function in addition to its role in mitochondrial fusion. Knockdown of Mfn2 results in altered mitochondrial bioenergetic function, as reduced glucose oxidation and decreased oxygen consumption in primary rodent muscle and muscle-derived cell lines is evident (Bach et al., 2003). Additionally, reduced substrate oxidation and mitochondrial membrane potential has also been observed in the same cell types, and overexpression of a truncated Mfn2 lacking fusion activity showed opposing effects (Pich et al., 2005). We and others recently demonstrated that removal of Mfn2 altered substrate preference and impaired thermogenesis in brown adipose tissue (BAT) (Boutant et al., 2017; Mahdaviani et al., 2017). These results collectively show that mitochondrial morphology and tissue function are intimately connected.

Part of the aforementioned intimate connection is fuel preference for the mitochondria, cell, and insulin secretion. Acute exposure to free fatty acids (FFA) acutely increases insulin secretion, particularly through monoacylglycerol and other species (Pi et al., 2007); conversely, chronic exposure to elevated FFA inhibits mitochondrial quality control and insulin secretion in β-cells (Erion et al., 2015; Molina et al., 2009; Twig et al., 2008; Wikstrom et al., 2007). Suggesting a

necessary balance in fatty acid content, other data shows either HSL activity or exogenous FFA are necessary for robust insulin responses to glucose. Hyperlipidemia resulting from short term caloric excess has been shown to increase insulin *in vivo* in the absence of hyperglycemia (Olefsky et al., 1975). To address the role of nutrient-induced inhibition of mitochondrial fusion in the development of β-cell dysfunction and diabetes, we investigated mitochondrial fusion proteins *in vivo*, *ex vivo,* and *in vitro*. Given our published data showing that Mfn2 expression in β-cells in vitro is reduced by high fat exposure (Molina et al., 2009) and that fragmentation and Mfn2 inhibition promote fatty acid oxidation (Mahdaviani et al., 2017), we hypothesized that Mfn2 downregulation in obesity could be responsible for lipid-induced insulin secretion at nonstimulating glucose levels characteristic of β-cells from obese subjects (C J Nolan et al., 2006). These findings contribute to the understanding of diabetes by demonstrating a secretion-inducing fuel-preference switch in the pancreatic β-cell which increases basal insulin secretion in response to free fatty acids, presenting a potential target for regulation of basal insulin secretion.

EXPERIMENTAL PROCEDURES

Generation and genotyping of βMfn2KO mice

The generation of $Mfn2^{loxP}$ mice has been previously described by Hsiuchen Chen (H. Chen, McCaffery, & Chan, 2007). Briefly, ES clones (129 strain) carrying targeted mutations were injected into C57BL/6 blastocysts. Founder chimeric mice

were bred to Black Swiss mice, and agouti offspring were bred to FLPeR mice to remove the neomycin resistance cassette. Resulting mice were maintained as homozygous stocks (Farley et al., 2000). B6.Cg-Tg(Ins2-cre)25Mgn/J mice (RIP-Cre) were obtained from JAX mice (Bar Harbor, ME) and bred with homozygous $Mfn2^{loxP}$ to generate F1, double heterozygous mice. F1 mice were then bred with the original $Mfn2^{loxP}$ mice in order to generate the *β*Mfn2KO mice. Littermates include $Mfn2^{loxP}$ +/+ RIP-Cre -/- and Mfn2 +/- RIP-Cre -/- which were used as WT controls. In addition, $Mfn2^{loxP}$ +/- RIP-Cre +/- were tested and found to possess a mild phenotype.

Genotyping was performed by PCR of tail snip lysates (Viagen, DirectPCR, Los Angeles, CA) obtained during the weaning of pups. Floxed Mfn2 transgene was detected using GoTaq Green Master Mix (Promega, Madison, WI) and the following primers: gaa gta ggc agt ctc cat cg and ccc aag aag agc atg tgt gc. The unexcised conditional band is 810bp and the WT is 710 bp. Cre transgene was detected in the same samples by following the genotyping protocol provided by JAX Mice using the following primers: gcg gtc tgg cag taa aaa cta tc and gtg aaa cag cat tgc tgt cac tt.

Confocal Microscopy

Confocal microscopy was performed on live cells in glass bottom dishes (MatTek, Ashland, MA) using an inverted Leica TCS SP2 confocal microscope or Zeiss LSM 710 DUO with a plan-apochromat 100x (NA = 1.4) oil immersion objective. Mitochondria were stained with 3.5nM TMRE (Invitrogen Molecular

Probes, Eugene, OR.) for 45 minutes prior to imaging. Insulin promoter mediated paGFP expression in the mitochondrial matrix was induced by lentiviral transduction. The generation and use of these constructs was previously described in detail (Molina et al., 2009).

Pa-GFP activation and imaging of mitochondria

Photoconversion of PA-GFPmt to its active (fluorescent) form was achieved by using 2-photon laser (750nm) to give a 375 nm photon-equivalence at the focal plane. This allowed for selective activation of regions that have submicron thickness and are less than 0.5 μm^2. Using the multi-track scanning mode of the Zeiss LSM-710 microscope, red-emitting TMRE was excited with a 1 mW 543 nm helium / neon laser set at 0.3% and emission was recorded through a BP 650–710nm filter. Activated PA-GFPmt protein was excited using a 25 mW 488 nm argon laser set at 0.2%. Emission was recorded through a BP 500–550 nm filter. Prior work from our lab has determined optimal concentrations of probes and laser power to avoid photobleaching in our models (Twig et al., 2008), which was utilized in this study to avoid similar artifacts.

Batch Insulin Secretion

Islets were cultured in RPMI 1640 media supplemented with 10% FBS and 50 U/ml penicillin and 50 µg/ml streptomycin overnight prior to insulin secretion assays. Insulin secretion was run in 5 technical replicates and collected in a parallel fashion. Islets were washed and preincubated at 2mM glucose for 30 min

in modified Krebs-Ringer bicarbonate buffer (KRB). This was followed by a 30 min incubation in media containing either 3 mM or 15 mM glucose. Media was collected and stored at –20°C for insulin measurement. Insulin was measured by radioimmunoassay (LINCO Research Inc., St. Charles, MO). Normalization was performed by lysing the cells and measuring total insulin content. In order to measure insulin content, islets from three different animals were measured per genotype. For each animal, islet insulin content was measured in triplicate. For each measurement, six islets were lysed and diluted for insulin and protein measurements. Insulin was measured using the HTRF Insulin Assay (Cisbio Bioassays). Total protein was measured using the Bio-Rad Protein Assay, which is based on the Bradford method. Insulin content is presented as nanograms of insulin per milligram of total protein.

Islet Perifusion

Islets were perifused in a column as described (Cunningham, Deeney, Bliss, Corkey, & Tornheim, 1996). A collection of 50 islets was laid between 2 layers of Cytodex microcarrier beads (Sigma). The column used was 0.4 cm in diameter and 4 cm high and contained in a temperature controlled environment at 37 °C. Perifusion reagents were pumped through the column at 0.3 ml/minute using an analog tubing pump (Ismatech REGLO pump, type ISM 827, model 78,016–30; Cole-Parmer Instrument Co., Chicago, IL). Islets were perifused with Krebs-Ringer Bicarbonate buffer with added 0.5 % BSA for 30 minutes to allow for equilibrium. Eluted samples were collected at 30 second intervals for 48 minutes.

Basal levels of insulin were determined with 3mM glucose perifusion for 6 minutes, response to 15mM glucose was measured for 32 minutes and 15mM glucose; KCl was perifused for 10 minutes.

Western Blot

Primary antibodies used include anti-Mfn2 (#56889, AbCam, Cambridge, MA), anti-Beta-Actin (#AB8227, AbCam, Cambridge, MA), and anti-porin (#AB15895, AbCam, Cambridge, MA).

qPCR

Total RNA was isolated from islets using the Qiagen RNesay Plus Mini Kit. cDNA was obtained from RNA by a reverse transcriptase reaction using Applied Biosystems High Capacity cDNA Reverse Transcription Kit. Changes in gene expression were detected with SYBR Green. All samples were normalized to 18S content, which served as an endogenous control.

Respirometry

Respirometry of whole murine islets was performed using the Seahorse Bioscience XF 24 platform (Agilent Technologies, Santa Clara, CA) as previously described (Ferrick, Neilson, & Beeson, 2008). βMfn2KO and wild type islets were isolated and allowed to recover after isolation in culture overnight before respirometry was performed. Islets were placed in a 24 well islet plate and the addition of an 80 micron screen kept islets in place directly under the oxygen sensors. Data was normalized by islet number. Drug concentrations were as

follows: oligomycin (5μM), FCCP (1μM), rotenone (5μM) and antimycin A (5μM) (Sigma). INS1 cells were transfected with a micro-RNA mfn2 KD delivered by adenovirus at a MOI of 500. After 3 days, mitochondria were isolated and respirometry was performed using the Seahorse XF 24 platform. In order to ensure the amount of mitochondria was consistent between groups; 40 μg of protein was loaded into every well.

Glucose Tolerance Test (GTT)

Mice were fasted (supplied with water ad libidum) for 12 hours overnight prior to the GTT. The volume (μL) of 10% glucose to be injected per mouse is determined by multiplying mouse weight (in grams) by 5, or 0.5mg/g body weight. Initial time zero blood glucose measurements were taken using a glucometer with a drop of blood obtained from the tail. After blood glucose for time zero is taken, the mice were given an intraperitoneal (IP) glucose injection and blood glucose measurements were taken at 15, 30, 60, 90, and 120 minutes. Lab chow was reinstated to cages once the last glucose measurement and blood sample was taken.

Fluorescent measurement of mitochondrial H_2O_2 production and Generation of ex-vivo knockout

A mitochondrially targeted fusion protein (Orp1-roGFP) of cytosolic ORP1 and redox-sensitive GFP (roGFP) (Morgan, Sobotta, & Dick, 2011) was transduced into dispersed Mfn2 fl/fl mouse islet cells using an adenoviral vector at

a MOI of 200 particles per cell. This virus was co-transduced with 200 MOI adenoviral Cre containing DsRed as a reporter of transduction. The MOI of each virus was determined to have over 90% transduction efficiency via titration and measurement of reporter fluorescence. The cells were then reaggregated in the presence of both viruses into a pseudo-islet (5,000 cells per reaggregated islet) by centrifugation at 1,643 *g* in a 96-well V-bottom plate and cultured overnight. Media was changed the following morning and the islets were cultured for 3 days in RPMI (11mM glucose; 10%FBS; 1% penicillin/streptomycin) before being transferred to glass-bottom confocal dishes in 3 mM glucose basal Krebs buffer (Table 1.2).

Islets were imaged after a 30-minute preincubation in basal buffer and then the glucose concentration was increased to 15 mM before imaging 20 minutes after this addition. For normalization, the fully reduced state was achieved by addition of 5 mM DTT for 15 minutes; the fully oxidized state was achieved by addition of 0.5 mM H_2O_2 for 10 minutes. For imaging experiments, 10mL of buffer was diluted after addition of appropriate glucose, 0.5mL of 200mM $CaCl_2$, and 0.25g of fatty acid free BSA (0.5% final). Volume was adjusted to 50mL after adjusting pH to 7.4.

The imaging plate (#627870, Greiner bio-one) containing 8 to 10 islets per condition (1 per quadrant) was imaged on an Olympus IX 70, equipped with an Andor Zyla VSC-03062 camera, incubation, and CO_2 environmental control. Wavelengths are expressed as wavelength (bandwidth). Images were acquired with 395(15)nm oxidized and 470(40)nm reduced excitation (ex) and 525(50)nm

emission (em) for both excitations. The exposure time each ex/em pair was determined at basal glucose during preincubation, and the baseline FI of both oxidized and reduced was set as close to equal as possible; e.g. the ratio of oxidized/reduced fluorescence was set to 1 at the outset of each experiment.

Compound additions (glucose, DTT, and/or H_2O_2) were performed as additions of 100X concentrated solutions added to the well for imaging. After addition of the compounds, the volume (500µL initial, increasing with each sequential addition) of each quadrant was gently yet thoroughly mixed a minimum of 15 times with a 1000µL pipet, after which the islets were incubated for the times indicated.

Metamorph image analysis software (Molecular Devices) was used to quantify whole islet average fluorescence in each channel after cropping and thresholding each image in the green channel (which had a larger signal/noise ratio) to remove background. The baseline ratio (oxidized/reduced FI) was set to 1 and other values expressed as fold-change for calculation and comparison between independent experiments. We then performed a Wilcoxon (nonparametric, paired) test for significance in which islets from each mouse were aggregated and each experiment was treated as an *n* value.

Representative image generation

Representative images were generated using FIJI (https://fiji.sc/). Images were cropped for detail, separated into respective channels, and the *window* and

level parameters were adjusted identically per channel in all images to emphasize the fluorescent structures in the images without manipulation of raw pixel values.

C12-BODIPY uptake

INS-1 cells transduced with adenoviral shRNA (Welgen, MA) overnight were cultured for 3 days to knockdown Mfn2. Mfn2-KD INS1 cells were incubated for 45 min with 200nM C12-BODIPY 558/568 in 11mM glucose RPMI (0.1% FBS), after which the media containing BODIPY-labeled FAs was removed, fresh, phenol-red-free DMEM media (1% FBS) was placed on the cells, and the cells were imaged in an Operetta high-content imager at 37°C with 5% CO_2 to evaluate BODIPY fluorescence inside the cells. These images were then quantified using the Operetta Harmony software for average cytosolic fluorescence after thresholding and removing background.

RESULTS

Mfn2 was reduced under HFD and in the ZDF rat

Previously, we published that reduced fusion activity fragments mitochondria upon exposure to excess palmitate (Molina et al., 2009). In order to investigate this effect in vivo, we examined the levels of the mitochondrial fusion protein Mfn2 in high fat diet fed mice, a model of diet induced obesity and diabetes. C57Bl6 mice were placed on a high fat diet (HFD, 58% kcal from fat: hydrogenated coconut oil, #D12331, Research Diets, New Brunswick, NJ) for 12 weeks vs. a

control diet with 11% kcal from fat (#D12329, Research Diets, New Brunswick, NJ). Glucose tolerance tests were performed weekly from weeks 8-12 to verify diet induced changes in glucose homeostasis. Impaired glucose tolerance became evident at week 12 (Supp. Fig. 1.2). Mfn2 protein expression levels after 12 weeks were reduced by 67 % compared with control mice while mitochondrial mass (by porin) was unchanged (Fig. 1.2A).

HFD feeding in mice induces both hyperglycemia and hyperlipidemia. To test if either or both of these two phenomena are required for reduction of Mfn2 expression in islets, we examined islets isolated from Zucker rats. Three animals from each experimental group (Zucker Lean, Zucker Fatty, Zucker Diabetic Lean, and Zucker Diabetic Fatty) were assayed at eight weeks of age. Comparison of the Zucker Fatty (Fig. 1.2B) and the Zucker Diabetic Fatty (Fig. 1.2C) to their corresponding lean control showed that Mfn2 was reduced in the Zucker Diabetic (by 41%), but not in the Zucker Fatty. These results suggest that the reduction of Mfn2 is inherently related to the increase in circulating triglyceride and compounded by hyperglycemia in the progression to overt diabetes.

Deletion of Mfn2 in β-cells induced mitochondrial fragmentation

To investigate the role of Mfn2 reduction in β-cell mitochondrial morphology, we created a mouse lacking Mfn2 in insulin secreting cells by using the Cre/LoxP system. Rat Insulin Promoter (RIP)-mediated Cre expression produced excision of Mfn2 (β-Mfn2KO) in β-cells. Tissue specific excision of Mfn2 from isolated pancreatic β-cells was confirmed by PCR (Supp. Fig. 2.2A) and western blot

(Supp. Fig. 2.2B). Comparison of Mfn2 expression in other tissues (liver, muscle, heart, fat, thymus, and brain) obtained from β-Mfn2KO indicated that these tissues are not significantly affected (Supp. Fig. 2.2C).

As Mfn2 deletion has been shown to change mitochondrial morphology to a fragmented state in different tissues, we determined whether this was the case in β-cells as well. In order to distinguish β-cells during this imaging, dispersed islet cells were transduced with adenovirus encoding for mitochondrial photo-activatable GFP (paGFP) driven by the Ins1 promoter, which is only active in β-cells. TMRE was used to stain mitochondria in all cells. After photoactivating different cells, we identified the β-cells within dispersed islets and found that β-cells from β-Mfn2KO mice show mitochondrial fragmentation (Fig. 2.2A). Indeed, cells in which photoactivation of GFP was not successful showed elongated mitochondria, supporting β-cell specific Mfn2 deletion and fragmentation (Fig. 2.2B). Since RIP-driven Cre has been shown to lead to expression in POMC neurons, all experiments were performed on islets isolated from body-mass matched WT and β-Mfn2KO mice (Fig. 3.2A) or from isolated islets from Mfn2 floxed mice transduced with adenoviral Cre ex vivo, eliminating potential complications from hypothalamic Cre expression.

β-Mfn2KO islets have increased insulin secretion at substimulatory glucose levels

To test the effects of Mfn2 deletion on β-cell function, GSIS was measured in islets isolated from wild type and β-Mfn2KO mice. Loss of Mfn2 expression induced an impairment of glucose tolerance by 50 days of age (Fig 3.2B). Mfn2

deletion induced a 2 fold increase in insulin secretion at basal (3mM) glucose when compared to WT islets (Fig. 3.2C). Excision of Mfn2 ex vivo initiated a similar increase in basal insulin secretion, demonstrating that acute excision is sufficient to produce basal hypersecretion (Fig 3.2D). On the other hand, insulin secretion after glucose stimulation was not different between WT and β-Mfn2KO islets. While islets were size matched, we also measured insulin content to verify that the size matching was done properly as well as to test whether Mfn2 deletion could alter steady state levels of insulin in islets. We did not detect a significant change in insulin content between size matched WT and β-Mfn2KO islets (Fig. 3.2E).

Mfn2 deletion in β-cells recapitulated the insulin secretion dynamics of obese islets

In order to better understand the changes induced by Mfn2 deletion in β-cell secretory function, we conducted islet perifusion experiments to quantify first- and second- phase insulin secretion (Fig. 3.2F). β-Mfn2KO islets perifused with 3mM glucose showed elevated insulin secretion when compared to WT islets, similar to the batch secretion experiments. Upon increasing the glucose concentration to 15mM, control islets exhibit a short decline in insulin secretion, followed by a large 5-fold increase in secretion, as expected with phase I insulin secretion. Phase I is followed by a rapid decrease in secretion, which is followed by a gradual increase in secretion, consistent with the classic Phase II of insulin secretion, as shown in wild type mouse islets. On the other hand, β-Mfn2KO islets exhibit no pre-phase I decrease and no peak during phase I. The absence of phase I secretion was instead replaced by elevated insulin secretion for the duration of

exposure to high glucose during phase II in β-Mfn2KO islets. Subsequent exposure to 40mM KCl caused a similar increase in insulin secretion between both groups, although the β-Mfn2KO islets continued to secrete at a higher rate overall. In order to visualize the oscillatory nature of phase II insulin secretion, the perfusion data was processed with the OOPSEG smoothing program (Bradley, Steil, & Bergman, 1995) and displayed in Fig. 3.2G. The β-Mfn2KO islets demonstrate disrupted oscillatory behavior in addition to impaired phase I and increased phase II secretion, phenomena also observed in human models of prediabetes.

Deletion of Mfn2 increased mitochondrial ATP-synthesizing respiration under basal glucose

Because insulin secretion and oxygen consumption are intimately related in the β-cell, we sought to determine if β-Mfn2KO islets demonstrate altered oxygen consumption in response to glucose or fatty acids using the Seahorse XF24 respirometer. β-Mfn2KO islets exhibit increased basal oxygen consumption, demonstrating an increased energy demand (Fig. 4.2A). Islets typically display an increase in oxygen consumption with an acute increase in glucose concentrations (from 3mM to 20mM); however, this response is significantly lower in β-Mfn2KO islets because they exhibited a two-fold increase in respiration under low, basal, glucose, when compared to WT islets (Fig. 4.2B). This increase in respiration was indeed mostly attributed to an increase in ATP synthesis capacity, as it was oligomycin sensitive (Fig. 4.2C). Therefore, these data show that increased basal oxygen consumption in β-Mfn2KO islets is through an increase in the capacity of

mitochondria to produce ATP, resembling β-Mfn2KO mitochondria from brown adipose tissue. A dramatically increased oxygen consumption was observed in Mfn2-KD INS-1 cells compared with scramble control INS-1 cells, suggesting that Mfn2 knockdown elicits an increase in fatty acid uptake (Fig 5.2E) and oxidation (Fig 4.2D).

Mfn2-deletion in β-cells sensitized insulin secretion to fatty acids

Increased basal insulin secretion is a hallmark of islets from obese and diabetic animal models. To determine the mechanism of increased insulin secretion at basal glucose concentrations, we first investigated cytosolic calcium in islets lacking Mfn2, given calcium's established role in GSIS. We observed no difference in cytosolic calcium levels between WT and β-Mfn2KO β-cells at basal (Fig. 5.2E) glucose conditions. Mfn2 inhibition has been shown to increase H_2O_2 levels in other cell types and H_2O_2 is a molecule known to enhance insulin secretion(Heart, Palo, Womack, Smith, & Gray, 2012; Pi et al., 2007). Therefore, we investigated mitochondrial matrix H_2O_2 production utilizing a reversible redox sensor Orp1-roGFP. However, no differences in mitochondrial H_2O_2 levels were detected between WT and β-Mfn2-KO islets. Indeed, only exogenous H_2O_2 was sufficient to significantly increase oxidation of the probe localized to the mitochondrial matrix (Figs. 5.2C and 5.2D).

Previous studies have shown that obesity or fat accumulation in β-cells is sufficient to induce fatty acid-mediated insulin secretion at basal glucose concentrations accompanied by an increase in fatty acid utilization (C J Nolan et

al., 2006). In order to investigate whether Mfn2 reduction could be responsible for sensitizing basal insulin secretion to fatty acids, palmitate-induced insulin secretion was markedly increased by 0.4mM palmitate in β-Mfn2KO islets (Fig. 5.2A), suggesting that Mfn2 downregulation in β-cells is sufficient to induce elevated insulin secretion in response to fatty acids at basal glucose concentrations. To determine if this increased sensitivity to fatty acids is accompanied by increased fatty acid utilization in cells lacking Mfn2, we transduced INS-1 832/13 cells with Mfn2 shRNA via an AAV vector (Mfn2-KD). We observed a significant increase in labeled 12-carbon FA uptake in the Mfn2-KD cells compared to their scramble-RNA transduced controls (Fig. 5.2B), suggesting an increase in FA uptake and utilization with Mfn2-KD.

DISCUSSION

Increased basal insulin secretion, loss of phase II oscillations, and increased insulin secretion in response to fatty acids are thought to contribute to the development of insulin resistance, but the relationship between mitochondrial morphology and these phenomena is unknown. Hyperinsulinemia has been the focus of historical and recent research, as studies show that it might be a trigger for insulin resistance and T2D (Reviewed in Czech 2017). Our results indicate that mitochondria play an important role in the observed increased insulin secretion through the reduction of Mfn2 and concomitant increase of fatty-acid induced insulin secretion.

Consequences of arrest of mitochondrial fusion

We and other labs have observed mitochondrial fragmentation in response to an excess nutrient environment. To address the mechanism, we examined Mfn2, which previous studies have shown is reduced in models of obesity and excess nutrients in muscle and adipose tissue (Bach et al., 2003; Le Blanc et al., 2012; Pich et al., 2005; Sorianello et al., 2012). Here, we report a decrease in Mfn2 expression in the β-cell in a rat model of obesity. Deletion of Mfn2 in the β-cell resulted in fragmented mitochondria in the absence of an excess nutrient environment. Mfn2 deletion was sufficient to recapitulate an obese-like phenotype in rodent β-cells, including altered responsiveness to fatty acids, which is characteristic of islets from obese/T2D subjects. One of the most compelling outcomes of deletion of Mfn2 is the capacity of free fatty acids (FFA) to promote insulin secretion under low glucose. This mimics previous findings from the Prenkti group showing islets from obese rats are more sensitive to fatty-acid induced insulin secretion at basal glucose (C J Nolan et al., 2006). The potentiation of insulin secretion in response to fatty acids may be of particular importance in states of insulin resistance or diabetes because these patients often have increased circulating triglyceride (Seigneur et al., 1994).

Deleting Mfn2 in brown adipose tissue (BAT) mitochondria increases their capacity for ATP-generating fat oxidation (Mahdaviani et al., 2017). In this regard, we showed that deletion of Mfn2 in β-cells increased respiratory capacity linked to ATP synthesis under low glucose. The preferred nutrient of β-cells to oxidize in low

levels of low glucose is fatty acids. Thus, our data demonstrate that inhibiting Mfn2 provides an extra capacity to take up and utilize fat for ATP synthesis in β-cells under low glucose.

Fatty acids regulate insulin secretion

Long-term exposure to saturated long-chain fatty acids, such as palmitate, has been shown to increase basal insulin secretion and blunt GSIS; however, acute exposure to saturated FFAs potentiates GSIS (Branstrom, Corkey, Berggren, & Larsson, 1997; El-Azzouny et al., 2014; Y.-P. Zhou & Grill, 1995; Y. Zhou & Grill, 1994). Exposure to palmitate has been shown to induce mild mitochondrial uncoupling (Carlsson, Håkan Borg, & Welsh, 1999). The data included herein suggest that Mfn2 downregulation may be involved in this switch in response from short term to long term exposure in β-cells by controlling the dose response of insulin secretion to palmitate, independently of ROS or Ca^{2+} alterations. This would fit with our data demonstrating a decrease in islet Mfn2 expression in HFD fed mice and ZDF rats. Specific mechanisms regulating Mfn2 expression have been described; decreased Mfn2 protein levels could be a result of phosphorylation and proteasomal degradation of Mfn2 (Chan et al., 2011; Ziviani et al., 2010), which has been shown in sarcoma U2OS cells in response to doxorubicin, an inducer of mitochondrial oxidative stress (Leboucher et al., 2012). Previous studies have shown an increase in glycerolipid/free fatty acid (GL/FFA) cycling in response to HFD in rats (C J Nolan et al., 2006; Christopher J. Nolan & Prentki, 2008; Christopher J Nolan et al., 2006). It is thought that this cycle alters

insulin secretion through signaling intermediates, such as monoacylglycerols (MAGs), which activate exocytotic machinery via Munc13 (Marc Prentki, Matschinsky, & Madiraju, 2013). Given that Mfn2 deletion results in similar effects, it is conceivable that GL/FFA cycling could increase sensitivity to exogenous fatty acids in our system, particularly given their increased utilization by β-cells. Other studies have shown an important role for the cell membrane fatty acid receptor GPR40 in the augmentation of insulin secretion by FFA (El-Azzouny et al., 2014). These two potential mechanisms are not mutually exclusive; increased cycling could also contribute to increased release of FFA from the cell, which GPR40 responds to by enhancing insulin secretion.

Limitations and future directions

Growing evidence indicates that alterations in β-cell mitochondrial function, including mitochondrial dynamics, contribute to the observed changes characteristic of β-cells in the development of T2D. This includes the changes in mitochondrial architecture, insulin secretion at basal glucose, and loss of phase I secretion and phase II oscillations. In this study, we evaluated the effect of *in vivo* and *ex vivo* knockout of Mfn2. Due to considerations regarding the RIP-Cre system utilized for *in vivo* work, we subsequently excised Mfn2 exogenously, which removes potential confounding variables from expression of Cre recombinase in specific neurons of the hypothalamus (Schrepfer & Scorrano, 2016). This approach isolates the pancreatic islet from any effects due to overeating driven by Cre expression in the hypothalamus and further elucidates the mechanism

involved in the observed hyperinsulinemia. While we clearly show increased oxidation of palmitate by measuring oxygen consumption, this does not prove all fatty acids are equally utilized by β-cells or even determine multiple species of lipid that exert the insulin secretion augmentation. Further study should focus on describing differential effects of various fatty acids and may point to dietary changes for individuals plagued by hyperinsulinemia. Indeed, other work has shown that mono-oleoylglycerol is also capable of stimulating insulin secretion, pointing to the diverse nature of these stimuli (Saadeh et al., 2012). Our data demonstrate that changes in mitochondrial network architecture may underlie the changes in patterns of insulin secretion. As such, these data suggest that restoration of mitochondrial architecture may serve as a potential approach to restore normal insulin secretion. We show that Mfn2, a mediator of mitochondrial fusion and organelle tethering plays an important role in mediating coordinated β-cell insulin secretion in response to glucose and fatty acid stimulation. This work provides evidence that nutrient induced alterations to β-cell mitochondrial dynamics can affect mitochondrial bioenergetic efficiency, capacity, and insulin secretion and thereby could contribute to the development of diabetes through an overt change in fuel utilization in the excess nutrient environment.

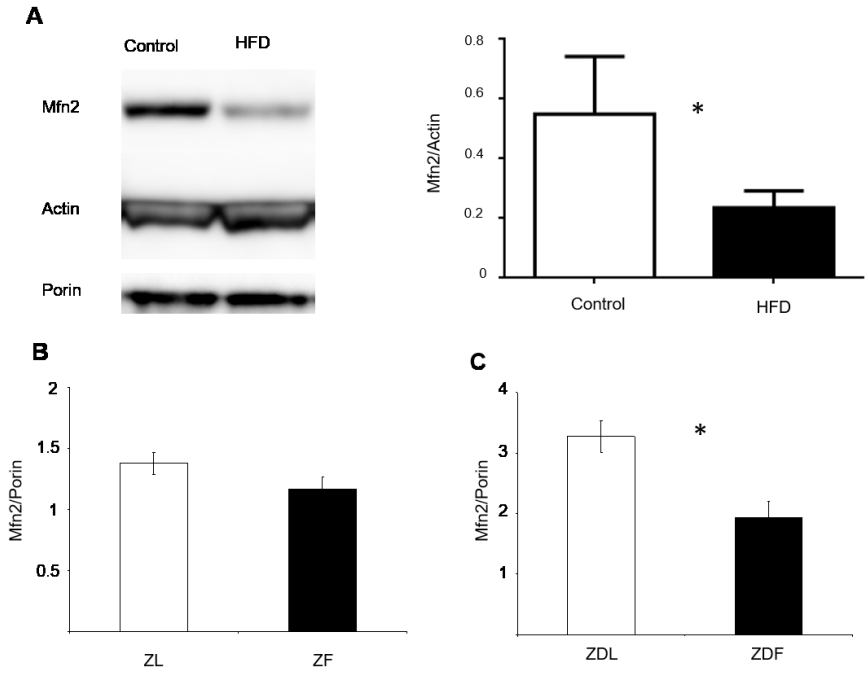

Figure 1.2. Mfn2 protein levels are decreased in pancreatic islets in models of obesity.

(A) Male C57Bl6 mice were provided with a high fat or a control diet for 12 weeks. Western blot analysis of protein lysates obtained from islets isolated from HFD mice reveal a decrease in Mfn2. B-Actin and Porin expression was equal in both sets of mouse islets tested (n=3 mice per condition) Student's T-Test, *p≤0.05. (B,C) Islets were isolated from 8 week old Zucker Lean (ZL), Zucker Fatty (ZF), Zucker Diabetic Lean (ZDL), and Zucker Diabetic Fatty (ZDF) and tested for Mfn2 protein expression (n=3 per group). Densitometric analyses of Mfn2/porin indicates that there is a 41% decrease in Mfn2 expression in ZDF rats compared to ZDL control ($p<0.05$) and no difference between ZF and ZL mice. Student's T-Test, *p≤0.05

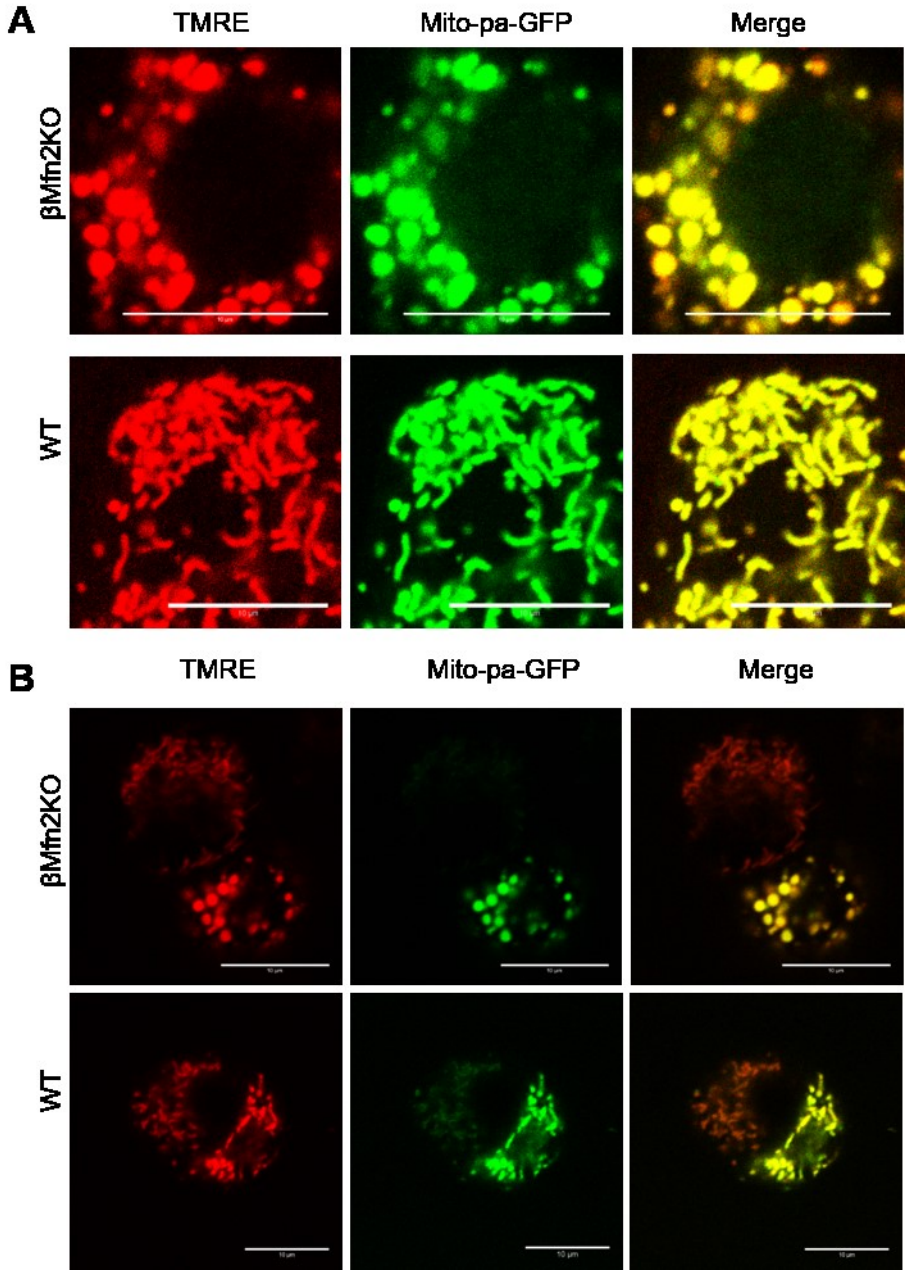

Figure 2.2. Excision of Mfn2 leads to β-cell mitochondrial fragmentation.

(A) β-cell mitochondria were labeled with TMRE and mito-paGFP (insulin promoter) for confocal imaging. β-cells were identified by 2 photon mediated photoconversion of paGFP and possess fragmented mitochondria. (B)

Representative images showing β-cells and non β-cells (no GFP expression) from dispersed islets in the same field of view. Mitochondrial fragmentation is only evident in the β-cells obtained from βMfn2KO samples. Cells from 3 mice were imaged for representative fragmentation in β-cells, all scale bars 10μm.

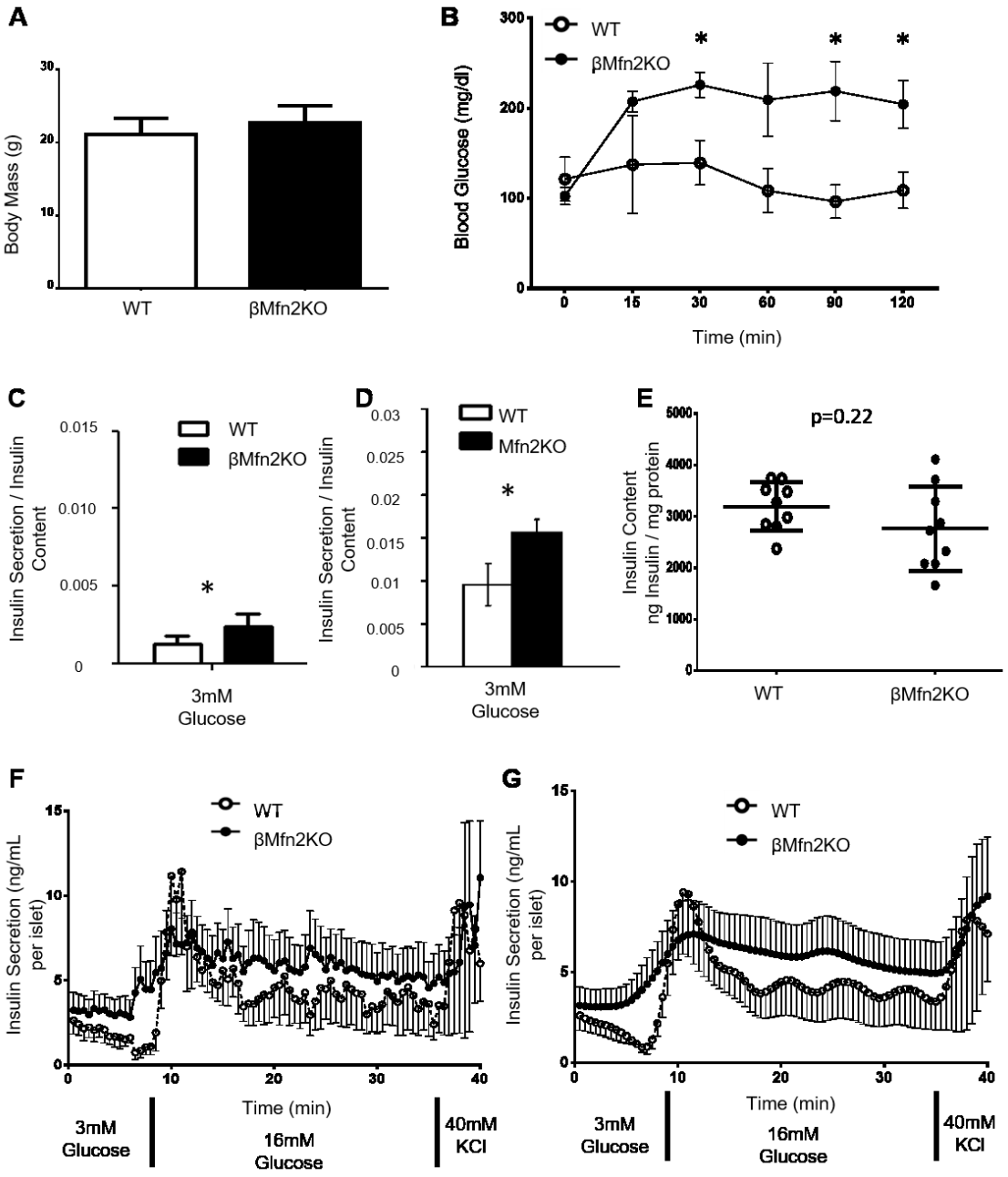

Figure 3.2. Deletion of Mfn2 in vivo and ex vivo induces altered insulin secretion profiles.

(A) No differences between WT and βMfn2KO animal body mass were observed at 56 days of age (n=3-4 mice per group). (B) βMfn2KO mice exhibit impaired glucose tolerance at 56 days of age compared to controls, *p≤0.05, n=3 mice per group. (C) βMfn2KO islets exhibit increased basal insulin secretion. n=7 and 8 animals for WT and βMfn2KO respectively, performed in technical triplicates, p≤0.05 by student's t-test. (D) Acute excision of Mfn2 *ex vivo* increases basal insulin secretion. CMV-Cre infected β-cells from floxed Mfn2 mice displayed increased basal insulin secretion compared with CMV-GFP control infected β-cells (n= 3 animals per genotype; performed in triplicate). (E) No differences in insulin content were observed in βMfn2KO islets compared with control islets (n=3 mice per group; technical triplicates of 10 islets each from each animal). (F) Basal, 3mM glucose, Islets were perifused with Krebs buffer for 3 minutes, followed by 15mM glucose Krebs buffer for 30 minutes, and finally 15mM glucose + KCl 40mM solution for 15 minutes. βMfn2KO islets (solid line) have increased basal insulin secretion, a more prolonged increase in insulin secretion upon addition of stimulating concentrations of glucose, and display disrupted oscillatory patterns of secretion compared with control islets. Error bars are shown in a single direction for clarity. n=4 separate animals with 3 technical replicates each. (G) To further demonstrate the oscillatory behavior of the secretion and loss thereof in the βMfn2KO islets, we utilized the OOPSEG smoothing program to smooth the data from panel (F).

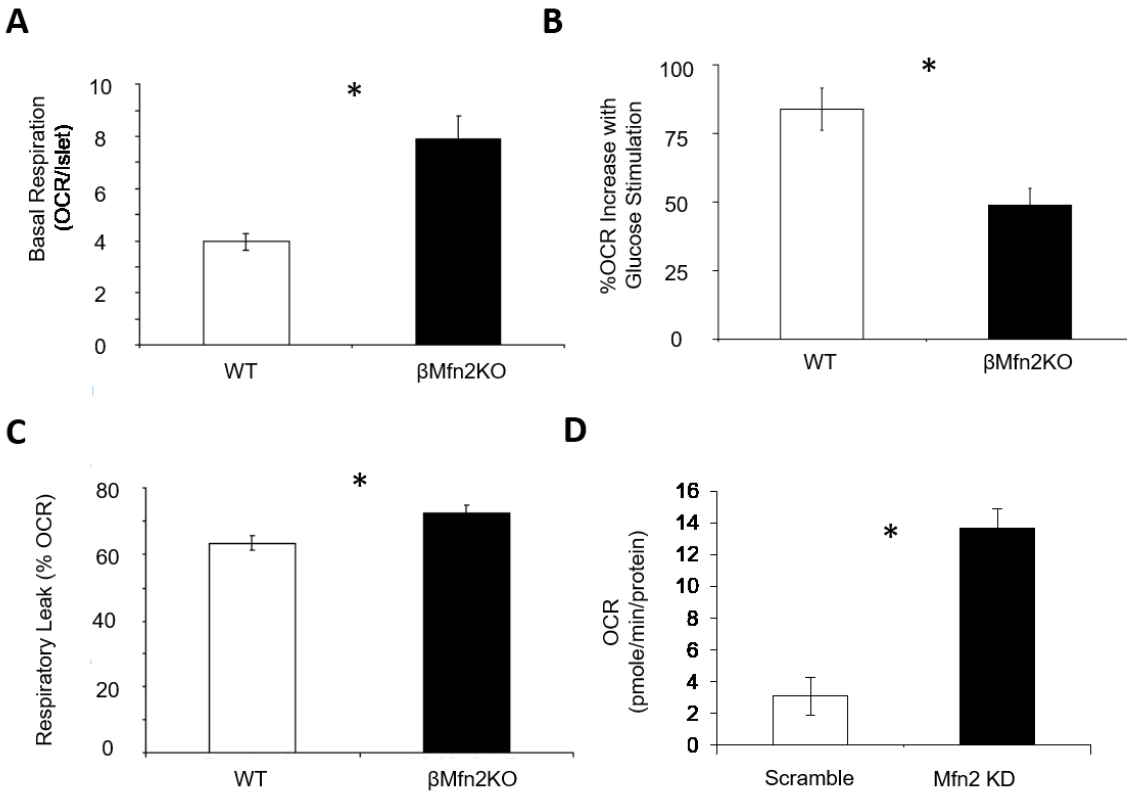

Figure 4.2. Mfn2 controls oxygen consumption and fatty acid metabolism in β-cells

(A) Representative trace showing quantification of Seahorse traces. (B) Basal oxygen consumption is 2 fold greater in islets lacking Mfn2 compared to controls ($p<0.001$, n=4 mice per group). (C) The percent increase in oxygen consumption with 20mM glucose stimulation is significantly blunted in the islets lacking β-cell Mfn2 ($p=0.002$, n=4 mice per group). (D) Respiration under 5μM oligomycin, to block ATP synthase, is 10% greater in islets lacking Mfn2 compared to control ($p<0.001$, n=4 mice per group). (E) INS1 cells with Mfn2KD exhibit an increase in

palmitate induced respiration (n=4 independent experiments), Student's T-Test, *p≤0.05

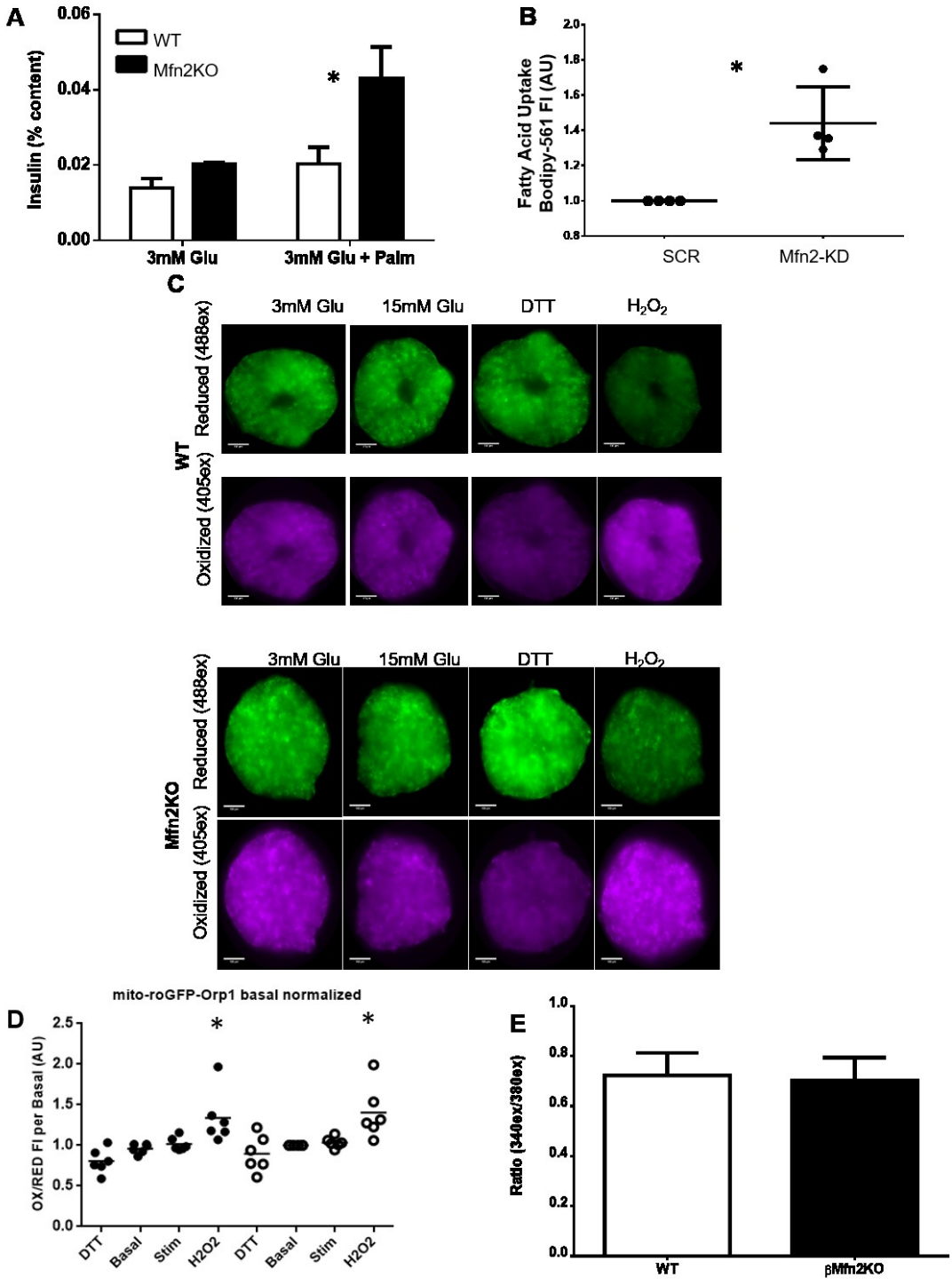

Figure 5.2. Mechanistic investigations of basal insulin secretion in β-cells lacking Mfn2

(A) Insulin secretion in response to 0.4mM palmitate. βMfn2KO animals display increased basal insulin secretion. When 0.4mM palmitate is added with 3mM glucose, βMfn2KO demonstrate a statistically significant increase in insulin secretion, which is not observed in control islets. Data is shown as mean ± standard deviation; n = 4 per group. (B) BODIPY-labeled 12-carbon fatty acid uptake is increased in Mfn2-KD INS-1 cells compared to scramble control cells, which were set at 1 for each experiment to facilitate comparison and normalization between experiments ($p \leq 0.05$, n=4 independent experiments). (C,D) Reaggregated primary islets transduced with mitochondrially targeted ORP1-roGFP with *ex-vivo* Mfn2 excision, n=6 independent experiments with 8-10 islets per condition. Mfn2-KO (black circles) show no difference in H_2O_2 production at 3mM Glu (Basal) or 15mM Glu (Stim) from the WT control (open circles). Only each genotype's oxidized control (H_2O_2) show a significant increase (*, $p \leq 0.05$) in detected H_2O_2. All scale bars are 100μm. (E) βMfn2KO cells do not have increased cytosolic calcium, suggesting a mechanism not involving calcium for induction of insulin hypersecretion at basal levels of glucose (n=3 mice per group).

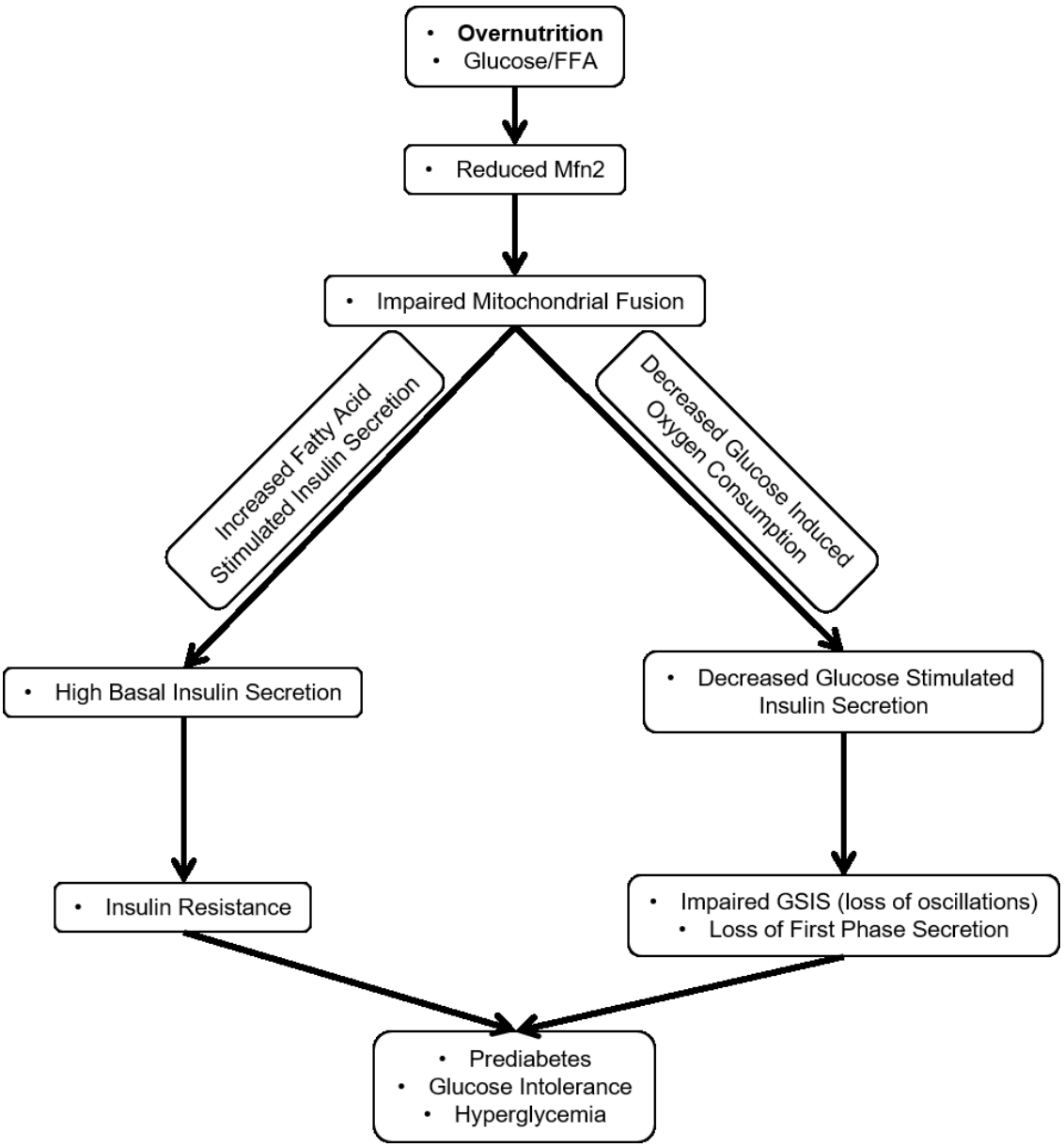
• Overnutrition
• Glucose/FFA
• Reduced Mfn2
• Impaired Mitochondrial Fusion
Increased Fatty Acid Stimulated Insulin Secretion
Decreased Glucose Induced Oxygen Consumption
• High Basal Insulin Secretion
• Decreased Glucose Stimulated Insulin Secretion
• Insulin Resistance
• Impaired GSIS (loss of oscillations)
• Loss of First Phase Secretion
• Prediabetes
• Glucose Intolerance
• Hyperglycemia

Figure 6.2. Scheme of progression to prediabetes via excess nutrient intake and mitochondrial fragmentation.

Excess nutrient consumption (*in vivo)* or excess glucose/FFA (*in* vitro) reduced Mfn2 expression. The loss of Mfn2 impairs mitochondrial function and alters GSIS and nonstimulated insulin secretion similarly to obesity. Elevated nonstimulated insulin secretion leading to hyperglycemia and eventual insulin resistance is compounded by impaired GSIS, eventually leading to prediabetic complications.

Compound	mw (g/mol)	Conc. (M)	MW*con	For 0.5 L
NaCl	58.44	0.595	34.7718	17.3859
HEPES	238.3	0.1	23.83	11.915
KCl	74.56	0.023	1.71488	0.85744
MgSO4	246.5	0.005	1.2325	0.61625
Na2HPO4	141.96	0.00075	0.10647	0.053235
KH2PO4	136.09	0.002	0.27218	0.13609
NAHCO3	84.01	0.025	2.10025	1.050125

Table 1.2 Krebs secretion and imaging buffer

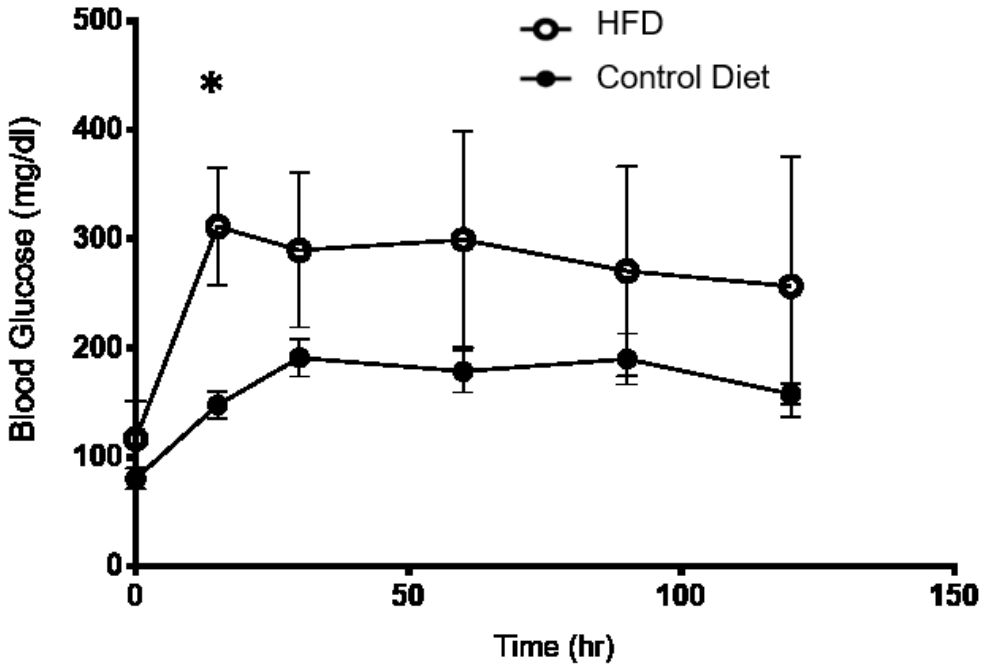

Figure S1.2. HFD mice exhibit impaired glucose tolerance after 12 weeks of age

HFD mice demonstrate impaired glucose tolerance via OGTT after 12 weeks of age compared to control diet fed animals, n=3 animals per diet, * $p \leq 0.05$ by student's t-test at each timepoint.

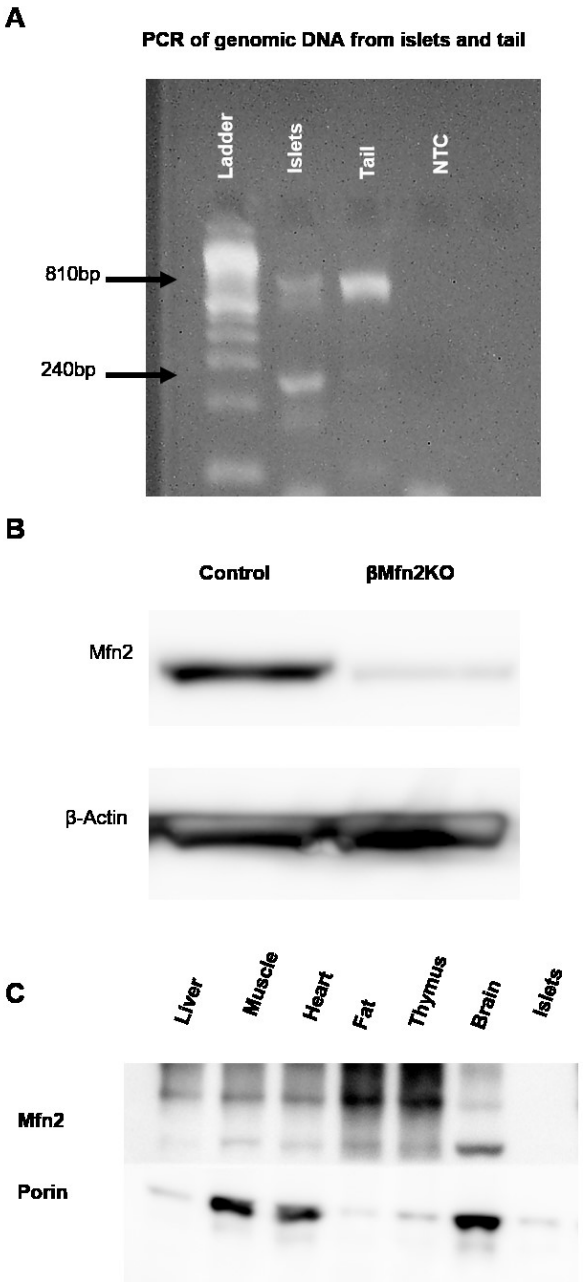

Figure S2.2. Validation of beta cell specific Mfn2 knockout.

(A) Mfn2 LoxP PCR of genomic DNA obtained from a tail blood sample and islet homogenate from a βMfn2KO animal. Lane 1 is the PCR product obtained using islet DNA as the template, the product is present at a 240bp excised band

demonstrating knockout of Mfn2. Any residual unexcised 810bp band is contributed by other cell types in the islet that would have Mfn2 excised under RIP. Lane 2 is the PCR product obtained using tail lysates and is present as the unexcised 810bp band. Lane 3 is the no template control. (B) Western blot of protein samples obtained from βMfn2KO and control littermate islets. Mfn2 protein is reduced in the islets of βMfn2KO islets and any present Mfn2 is attributed to non-beta cell islet cells. (C) Tissue specificity of the beta cell specific Mfn2 knockout was measured in tissue samples obtained from a βMfn2KO mouse. Mfn2 expression was measured by western blot and was found to be present at varying degrees in all tissues tested except for isolated pancreatic islets.

CHAPTER THREE: Metabolic Characterization of Adenovirally-delivered Mfn2 Knockdown in the INS-1 Cell Line

Ilan Benador*[,1,2], Nathanael Miller*[,1,2], Jin Li[1], Daniel Braas[1], Orian Shirihai[1].

***Equal contributions from these authors**

1. Division of Endocrinology, Department of Medicine, David Geffen School of Medicine at UCLA, Los Angeles, CA, USA

2. Obesity Research Center, Department of Medicine, Boston University School of Medicine, Boston, MA, USA

ABSTRACT

Mitofusin 2 was previously shown to govern basal insulin secretion and FAO in primary pancreatic islets. Because primary islet tissue is limited, utilizing cell lines as models of disease and primary tissue is beneficial. Metabolic characterization of cell lines provides insight into their metabolite profiles, oxygen consumption, ROS production, and mitochondrial function. Here, we investigated the role of Mfn2 loss-of-function in INS-1 cells, a model of pancreatic β-cells. While adenovirally-transduced Mfn2 siRNA reduced Mfn2 expression and fragmented mitochondria, it did not affect insulin secretion in either the basal or glucose-stimulated state. Regardless of the lack of functional consequences, INS-1 cells with Mfn2-KD

exhibited increased ROS production and FFA uptake, while ETC activity was impaired, even without reduced ETC component expression. This investigation paves the way for further characterization of mitochondrial fragmentation and its consequences, particularly fusion-independent functions of Mfn2 utilizing modulators of its activity.

INTRODUCTION

Metabolism sits at the intersection of environment and genetics, and as such serves as a hub to investigate cellular and mitochondrial dysfunction. Here we describe a systematic approach to metabolic phenotyping in a model of pancreatic beta cells for the study of mitochondrial fragmentation. Given the pancreatic beta cell's unique position as a nutrient signal integrator, characterization of its nutrient breakdown is critical to understanding its function. Prior work from our lab has shown that mitochondrial morphology is both governed by available fuel and alters cellular metabolism (Molina et al., 2009; Twig et al., 2008; Wikstrom et al., 2007). Because mitochondria fragment in response to obesity and diabetes (Molina et al., 2009), we induced fragmentation via an adenovirally-delivered shRNA for Mitofusin 2 (Mfn2-KD) and characterized the metabolic consequences thereof.

Previous studies focusing on Mfn2 loss of function have focused on other cell types, such as mouse embryonic fibroblasts (H. Chen, Chomyn, & Chan, 2005) and skeletal muscle (Pich et al., 2005) and demonstrate that Mfn2 independently regulates both mitochondrial dynamics and metabolic activity in mitochondria, as evidenced by the glucose oxidation-enhancing effects of overexpression of a fusion-incompetent truncated Mfn2 (Pich et al., 2005). Because knockout of Mfn2 resulted in a greater sensitivity to palmitate-induced insulin secretion at nonstimulatory glucose concentrations (Ch. 2), we further investigated the consequences of Mfn2 loss-of-function. In this study, we focused on some of the

most likely modulators of insulin secretion in response to mitochondrial fragmentation: ROS (Pi et al., 2007), mitochondrial mass and function (Molina et al., 2009; Patterson et al., 2014; Wikstrom et al., 2007), and fatty acid metabolism (Christopher J Nolan et al., 2006).

Oxygen consumption measurement can provide information on fuel dependence, metabolic efficiency, and can be used in conjunction with other techniques to derive flux through metabolism, for instance measuring oxygen consumption in response to fatty acid stimulation. Oxygen consumption measurements also provide information such as mitochondrial inner membrane leak and non-mitochondrial oxygen consumption.

Given the importance of the mitochondria to the cell and our previous work showing the disruption of mitochondrial dynamics, particularly fusion (Molina et al., 2009), and the role of mitofusin 2 (Mfn2) in the response to excess nutrients (Ch. 2) we knocked down Mfn2 in INS-1 cells (Asfari et al., 1992) to investigate their metabolic response to mitochondrial fragmentation. By using an adenovirally-delivered siRNA, we were able to investigate the effects of an acute reduction in Mfn2 in a beta cell line and determine its functional consequences on the cells.

MATERIALS AND METHODS

Viral Transduction of Mfn2-siRNA (Mfn2-KD)

An siRNA-containing Adeno-associated virus was purchased from Welgen (Cambridge, MA) containing mKate2 as a marker of transduction. The effective

multiplicity of infection (MOI) was determined by high-throughput imaging of cells treated with increasing MOIs of virus and measurement of mKate2 fluorescence. The MOI of the KD virus was determined to be 200 for >90% transduction efficiency and 1700 for the scramble control (SCR). The large difference between these MOIs is a result of the quantification of viral particles performed by Welgen. The concentration of particles is measured optically, not as plaque-forming units, meaning each virus can have different portions of active viral particles.

Cell Culture

INS-1 cells were plated at 10,000 cells per well in 100uL in the presence of MOI 200 (KD) or MOI 1700 (SCR) on 96-well plates (Corning #3603) for high throughput imaging. A Seahorse utility plate was utilized for respirometry; cells were plated at a density of 2,000 cells per well in 150uL. Six-well plates were used for metabolomic experiments and plated at a density of 500,000 cells per well in 2mL of media. The cells were cultured in INS-1 medium overnight with the virus, then given fresh media the following day. The cells grew out for an additional 3 days (37°C, 5% CO_2), at which point they were assayed.

High Throughput imaging

Cells were washed with Imaging Media without phenol red once, then stained with Hoechst nuclear dye (1µg/mL) and one of the following: DHE (10 µM), Mitotracker Green (200 nM), or BODIPY 533 (200 nM) for 45 minutes, after which they were washed twice with imaging media and immediately imaged on an

Operetta high content imager. The separation of various dyes was necessary due to spectral overlap with each other. Each genotype was imaged in triplicate. The DHE stained cells were imaged first due to the time-sensitive nature of this irreversible ROS probe.

Fatty acid uptake measurements

INS-1 cells transduced with adenoviral shRNA (Welgen, MA) overnight were cultured for 3 days to knockdown Mfn2. Mfn2-KD INS1 cells were incubated for 45 min with 200nM C12-BODIPY 558/568 in 11mM glucose RPMI (0.1% FBS), after which the media containing BODIPY-labeled FAs was removed, fresh, phenol-red-free DMEM media (1% FBS) was placed on the cells, and the cells were imaged in an Operetta high-content imager at 37°C with 5% CO_2 to evaluate BODIPY fluorescence inside the cells. These images were then quantified using the Operetta Harmony software for average cytosolic fluorescence after thresholding and removing background.

Image Analysis

Images were analyzed in the Operetta Harmony software, which was used to quantify fluorescence intensity of these dyes plus identification of transduced cells via mKate2, the reporter included with the adenovirus used for transduction.

Confocal Imaging

INS-1 cells were plated on Quadrant confocal dishes and imaged on a Zeiss LSM-880 microscope with a 63X oil immersion objective (1.4 NA) equipped with

an Airyscan detector (Weisshart, 2014). Prior to imaging, cells were stained with mitotracker green for 45 min and washed thrice. The reporter fluorophore mKate2 was used to identify transduced cells. Images were quantified using FIJI (www.fiji.sc) for mitochondrial architecture.

Respirometry

The Agilent Seahorse XF96 Extracellular Flux Analyzer was utilized to measure oxygen consumption from Mfn2-KD and SCR control cells. Drug concentrations were as follows: oligomycin (5μM), FCCP (1μM), rotenone (5μM) and antimycin A (5μM) (Sigma). The protocol for mitochondrial stress analysis was followed as published (Nicholls et al., 2010; Seahorse, 2017). Data were compiled and analyzed in Seahorse Wave and Graphpad Prism softwares.

Metabolomics

The experiments were performed as described in (Thai et al., 2014). Briefly, cells were seeded in 6 well plates, so that the final cell count at the time of metabolite extraction was about $7*10^5$ and even across all cell lines. Medium was changed with medium containing U-^{13}C-glucose or U-^{13}C glutamine 24h before metabolite extraction. To extract intracellular metabolites, cells were briefly rinsed with cold 150 mM ammonium acetate (pH 7.3), followed by addition of 1 ml cold 80% MeOH on dry ice. Cells were detached with cell scrapers, suspensions transferred into Eppendorf tubes and 10 nmol D/L-norvaline was added. After

rigorously mixing, the suspension was pelleted by centrifugation ($1.3*10^4$ rpm, 4 °C). The supernatant was transferred into a glass vial, metabolites dried down under vacuum, and resuspended in 70% acetonitrile. For the mass spectrometry-based analysis of the sample, 5 µl were injected onto a Luna NH2 (150 mm x 2 mm, Phenomenex) column. The samples were analyzed with an UltiMate 3000RSLC (Thermo Scientific) coupled to a Q Exactive mass spectrometer (Thermo Scientific). The Q Exactive was run with polarity switching (+3.50 kV / -3.50 kV) in full scan mode with an m/z range of 65-975. Separation was achieved using A) 5 mM NH_4AcO (pH 9.9) and B) ACN. The gradient started with 15% A) going to 90% A) over 18 min, followed by an isocratic step for 9 min and reversal to the initial 15% A) for 7 min. Metabolites and isotopomers thereof were quantified with TraceFinder 3.3 using accurate mass measurements (≤ 3 ppm) and retention times. For isotopologue distribution measurements, data was corrected for naturally occurring ^{13}C as described (Moseley, 2010). Data analysis, including principal component analysis and hierarchical clustering was performed using the statistical language R. Fractional contributions were calculated using the formula $FC = \frac{\sum_0^n i*m_i}{n\sum_0^n m_i}$ as described (Fendt et al., 2013), where m_i denotes the intensity of the isotopologue, and n marks the number of carbons in a given metabolite.

Insulin secretion

INS-1 cells at 60-80% confluence were incubated for 2hr in 2mM glucose RPMI culture media (37°C, 5% CO_2) then incubated in 2mM glucose secretion

buffer for a 1hr pre-incubation in a 37°C water bath, ensuring the water was in contact with the bottom of the plate for efficient heat transfer. Following this pre-incubation, the cells were incubated in the respective conditions (in triplicate) for 45min in a 37°C water bath for insulin secretion, with 2mM glucose as basal and 12mM glucose as stimulated insulin secretion. The media was collected from the wells and insulin content measured by the HTRF Insulin Assay (Cisbio Bioassays). Data was normalized to cell counts per well imaged on the Operetta and calculations performed in Graphpad Prism.

Insulin Measurements

An HTRF insulin assay kit was used to measure insulin secretion (CisBio, Bedford, MA). The assay consists of a FRET-based sandwich immunoassay with Europium Cryptate (Eu-K) and allophycocyanin (XL665) antibodies. Secretion samples were appropriately diluted in a 96-well plate after which 5uL of sample and 5uL of the antibody mix were dispensed into white 384-well plates (#784076, Greiner Bio-One), which was protected from light with aluminum foil and incubated overnight at room temperature. Wavelengths are expressed as wavelength (bandwidth). A Tecan Infinite M1000 or Spark 10M plate reader was used to measure time-resolved fluorescence at 317(20)nm excitation and emission wavelengths of 665(20)nm (XL665) and 620(20)nm (Eu-K). Insulin concentration of the samples was calculated from an insulin standard curve in the same plate. Values that did not fall within the standard curve were excluded.

RESULTS

Knockdown of Mfn2 fragments mitochondria

Adenovirally-delivered shRNA for Mfn2 results in fragmented mitochondrial morphology compared to the Scrambled (SCR) control in INS-1 cells (Fig 1.3A). Super-resolution images show mKate2, the marker of transduction in the cytosol, and mitotracker green localizes to mitochondria. Transduction efficiency in all conditions exceeded 90% (Fig 1.3B), and transduction of the shRNA did not affect cell growth significantly (Fig 1.3C).

Knockdown of Mfn2 does not change mitochondrial mass

We utilized the Operetta high content imager in order to investigate the consequences of limiting mitochondrial fusion on mitochondrial mass, measured as the average intensity of mitotracker green per cell (Fig 2.3A). Even though mitochondrial dynamics is essential for mitochondrial quality control, mitochondrial mass was unchanged (Fig 2.3B). It is possible that the relatively short time course of these experiments (72-96 hr) was insufficient to induce dysfunction of mitochondrial quality control and exert an effect on mitochondrial mass.

Knockdown of Mfn2 Increases labeled fatty acid uptake

Mfn2-KD INS-1 cells were incubated for 45 minutes with 12-carbon Bodipy-533, which enters cells in a manner similar to 16-carbon fatty acids. Average fluorescence intensity per cell was quantified as a measure of uptake. Previous

publications have shown this labeled fatty acid is degraded in a regular fashion and traffics in a manner similar to unlabeled fatty acids (Rambold, Cohen, & Lippincott-Schwartz, 2015), and Mfn2-KD INS-1 cells exhibited significantly increased FFA uptake (Fig 2.3C).

Knockdown of Mfn2 increased ROS production

Given the arrest of mitochondrial dynamics that accompanies loss of fusion, Mfn2-KD cells were incubated with dihydroethidium (DHE) for 45 minutes and then imaged with the Operetta high content imager (37°C, 5% CO_2). We observed a significant increase in DHE positive cells with Mfn2-KD compared to the SCR control, suggesting an increase in ROS production as a result of the reduction in Mfn2 expression (Fig 2.3D). This is consistent with other studies showing reduced mitochondrial activity and increased ROS production from HeLa cells using a similar shRNA approach to knockdown Mfn2 (Ding, Gao, Zhao, Wang, & Zheng, 2015). In HeLa cells, this increased ROS production is the result of dysfunctional mitochondria accumulating in the cytosol due to impairment of mitophagy, a mechanism that could also explain our results here.

Insulin secretion from Mfn2-KD cells is unchanged

Both basal (2mM glucose) and Glucose Stimulated (12mM glucose) insulin secretions were unaffected in the Mfn2-KD cells (Fig 2.3E). This phenotype was unexpected because in primary β cells basal insulin secretion is significantly increased with the loss of Mfn2 (Ch. 2). This functionally different response in

primary cells and a model thereof led us to investigate why these two systems exhibit different phenotypes.

Mfn2-KD reduces overall oxygen consumption in INS-1 cells

Loss of Mfn2 expression significantly reduces basal oxygen consumption (Fig 3.3A) as well as oligomycin-resistant oxygen consumption, which is proton leak across the inner mitochondrial membrane (Fig 3.3B). In addition, ATP linked oxygen consumption (Fig 3.3C) and maximal respiration (Fig 3.3D) are decreased. This result, paired with the increased ROS production above, suggest cells with early mitochondrial dysfunction that has not manifested other functional effects such as impaired insulin secretion. The reduced oxygen consumption in Mfn2-KD cells suggested possible substrate handling deficiencies in Mfn2-KD cells, which we investigated using footprint and metabolomics approaches.

Mfn2-KD does not change TCA substrate uptake

In order to investigate the changes in substrate uptake, we used the Nova Bioanalyzer and did not observe a difference between the knockdown and scramble conditions in glucose utilization (Fig 4.3A), glutamate production (Fig 4.3B), or glutamine production (Fig 4.3C). The Mfn2-KD exhibited a trend of more glutamine production that was insignificant upon statistical analysis. Thus, it appears that Mfn2-KD INS-1 cells respond to fragmentation with a decrease in respiration and no change in oxidized substrate preference, regardless of the increased uptake of labeled fatty acids.

Mfn2-KD alters metabolite profiles in INS-1 cells

Utilizing universally-labeled ^{13}C-Glucose, we performed tracing experiments for the carbons derived therefrom. When analyzed by mass spectrometer, we observed an increase in Phosphocreatine. This increase could be a storage mechanism for high-energy phosphates derived from additional flux through the ETC, as shown previously in neurons (Meyer et al., 2006).

Mfn2-KD reduces ETC activity without reducing mitochondrial ETC protein

Upon knockdown of Mfn2, we observed no change in expression of several ETC components when quantified by densitometry of western blots using FIJI (Fig 5.3). However, the ATP/ADP ratio was unaffected, suggesting an overall reduction in high-energy adenosine nucleotides. This finding is similar to previous findings in heart tissue with Mfn2KO, suggesting a common governing mechanism between these two metabolically demanding tissues (Mourier et al., 2015).

DISCUSSION

Mfn2 was shown in the previous chapter to have a functional role in regulation of insulin secretion. As a result of these findings, we set out to determine the mechanism of this regulation in a pancreatic β-cell line utilizing high-throughput techniques. Knockout of Mfn2 in primary beta cells increased basal insulin secretion and basal respiration, in addition to more fatty acid oxidation (Ch. 2). INS-1 cells are frequently used as a pancreatic beta cell model (Asfari et al., 1992; Molina et al., 2009; V Poitout, Olson, & Robertson, 1996; Roduit et al., 2004; Skelin, Rupnik, & Cencic, 2010; Wikstrom et al., 2007). However, we observed no

change in insulin secretion between the Mfn2KD and SCR groups. Perhaps this disparate phenotype between the two is the result of a knockout versus knockdown of Mfn2. Alternatively, INS-1 cells are immortalized for cell culture, which have a different glucose metabolism when compared to primary tissue models. Regardless of the mechanism for the difference, we have demonstrated that knockdown of Mfn2, validated by imaging and western blots, affects mitochondrial morphology without significantly changing insulin secretion.

Mfn2-KD increased ROS formation and FFA uptake independent from altering insulin secretion

Mfn2-KD cells exhibited increased FA uptake, which suggests an alteration in fuel preference in INS-1 cells. Thus, even in the absence of a functional change in GSIS, forced mitochondrial fragmentation by Mfn2 knockdown induced a fuel switch and decreased oxygen consumption, similar to previous findings in HeLa cells with Mfn2 knockdown induced via shRNA (Ding et al., 2015).

ROS have been shown to be instrumental to insulin secretion (Pi et al., 2007), in addition to being increased in excess nutrient conditions and stress (Criddle et al., 2006). Because insulin secretion was increased in primary β-cells in Ch. 2, we investigated the effect of Mfn2-KD on ROS production. Interpretation of ROS measurements presents challenges, particularly for the probe DHE (Laurindo, Fernandes, & Santos, 2008). However, this probe was specifically chosen because interpretation of results can be aided in the future by HPLC and quantification of specific oxidized products, such as ethidium and oxyethidium.

Separation of these two fluorescent products provides more accurate information of what ROS species oxidized DHE (Fink et al., 2004; Laurindo et al., 2008; Nazarewicz, Bikineyeva, & Dikalov, 2013; Tollefson, Kroczynski, & Cutaia, 2003). While this granularization was not performed on the samples in this project, such methods are well-suited to a high-throughput screening approach, because many other utilized techniques overlap with the tools needed for column separation of metabolites for metabolic screening. Further investigations should include quantification of the oxidized products to elucidate their electron donors, which may further illuminate the source of increased ROS production in Mfn2-KD cells.

This change in morphology without alterations in function certainly warrants further investigation. Perhaps Mfn2 is the primary link between morphology and metabolism, in such a way that low levels of expression after knockdown are sufficient to preserve “normal” metabolism observed in WT INS-1 cells. Other labs have shown that Mfn2 affects metabolism independently of its fusion activity (Pich et al., 2005), which means these two functions are functionally distinct. A possible explanation for this differential behavior could be the necessary dimerization of Mfn’s for fusion activity, meaning the Mfn oligomers may be functionally distinct from monomers. An alternative hypothesis is that INS-1 cells modulate insulin secretion in manners dissimilar from primary β-cells. Future experiments should investigate not only additional manipulations of morphology by changing Drp1, OPA1, or Mfn1 expression, but also include the truncated, fusion-incompetent form of Mfn2 or other modulators of mitofusin activity such as small peptides (Franco et

al., 2016). In addition, further investigation of the difference between immortalized cell models and their primary counterparts, specifically beta cells, will provide better quality control to the field of obesity research because of the important role mitochondria and metabolism play in pathology.

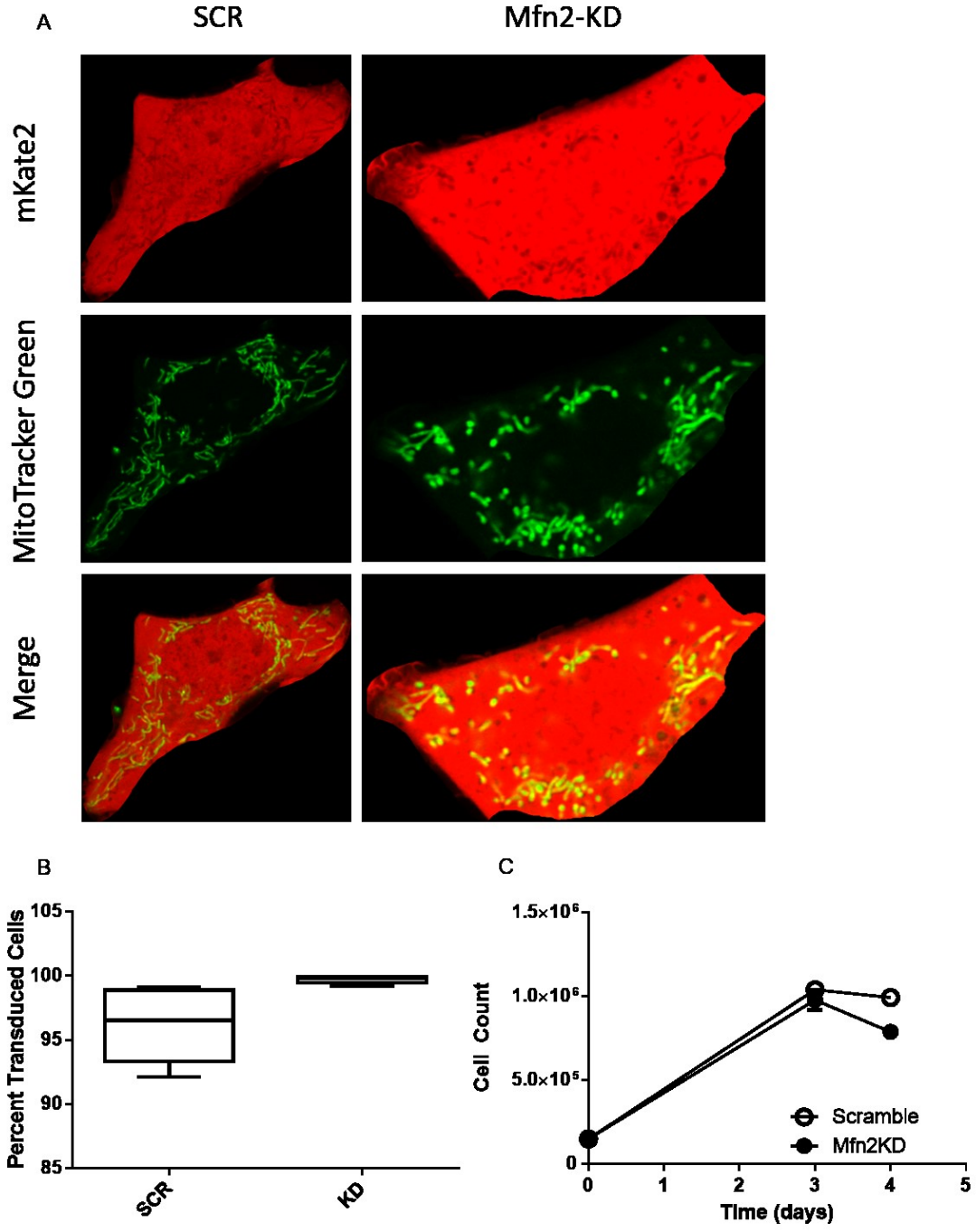

Figure 1.3. Mfn2 Knockdown results in fragmented mitochondria and does not change cellular proliferation.

(A) Mitochondrial fragmentation is evident 72 hours after transduction with Mfn2 shRNA knockdown adenovirus, mKate2 used as marker of transduction. (B) Transduction efficiency for both conditions exceeded 90% and (C) did not affect cellular proliferation significantly in the timeframe studied. Error bars represent SEM for 3 independent experiments, *$p \leq 0.05$ by student's t-test.

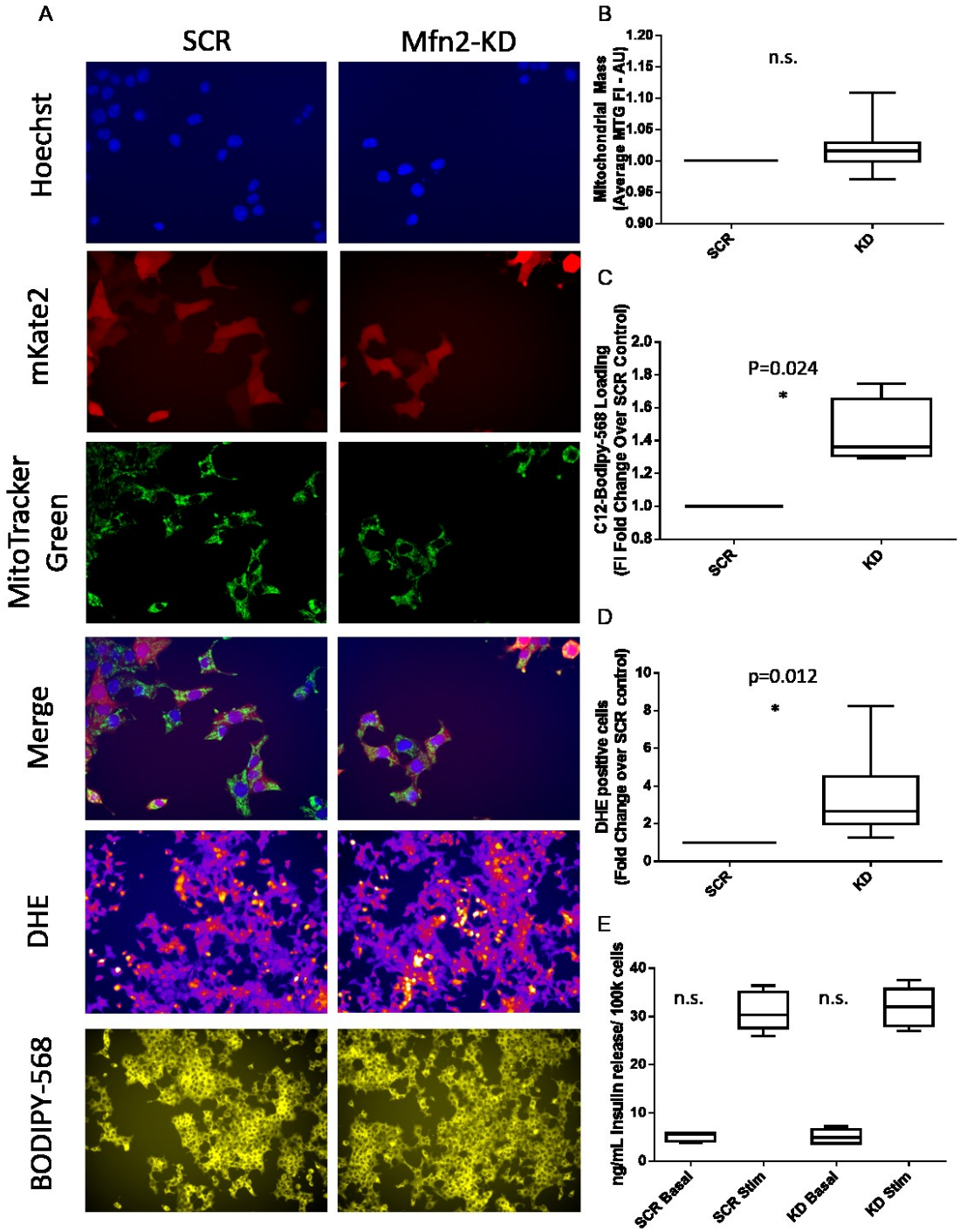

Figure 2.3. High-throughput imaging of Mfn2KD INS1 cells reveals metabolic differences without functional consequences.

(A) High-content images acquired on the Operetta High Content Imager (Perkin Elmer), showing nuclei (Hoechst), transduction efficiency (mKate2), mitochondrial mass (mitotracker green), ROS production (DHE), and FFA accumulation (BODIPY-568). Note the fields for DHE and BODIPY-568 are from different wells than the other images due to spectral overlap of the probes. (B) Mfn2-KD cells do not have altered mitochondrial mass, but do exhibit changes in fluorescently labeled FA uptake (C) and ROS production (D). Despite these metabolic differences, Mfn2KD cells are functionally similar to the SCR control when evaluating GSIS (E). Error bars represent SEM for 3 independent experiments, *$p \leq 0.05$ by student's t-test.

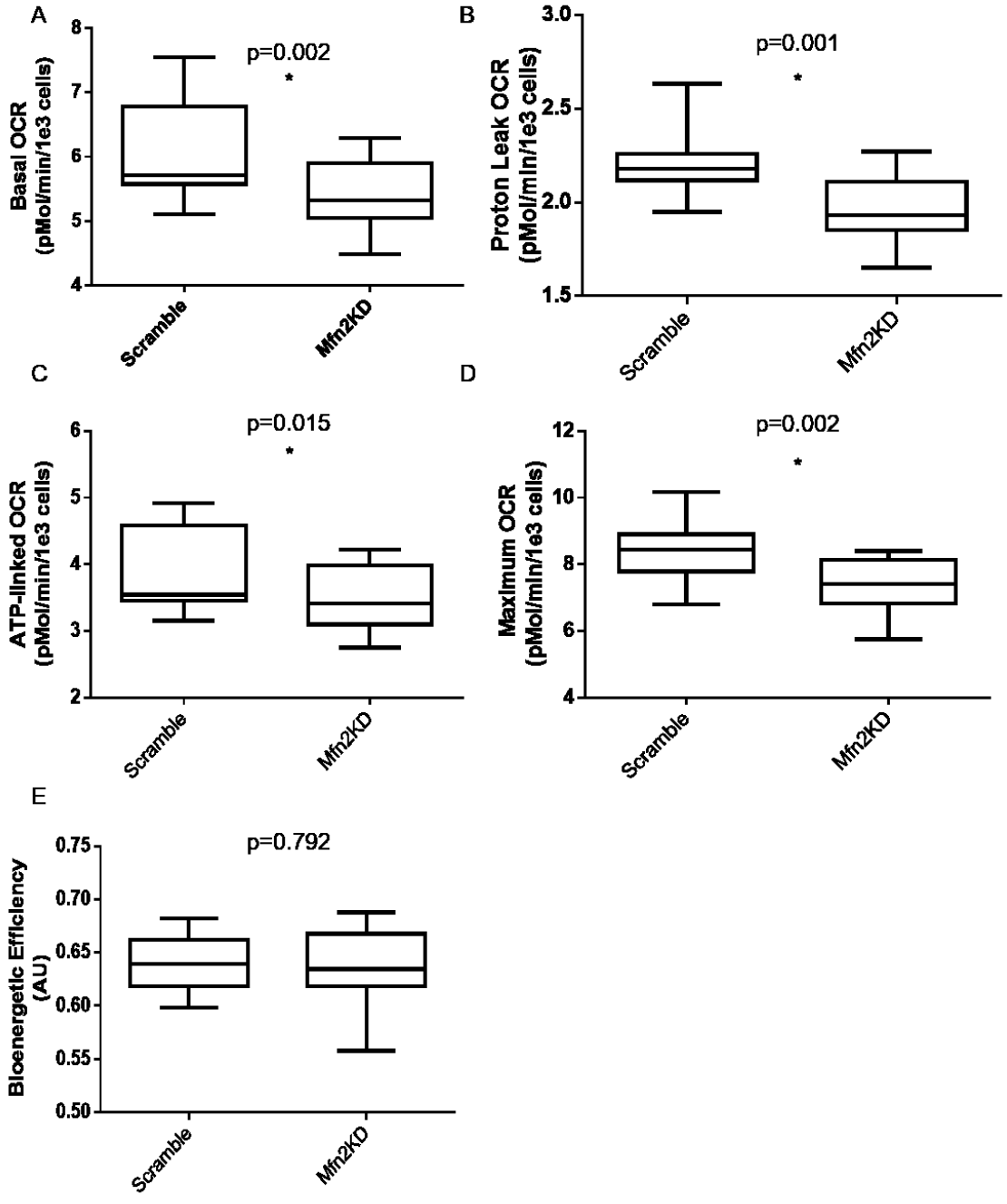

Figure 3.3. Mfn2KD cells exhibit reduced mitochondrial activity.

Mfn2KD INS1 cells demonstrate significantly reduced oxygen consumption, including (A) basal oxygen consumption, (B) proton leak, (C) ATP-linked

respiration, (D) maximal oxygen consumption. These changes do not alter bioenergetic efficiency, a measurement of basal respiration per proton leak (oligomycin-resistant respiration). (E). Error bars represent SEM for 3 independent experiments, *p≤0.05 by student's t-test.

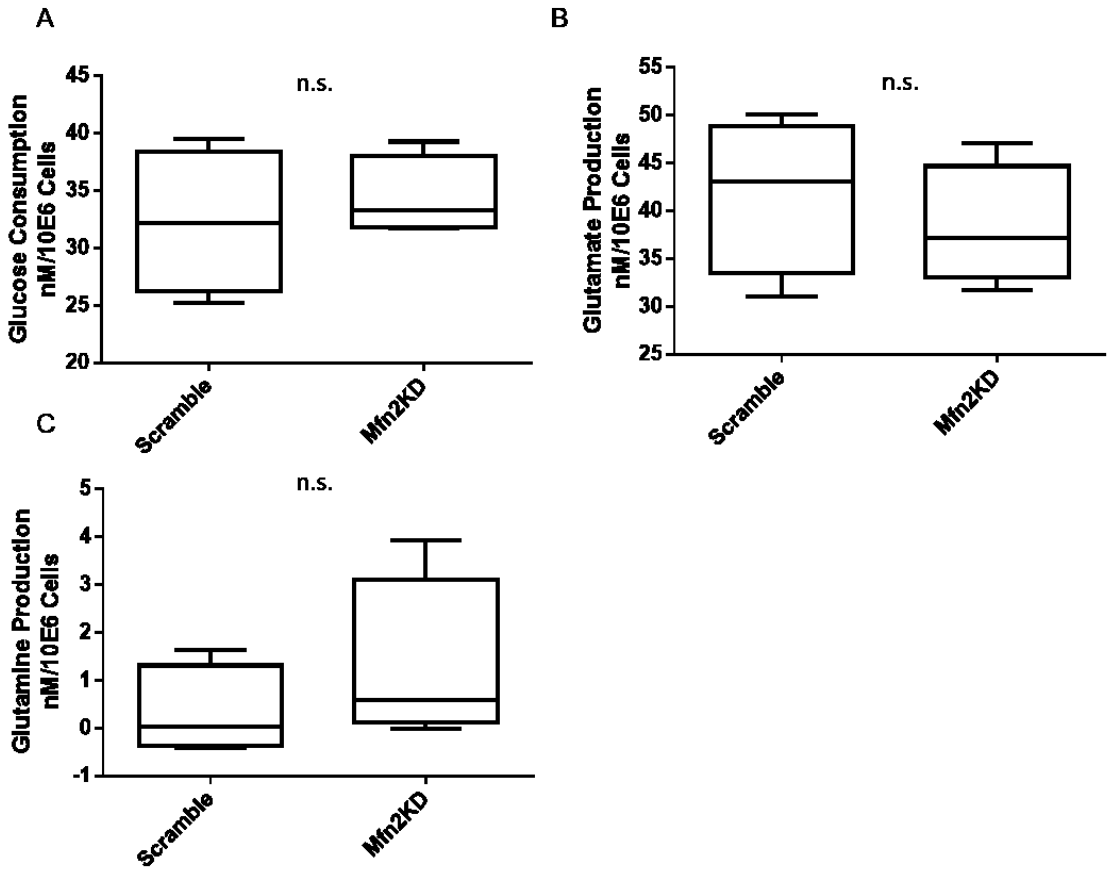

Figure 4.3. Substrate uptake and nontargeted metabolomics reveal nonsignificant differences between Mfn2KD and SCR cells.

Mfn2-KD cells do not significantly alter nutrient uptake compared to SCR controls in a 24 hour period compared to SCR controls, including glucose uptake (A), Glutamate Production (B), or Glutamine production (C). Error bars represent SEM for 3 independent experiments, *p≤0.05 by student's t-test.

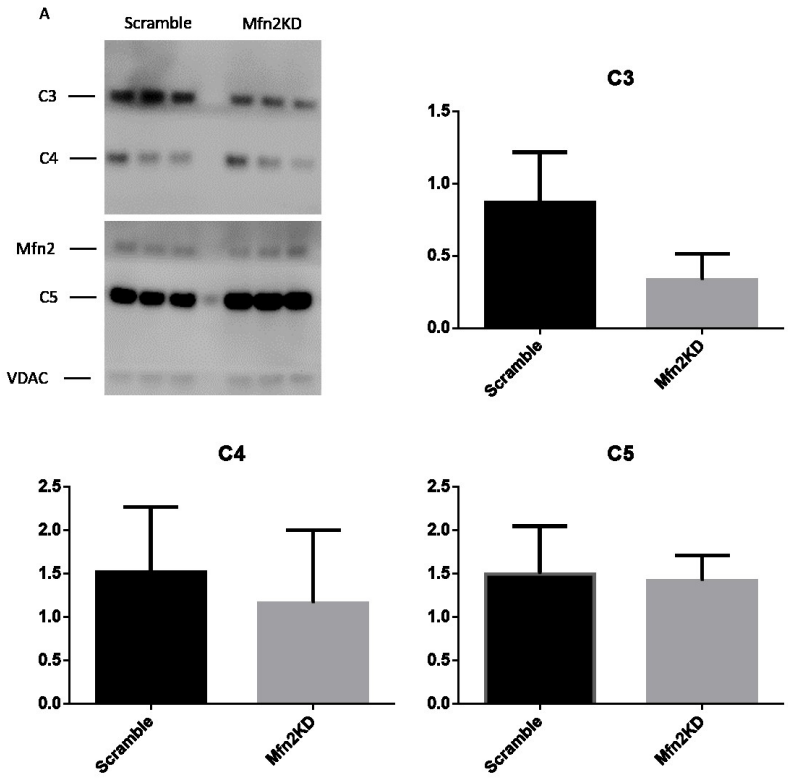

Figure 5.3. Mfn2KD cells maintain ETC machinery in the face of reduced respiration.

(A) Representative blots of ETC proteins; (B) through (D) are Mfn2KD INS-1 cells do not alter ETC component expression when compared to their SCR controls, despite the impaired respiration in Fig. 3.3. Error bars represent SEM for 3 independent experiments, *p≤0.05 by student's t-test.

CHAPTER FOUR: High-Throughput Quantification of Mitochondrial Morphological Parameters in Brown Adipose Tissue Using Advanced Image Segmentation

Nathanael Miller *[,1,2], Dane Wolf *[,1,2], Nour Alsabeeh[1,2], Kiana Mahdaviani[2], Orian Shirihai[1]

*Equal contributions from these authors

1. Division of Endocrinology, Department of Medicine, David Geffen School of Medicine at UCLA, Los Angeles, CA, USA

2. Obesity Research Center, Department of Medicine, Boston University School of Medicine, Boston, MA, USA

ABSTRACT

Digital image analysis of high-resolution micrographs is a challenging field that provides vast amounts of data. Here, we describe a novel method of segmenting Brown Adipose Tissue (BAT) that provides a granular approach to quantifying subcellular structures, particularly mitochondria in relation to lipid droplets. In addition, we lay out a novel machine-learning based mitochondrial segmentation method that eliminates the bias of manual mitochondrial segmentation and improves object recognition compared to conventional thresholding analyses. By

applying these methods, we discovered a significant difference between cytosolic and peridroplet BAT mitochondrial H_2O_2 production, and validated the machine learning algorithm in BAT via norepinephrine-induced mitochondrial fragmentation and comparing manual analyses to the automated analysis.

INTRODUCTION

Image acquisition and analysis are critical tools for the quantification of mitochondrial parameters. Imaging data can provide not only morphological measurements(Joshi, Crouser, Julian, Schanbacher, & Bauer, 2000), but also membrane potential ($\Delta\Psi$), mitochondrial mass, ROS production, and calcium, among others. A major challenge facing the microscopist is the quantification of imaging data without biasing the results of the study. Automated image analysis provides an unbiased, repeatable, and high-throughput method to quantify high-resolution micrographs. The use of macros (a set of instructions for a computer to perform repeatedly) is the most amenable way to increase image analysis throughput with current tools (Mutterer & Rasband, 2012). A macro reduces the amount of time to analyze a single image while ensuring that subsequent images are analyzed in an identical manner.

Brown Adipose Tissue (BAT) provides a unique case due to its high density of (frequently overlapping) mitochondria in the cytosol packed tightly with and around lipid droplets. Previous work in other cell types has focused on quantifying the entire network or manual classification of network morphology (Cribbs & Strack, 2009; Leonard et al., 2015; Mahdaviani et al., 2017; Valente, Maddalena, Robb, Moradi, & Stuart, 2017), while this work focuses on direct quantification of individual mitochondria. Improvements in computer processing power and graphical handling enable a novel solution to this difficult problem: machine

learning. Simply, machine learning is the process of humans training a computer program to perform a task. This differs from programming because the underlying architecture for decision-making has been written by a programmer and the human trainer simply segregates objects into different classes (bins, types of objects, etc.), which the computer then analyzes to build a decision tree to arrive at a similar classification scheme as the human trainer. This type of machine learning is referred to as a random forest model and is one of many iterative machine learning algorithms (Breiman, 2001).

Due to considerations of cost and transparency, the open-source programs ImageJ (https://imagej.nih.gov/ij/) and its plugin-rich counterpart FIJI (Schindelin et al., 2012) (http://fiji.sc/) are utilized for these analysis protocols and data. FIJI provides several plugins not available in stock ImageJ that greatly expedite analysis. Chief among these tools is the WEKA trainable segmentation plugin (Arganda-Carreras et al., 2017), which enables rapid training and deployment of machine-learning segmentation protocols. Tools of this nature are incredibly resource intensive and, as such, must be used on computers with sufficient processing and graphical power. Both ImageJ and FIJI are open-source and widely documented, providing ideal tools for scientific use.

Similar tools have previously been utilized to quantify mitochondria, albeit in a more limited manner. Koopman *et al*. introduced the concept of using a machine learning classifier to morphologically characterize and bin mitochondria

(Koopman, Visch, Smeitink, & Willems, 2006). This technique has been further refined by other groups (Leonard et al., 2015; Valente et al., 2017). Both of these approaches did not fully quantify mitochondrial morphology, but rather quantified the population of each type of mitochondrion, e.g. tubular vs. punctate. Previous work has also described what parameters best define mitochondrial morphology (Joshi et al., 2000). While the conventional approach of manual thresholding for segmentation is valid, it is subject to the analysts' bias (Cribbs & Strack, 2009). Combining these above approaches – using machine-learning to segment mitochondria which are then individually quantified using established parameters – provides the most robust and accurate quantification to date. Software exists to perform a similar segmentation routine (Harwig et al., 2018), but it is not easily adaptable as an ImageJ script, while the methods provided here are cross-platform and usable within ImageJ or FIJI. Additionally, the data outputs from these two methods are not identical and may in fact complement each other.

These tools are significantly more effective when the input micrographs are of high quality and resolution. Poor signal-to-noise ratio, low fluorescence in samples, and many other caveats of fluorescent microscopy influence the efficacy of image analysis. A recent publication details the ideal input image quality and common problems and artifacts encountered with analyses of this type (Harwig et al., 2018). The methods contained herein provide tools to segment and quantify lipid droplet number, morphology, and intensity in brown adipocytes (BAT). We also describe a novel approach to segment mitochondria within these same cells

in order to investigate mitochondria immediately adjacent to lipid droplets versus mitochondria in the rest of the cytosol. While such granulated approaches have been performed in the past (Glancy et al., 2015), they were undertaken in muscle tissue and revealed a novel energy conduction pathway along a mitochondrial network. Here we show a phenotypic difference between mitochondria immediately adjacent to the lipid droplet and the mitochondria distributed within the cytosol. Moreover, we provide a method for improved mitochondrial segmentation and measurement via the WEKA trainable segmentation plugin. Not only is this approach different from previous mitochondrial machine learning classification schemes (Leonard et al., 2015), but it provides an open and transparent tool with the potential to be refined and improved. The development of a WEKA classifier for mitochondrial segmentation expands the available input images significantly; a WEKA classifier is much better at segmenting poorly-acquired images than most conventional methods, preventing the issues mentioned above from excluding images from analysis. More importantly, input images from lower quality microscopes are generally accepted and properly segmented, assuming sufficient quality.

The method contained herein has been validated on images from several different microscopes and collection tools, but all images were in focus and sufficiently magnified that a human could recognize individual mitochondria within the cytoplasm of the cell. This level of detail is generally acquired by an objective lens of 60X magnification or higher, with a NA of 1.4. All images were initially

acquired with at least 1024 x 1024 pixels. The high resolution images permit detailed manual cropping of the cell from its field of view, a necessary step to ensure robust segmentation of mitochondria. More detailed metadata of the images used in this method are contained in the methods.

Brown adipocytes provide an ideal test case for these tools. Not only do the mitochondria in the cytosol differ from those surrounding lipid droplets (Benador et al., 2018), but also BAT mitochondria fragment upon norepinephrine-induced thermogenesis (Wikstrom et al., 2014), meaning accurate quantification of these phenomena can demonstrate the validity of our analysis protocols.

MATERIALS AND METHODS

Viral Transduction of ROS reporters

Mitochondrially-targeted Orp-1 roGFP (Morgan et al., 2011) was adenovirally transduced into primary BAT isolated from 12-16 week old C57BL/6J mice overnight at a MOI of 2000 particles per cell. This resulted in >90% transduction. After an overnight incubation at 37°C and 8% CO_2, the cells were given fresh media without viral particles and cultured for 72 hours prior to imaging.

Microscopy

Images of BAT were obtained on a Zeiss LSM 710 or LSM880 microscope equipped with a plan-apochromat 100X (NA=1.4) oil immersion objective. Images

were taken with a digital zoom of 1 or above. Images were at least 1024 x 1024 px.

Validation of machine learning classifier

The WEKA segmentation classifier was validated for several cell types (hepatocytes and INS-1 data not shown, BAT included) against human recognition of objects. Briefly, a human created ROIs manually around each mitochondrion in a cell, usually more than 100 mitochondria per cell. These individual regions were quantified identically to the WEKA-generated or threshold-generated ROIs of the same cells. All three analyses performed by the same human and they manually thresholded at a level that facilitated object recognition, typically ~10% of the maximum fluorescence intensity.

All images were high resolution images of single cells cropped from a larger field of view. This cell-level analysis facilitates granular analysis of the data and examination thereof on a cell by cell basis.

Training images used for WEKA training set

Images used for training of the classifier were high resolution and super resolution micrographs at resolutions above 512 x 512 px. Training was performed on manually cropped individual cells from different fields of view, more than 4 independent experiments, and on 2 different fluorescence markers of mitochondria: mitotracker green and TMRE. This broad training set increased

accuracy and flexibility of segmentation. Input images for segmentation should be of as high resolution as possible, but maximum pixel size utilized for analysis was 0.07 μm per px. Some enhancements can improve poor quality images for analysis, such as a previously published filtering method utilizing a median filter (Smith, Kovats, Lee, & Cano, 2006) or utilizing built in background subtraction in ImageJ, such as the rolling ball algorithm. Figures 3.4 and 4.4 illustrate lower-quality, lower-resolution (0.165 μm per px) images that are still accurately segmented by the classifier.

RESULTS

Mitochondrial morphological parameters describe mitochondrial networking

Image analysis frequently measures fluorescence intensity, both for quantification and sorting of cells. Additional commonly-measured parameters include area and perimeter of the region of interest (ROI). As previously established (Joshi et al., 2000; Koopman et al., 2006; Leonard et al., 2015; Molina et al., 2009; Nguyen, Beyersdorf, Riethoven, & Pannier, 2016; Twig et al., 2006; Wikstrom et al., 2007), mitochondrial morphology can be described by various shape descriptors (Table 1.4). Chief among these shape descriptors is the circularity measurement (Circ), which compares the perimeter of the region of interest to the perimeter of a perfect circle of the same area. This measurement is primarily used to describe branching of the network, because it equals 1 when measuring a perfect circle, and much less than 1 for a starfish shape. Form factor

(FF) is another frequently used shape descriptor, and is simply the inverse of circularity, meaning a starfish shape has a FF much greater than 1, while a perfect circle still has a FF of 1. Another frequent shape descriptor used for analysis of mitochondrial morphology is the aspect ratio (AR). AR measures the ratio of the long axis length of the ROI to the short axis length, and is a measure of elongation of the object. Solidity measures the concavity of the ROI, which can also be interpreted as branching or connectivity. Utilizing these parameters, mitochondria may be described in morphological as well as fluorescent detail.

Segmentation of cytosolic mitochondria versus peridroplet mitochondria reveals significant differences in H_2O_2 production

Brown adipose tissue (BAT) is specialized to utilize energy to produce heat upon activation by norepinephrine (Wikstrom et al., 2014). This specialization depends heavily on mitochondrial dynamics. Cell biologists have hypothesized (Wikstrom et al., 2007) that mitochondria may specialize into different populations within a cell, but evidence for this hypothesis is rare due to the difficulty of segmentation for analysis. A previous publication has supported this hypothesis in muscle, (Glancy et al., 2015) but other cell types remain to be analyzed in such a way. For instance, a question of interest is: How different are peridroplet mitochondria from their cytosolic counterparts? The analysis of these images proved to be challenging – how does one segment mitochondria in the cytosol apart from mitochondria immediately surrounding lipid droplets? By selectively

labeling lipid, we can visualize the droplets in order to segment the mitochondria around them. While this approach is somewhat limited in its morphological analysis, an additional level of subsegmentation could be added in order to separate each mitochondrion from its neighbors and measure each one's morphology in addition to measuring the average fluorescence intensity of the whole population. Here, we demonstrate a novel segmentation method for BAT mitochondria using a lipid label as the seed for the analysis.

The original image contains 4 channels, not all of which are useful to the analysis: Nile red (lipid), ORP1-roGFP (redox status, 2 channels), and bright field (BF). The BF channel is immediately discarded upon beginning analysis; it is a quality control channel included for manual review. The roGFP probe is a redox sensitive GFP fused to ORP1, which is itself a H_2O_2-specific antioxidant enzyme from yeast, making this probe a tool to measure H_2O_2 production in the mitochondrial matrix (Morgan et al., 2011). Nile Red is a lipophilic dye that marks lipid compartments selectively; it is used to locate and segment lipid droplets within BAT cells.

In order to evaluate cytosolic versus peridroplet mitochondria, the first step is to segment the lipid regions, which is accomplished with a basic automated thresholding step (Otsu method). This binarized image is then used for several other operations within the analysis. First, it is used to subtract the small amount of fluorescence bleed-through from Nile red into the reduced roGFP channel.

Second, it is used as the seed for peridroplet-mitochondria recognition. This segmentation is accomplished by dilation of the lipid region *n* times, where *n* is user-defined at the outset of analysis. This step is user-defined because of several considerations, primarily due to artifacts resulting from diverse input images. Because images may be taken at different magnifications and metadata is not always present to convert pixel units to SI units, allowing the user to define the peridroplet region in pixel units removes potential bias and bugs from the analysis itself while providing extensive customization for various inputs. After dilation and automated segmentation, the region immediately surrounding the lipid droplet is measured.

After the peridroplet region is measured, the dilated lipid image is used to subtract all peridroplet fluorescence from the cytosolic image, leaving only objects not analyzed in the previous step. This cytosolic image is then automatically thresholded using the MinError method in FIJI, then segmented using the “analyze particles” tool. This segmented image is then measured for the cytosolic data. Once these measurements are saved as a .csv file, they can be handled like other data arrays in various programs.

When segmented to recognize separate subcellular populations of mitochondria, we found that cytosolic mitochondria produce significantly more H_2O_2 than peridroplet mitochondria (Fig 2.4). The addition of menadione, a mitochondrial toxicant that induces ROS formation via redox cycling (Criddle et al.,

2006) was used as a positive control and elicited a significant increase in H_2O_2 production in treated cells.

Trainable WEKA segmentation is significantly more effective at mitochondrial segmentation compared to conventional thresholding methods

Trainable WEKA segmentation is a plugin for FIJI that enables machine-learning based image segmentation. Previously, work has focused on classifying and counting mitochondria using machine learning (Leonard et al., 2015), but this approach outputs much less useful data than possible. Frequently, these approaches only provide counts of objects contained in each class. With these known limitations, we set out to 1) improve mitochondrial segmentation for analysis and 2) utilize machine learning in a novel way to that end.

Machine learning is a complex field with many different algorithms available, each with tradeoffs between speed, accuracy, processor utilization, and other system requirements. The FastRandomForest (Breiman, 2001) algorithm attempts to mitigate some of the system requirements and speed up computation, which is part of why it is commonly used in this context. To the user, the algorithm is mostly a backend affair, and once selected is not seen again during training. WEKA provides a graphical user interface (GUI) useful for training a classifier. Within this GUI, the user defines the number and names of each class to be trained (in this example, the two classes are “mitochondria” and “background”). After defining and naming classes, the user trains the classifier, which entails using any of FIJI’s

selection tools (line, rectangle, circle, etc.) to define regions of an image belonging to a certain class. In Figure 3.4, this iterative process is demonstrated while training the classifier to distinguish mitochondrial signal from background noise. Panel F represents the final classification of the image, showing mitochondria in red and background in green. The final set of instructions for segmentation are stored in a file called a classifier with extension ".model" This published classifier is the product of over 100 training images containing tens to hundreds of discrete data points and used for subsequent analysis of new image sets (Fig 4.4).

Because manual analysis of hundreds of images is time consuming, the WEKA classifier needed to be incorporated into a high-throughput analysis method. The analysis workflow into which it was incorporated is shown in Figure 4.4. WEKA segmentation provided a much cleaner, closer segmentation of the mitochondria than conventional filtering and thresholding methods. The output of the classifier is a probability map: an image where the pixel intensity value represents the computer's certainty from 0 to 1 that a specific pixel belongs to a certain class (in Figure 4.4, the "mitochondria" class is shown). This probability map can be manually or automatically thresholded for certainty level, but adding a manual step at this point ensures data quality with a human checkpoint evaluating the classifier output.

When INS-1 cells were segmented with WEKA segmentation, the number of detected mitochondria increases twofold (Figure 5.4A). This increase is

attributable to the more accurate detection of background between proximal mitochondria compared to conventional thresholding, resulting in fewer mitochondria being combined when in fact they are discreet objects. As a result of the increased separation of mitochondria, mitochondrial perimeter is significantly decreased in WEKA-segmented measurements (Figure 5.4B). This decreased perimeter is the result of WEKA segmenting mitochondria while ignoring much of the airy fluorescent haze surrounding the mitochondria. As a consequence of this cleaner, closer segmentation, aspect ratio is increased (Figure 5.4C), circularity is decreased (Figure 5.4D), and solidity is decreased (Figure 5.4E). As an analogy, if outlining an object left a 1mm gap between the object and its outline, the object would be measured as being more round (circularity approaching 1, aspect ratio approaching 1, and solidity approaching 1). However, if the outline is more accurate and leaves only a 0.1mm gap between the object and the outline, the outline's shape will more closely match the shape of the object, and its measurements would diverge from 1 because the object would be measured as less round. This increased accuracy of segmentation is illustrated in Figure 4.4 by comparing the traditionally thresholded image to the WEKA-segmented image.

Detection of NE-induced mitochondrial fragmentation in BAT validated WEKA segmentation

BAT mitochondria fragment upon stimulation with NE (Wikstrom et al., 2014). Due to the obvious phenotype, this model was used to validate WEKA segmentation. WEKA segmentation was compared to the traditional thresholding

approach and to manual human segmentation of mitochondria by ROI drawing. While manual analysis exhibited the largest dynamic range and provided the most robust results (Fig 6.4), which is to be expected, traditional thresholding provided the least robust results – it is hampered by the background-increasing airy haze surrounding objects inherent to confocal microscopy. WEKA segmentation yielded significant decreases in mitochondrial connectivity (Circ and solidity), while also demonstrating a decreasing trend in AR upon fragmentation. This trend in AR is mitigated by an artifact inherent to the WEKA classifier included herein. Due to the inherent difficulty in mitochondrial segmentation, it splits larger objects into smaller ones, such as the very elongated filamentous mitochondria in nonstimulated BAT. However, this aggressive splitting is necessary to retain mitochondrial recognition, as evidenced by WEKA segmentation's trend to detect more mitochondrial objects. While it may be possible to reduce the impact of this artifact by utilizing a BAT image training set rather than a mixed image training set, it would also decrease the flexibility of the classifier. Alternatively, due to the higher throughput of analysis enabled by the WEKA classifier and macro, larger sample sizes would also offset this artifact.

DISCUSSION

Due to the increasing size (terabytes), quantity, and quality of data produced by digital microscopy in science, rapid, repeatable, and novel methods for processing these data are required. Given the difficulty of accurate image segmentation in service of unbiased measurements, we have created a novel

segmentation method to observe subpopulations of mitochondria within cells. Segmentation of images in creative ways provides additional granular approaches and resolution in existing and newly and formerly acquired images, providing additional ways to extract as much data as possible from micrographs. This peridroplet analysis methodology may be expanded by others to address similar hypotheses: for instance, are lysosomes near the nucleus distinct from those at the cell periphery? By adapting the above approach to dilate the nuclear region instead of a lipid region, such an investigation is possible. Such investigations are rare (Leonard et al., 2015), partly because light microscopes only recently achieved sufficient resolution to facilitate this type of analysis (Weisshart, 2014). While the biological implications of this ROS formation we discovered remains to be elucidated, a recent publication suggests that cytosolic mitochondria are more oxidative, while the peridroplet mitochondria are essential for lipid droplet formation (Benador et al., 2018). The increased ROS formation observed here suggests that the enhanced oxidative capacity comes at the cost of potential oxidative damage. Additionally, a novel machine learning segmentation method for mitochondria more accurately segments mitochondria than traditional methods. By combining this segmentation protocol with a high-throughput approach to image analysis, we have designed a workflow that expedites an unbiased analysis of mitochondrial parameters. These tools will not only enable more time-and cost- effective research, but also provide a platform from which other scientists may improve and build better analysis protocols.

Subcellular objects pose a unique challenge in advanced light microscopy, partly due to the refraction limit of light microscopes (Abbe, 1873). Some tools, including the Airyscan detector from Zeiss (Weisshart, 2014), provide novel ways to approach super resolution light microscopy and further enhance the quality of micrographs. With these improvements in imaging technology, image analysis is becoming more approachable and more necessary. While the above WEKA method largely utilized super resolution micrographs, the recognition of subpopulations of mitochondria was performed on images acquired without super resolution techniques. In fact, the WEKA classifier is sufficiently accurate to segment mitochondria from non-super resolution micrographs, as demonstrated in Fig. 4.4. Indeed, the images analyzed in Fig. 6.4 were not super-resolution images; WEKA segmentation accurately detected mitochondrial fragmentation from these images. However, no analysis is perfect, and the quality of input images can seriously hamper analysis. Other common issues and their simple solutions have been published recently by another group (Harwig et al., 2018). This provides a new tool to analyze and accurately quantify mitochondrial parameters from images of insufficient resolution to apply conventional thresholding techniques, again as illustrated in Fig. 4.4. This increased flexibility and accuracy will provide more robust analyses within the field going forward.

Parameter	Information	Units	Notes
Fluorescence Intensity (FI)	Brightness of fluorophore	A.U.	Can be sum or average of all intensity for entire region. Ratios of multiple fluorophores are possible
Area (A)	Cross-sectional area of region	Pixels (px), μm^2	
Perimeter (P)	Distance around region	Pixels (px), μm	
Circularity (Circ)	Branching $\frac{4\pi(Area)}{(Perimeter)2}$	A.U.	$0 < Circ \leq 1$; Circ is 1 for a perfect circle; less than 1 for branched structures Circ = FF^{-1}
Form Factor (FF)	Branching $\frac{(Perimeter)2}{4\pi(Area)}$	A.U.	$1 \leq FF < \infty$; FF is 1 for a perfect circle; more than 1 for branched structures FF = $Circ^{-1}$
Aspect Ratio (AR)	Elongation $\frac{Long\ Axis}{Short\ Axis}$	A.U.	AR measures elongation, not branching
Solidity	Concavity $\frac{Object\ Area}{Convex\ Hull\ Area}$	A.U.	Creates a fully convex shape (hull) surrounding the object and measures the ratio of the object area to the convex hull area

Table 1.4. Common mitochondrial morphology parameters.

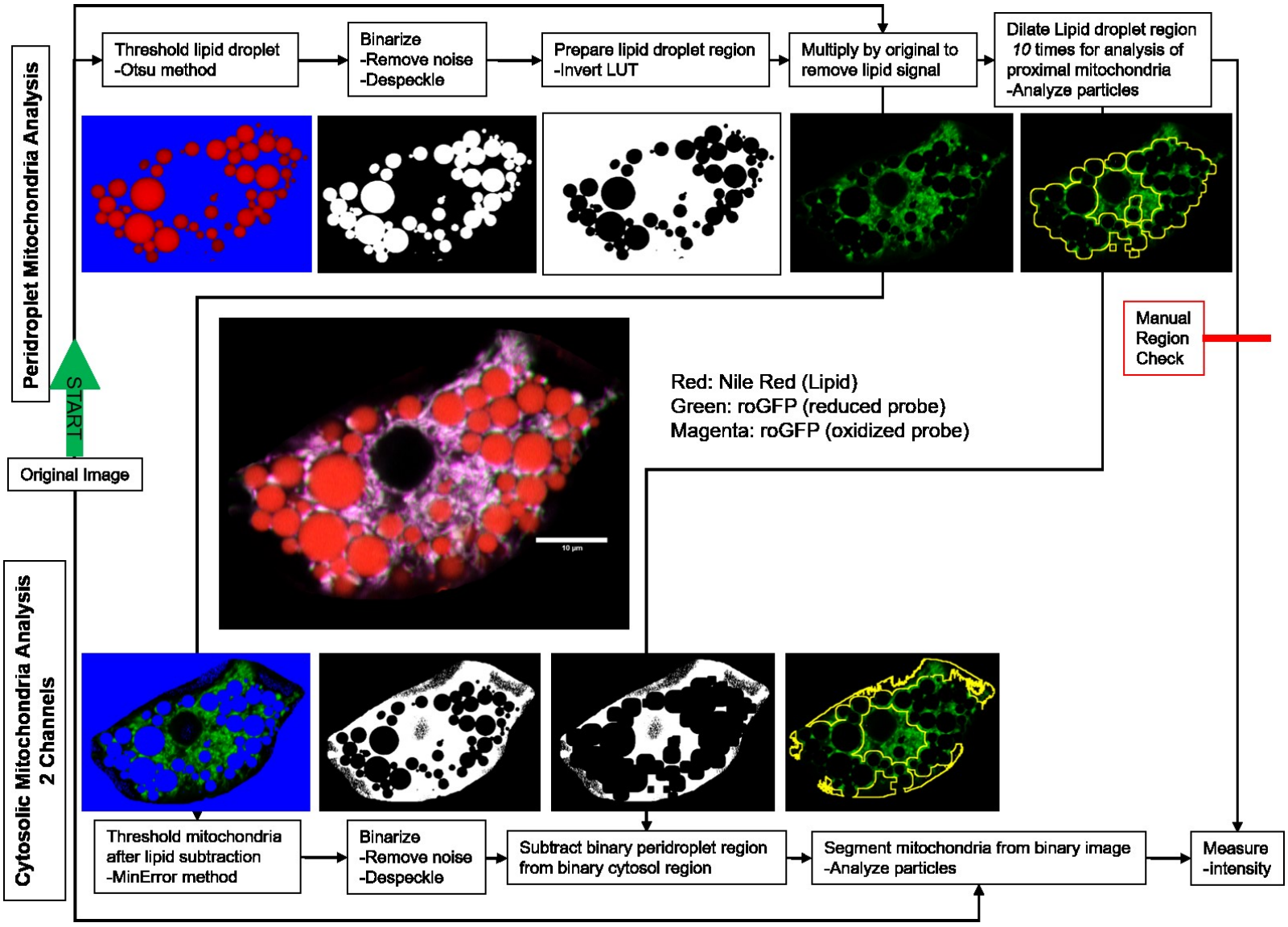
Peridroplet Mitochondria Analysis
Threshold lipid droplet
-Otsu method
Binarize
-Remove noise
-Despeckle
Prepare lipid droplet region
-Invert LUT
Multiply by original to
remove lipid signal
Dilate Lipid droplet region
10 times for analysis of
proximal mitochondria
-Analyze particles
Manual
Region
Check
START
Original Image
Red: Nile Red (Lipid)
Green: roGFP (reduced probe)
Magenta: roGFP (oxidized probe)
Cytosolic Mitochondria Analysis
2 Channels
Threshold mitochondria
after lipid subtraction
-MinError method
Binarize
-Remove noise
-Despeckle
Subtract binary peridroplet region
from binary cytosol region
Segment mitochondria from binary image
-Analyze particles
Measure
-intensity

Figure 1.4. Schematic representation of quantification of peridroplet and cytosolic mitochondria in Brown Adipose Tissue.

The original mutli-channel image is split into its component channels, which are then filtered for analysis. The lipid droplet is labeled with Nile Red dye, and this image region is used for recognition and segmentation throughout the analysis. The Nile red image is binarized and used multiple times in the analysis. First, it is used to subtract fluorescence bleed-through in the roGFP channel from the Nile Red. Then, the lipid droplet region is dilated *n* times, with *n* being empirically determined by the user to encompass peridroplet mitochondria. This dilated lipid region is then used to quantify the mitochondrial signal contained within. The cytosolic analysis builds on the previous steps, utilizing the dilated lipid region to remove any mitochondrial fluorescence in that region from the cytosolic image. The cytosolic image is then binarized, segmented, and measured similarly to the peridroplet image. Scale bar shown in original image is 10μm and is intentionally left out during analysis. Manual steps are outlined in red.

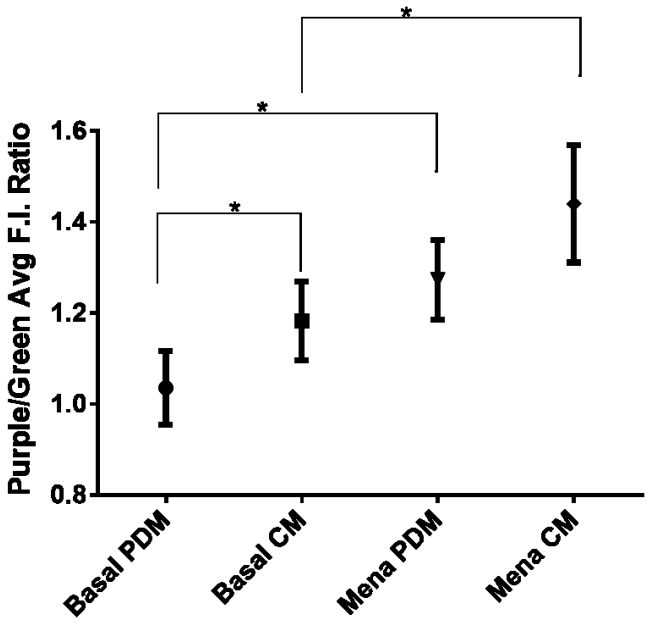

Figure 2.4. BAT mitochondria produce different amounts of H_2O_2 depending on their localization in relation to lipid droplets.

BAT cytosolic mitochondria (CM) produce significantly more H_2O_2 than their peridroplet (PDM) counterparts. Addition of menadione increased ROS production significantly in both mitochondrial populations.

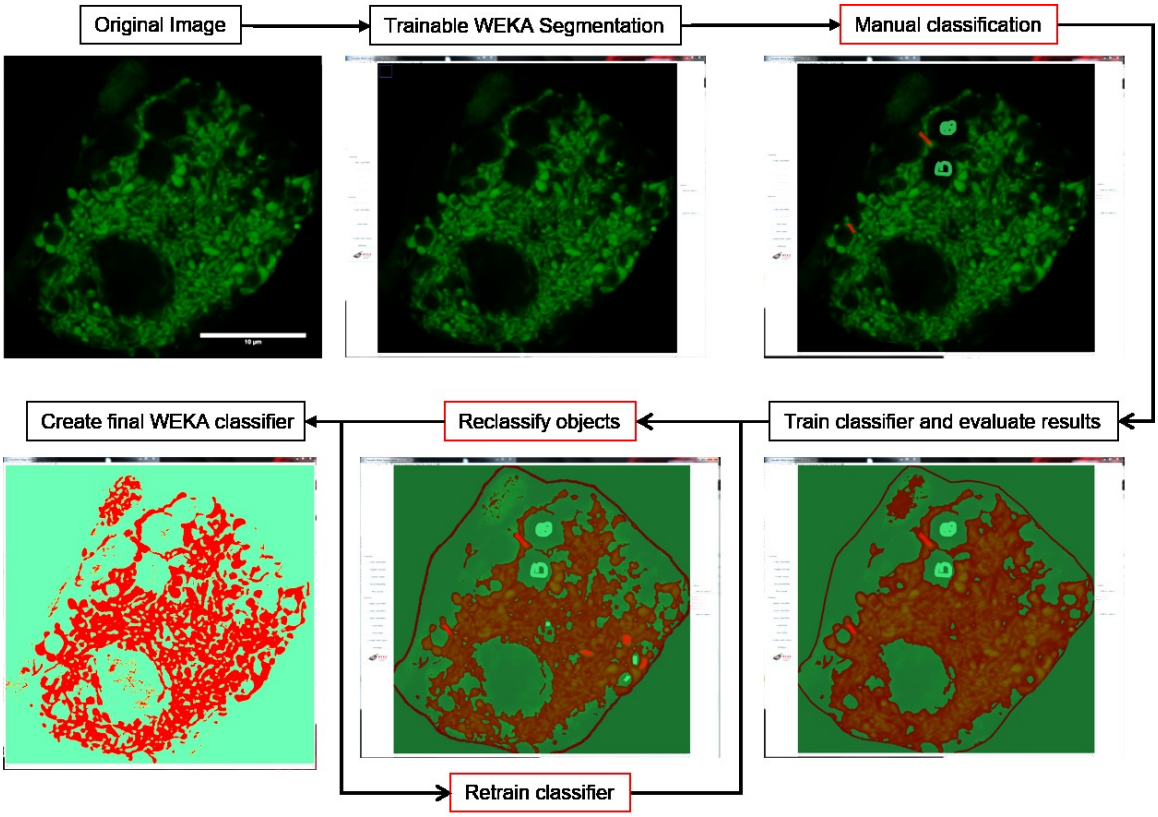

Figure 3.4. Representation of iterative training of the machine learning classifier using the WEKA trainable segmentation plugin for FIJI.

Once an image is opened in FIJI, WEKA trainable segmentation can be called from the plugins menu. WEKA is capable of using several machine learning algorithms, with the most fitting being FastRandomForest considering time and processor utilization. Options set within the WEKA GUI can control the parameters used for machine learning, though several of these require additional plugins. Once open, the user defines the number and name of each class of object. Once the classes are defined, the user can use any selection tool available in FIJI (line, rectangle, circle, etc.) to define what image objects belong to which class. Upon clicking “train

classifier," the computer then calculates the best segmentation algorithm and returns a map of the classes overlaid over the training image which can be used to refine the class segmentation with subsequent rounds of assignment and training. Once WEKA returns a satisfactory segmentation of the image, the user can finalize the classifier to be used on new data sets. Scale bar shown in original image is 10μm and is intentionally left out during analysis. Manual steps are outlined in red.

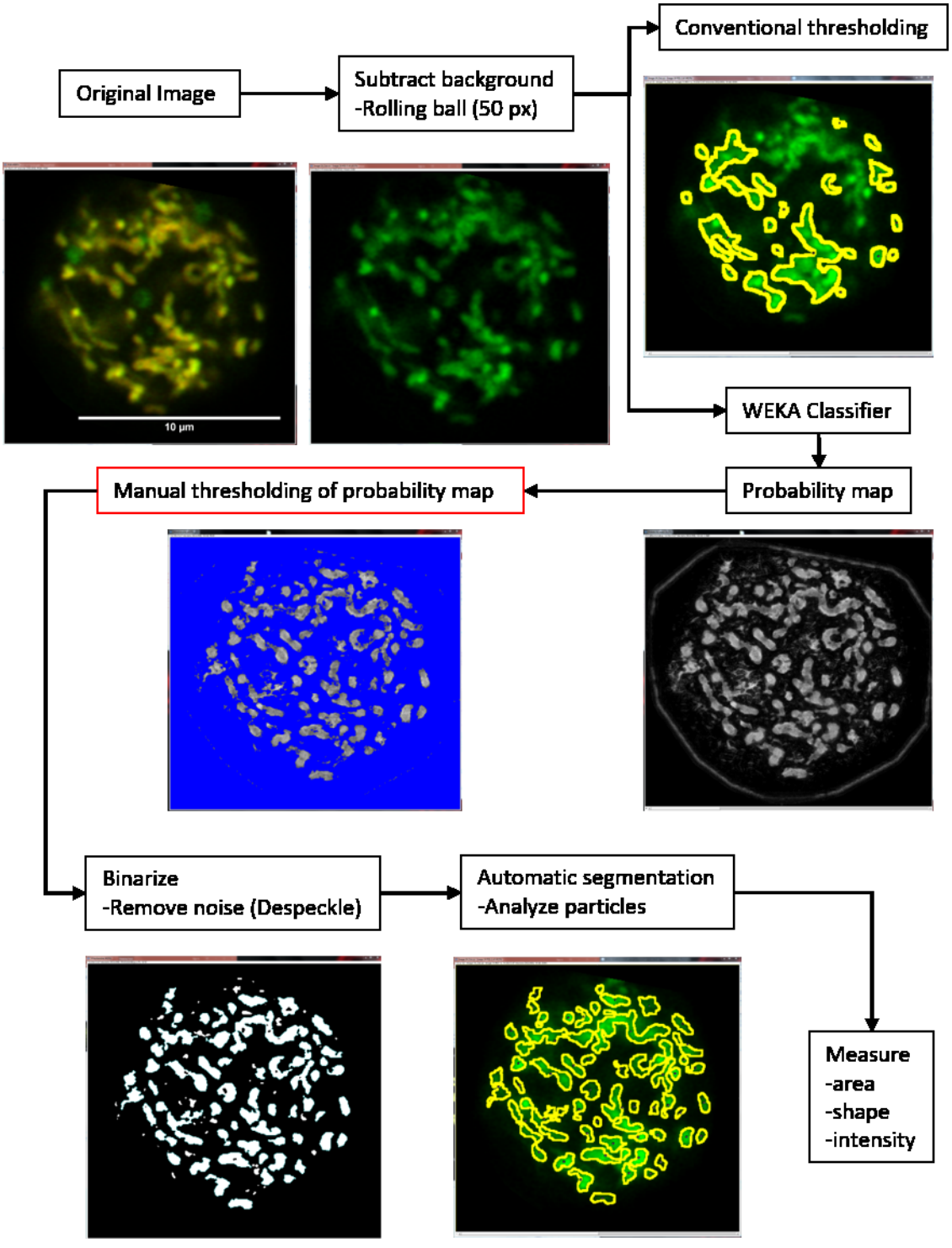
Original Image
Subtract background
-Rolling ball (50 px)
Conventional thresholding
10 µm
WEKA Classifier
Probability map
Manual thresholding of probability map
Binarize
-Remove noise (Despeckle)
Automatic segmentation
-Analyze particles
Measure
-area
-shape
-intensity

Figure 4.4. Workflow for a WEKA-based mitochondrial segmentation and analysis.

The original image is initially filtered to remove uneven background using the rolling ball algorithm with a diameter of 50 pixels. This facilitates better recognition of mitochondria by the WEKA classifier. Shown at this branch point for comparison is traditional threshold-based segmentation of mitochondria in the same image. Once the image is classified with the WEKA classifier, it returns a probability map. A probability map is the algorithm's best guess at which class each pixel in an image belongs to, in this case mitochondria or background, with a probability from 0 to 1. The user manually thresholds the certainty of the classification for best mitochondrial segmentation (though this step may be automated with validation). After the thresholding step, the image is binarized, the mitochondrial objects segmented for measurement, and then measured. Scale bar shown in original image is 10μm and is intentionally left out during analysis. Manual steps are outlined in red.

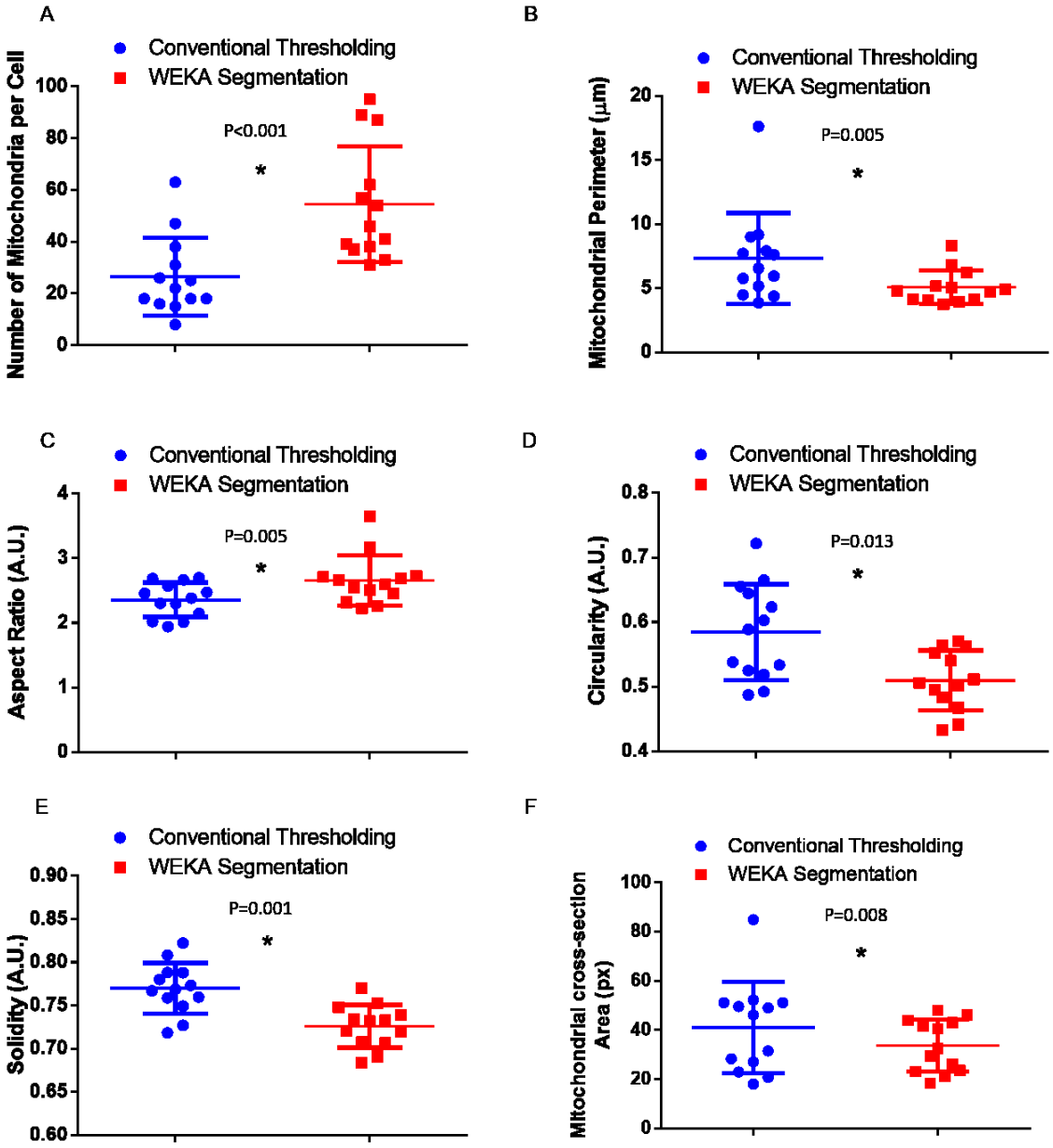

Figure 5.4. Comparison of mitochondrial morphological measurements segmented with WEKA segmentation versus traditional thresholding.

WEKA segmentation is significantly better at recognizing, separating, and quantifying individual mitochondria (A). Because of this more accurate segmentation, the mitochondrion is measured much more closely to its actual boundaries instead of the airy haze surrounding it. As a result, the Perimeter readout is significantly reduced (B). This more accurate segmentation provides more accurate measurements of Aspect Ratio (C), Circularity (D), and Solidity (E), and cross-sectional area (F). Better object recognition leads to improved dynamic range of measurements. Each point represents an individual image, error bars SEM. * $p \leq 0.05$ by t-test.

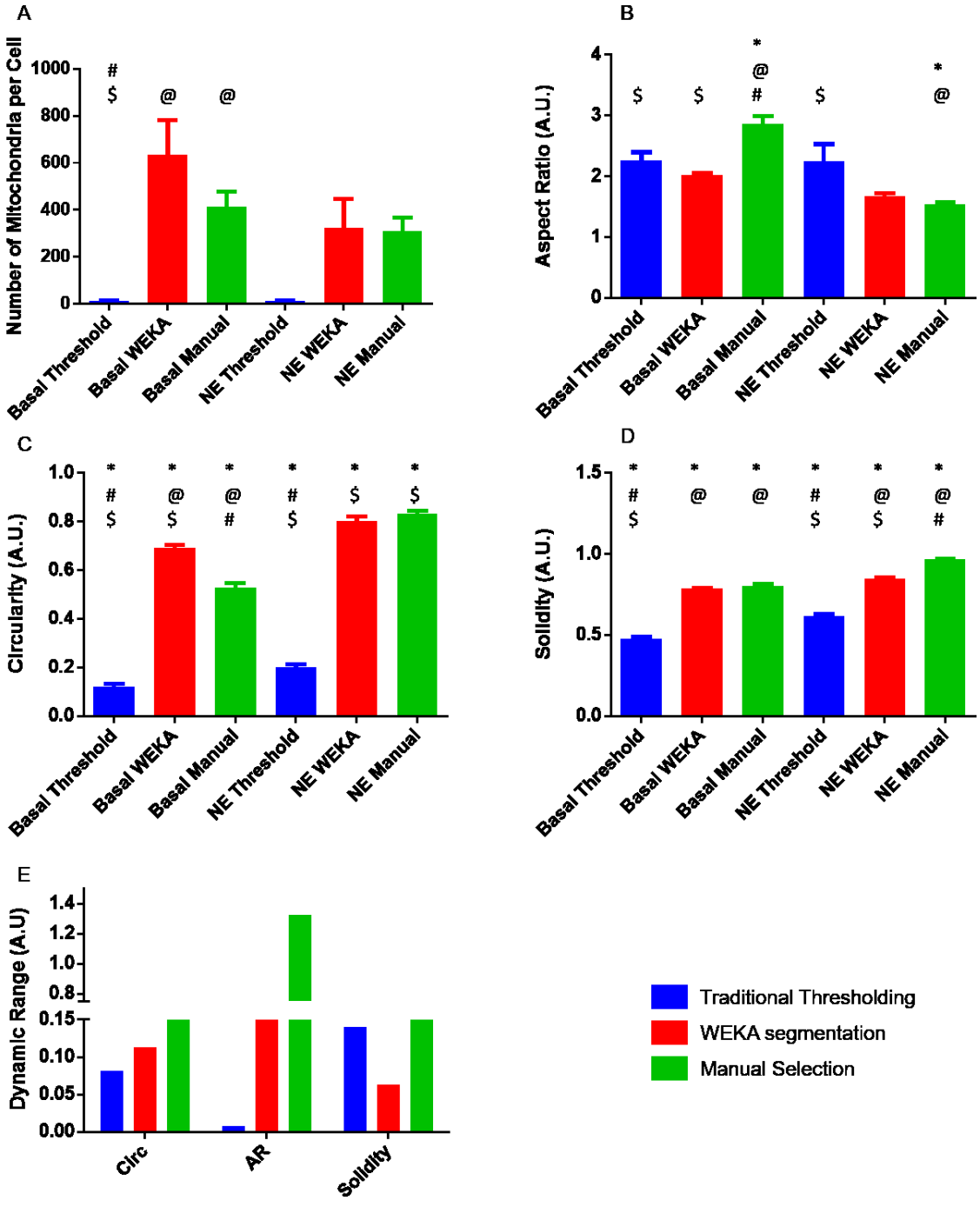

Fig 6.4. WEKA segmentation detects mitochondrial fragmentation in NE-activated BAT

A clear trend was exhibited by traditional thresholding to detect fewer mitochondrial objects per cell due to background fluorescence and airy haze surrounding mitochondrial objects in the images (A). WEKA segmentation detected significantly more mitochondrial objects than traditional thresholding but was not significantly different from manual ROI creation. The WEKA classifier more aggressively splits long filaments than a human analyst, leading to a trend of increased mitochondrial objects in the basal (nonstimulated) condition compared to manual analysis (A). This largely unavoidable bias is also evidenced by the significant decrease of AR with WEKA segmentation when compared to manual analysis (B). This artifact inherent to the algorithm necessitates a larger sample size for observed trends to be significant. However, Circ (C) and Solidity (D) exhibit significant increases with NE-activation of brown fat, suggesting reduced mitochondrial connectivity upon activation and validating the WEKA-based segmentation approach. WEKA segmentation increases dynamic range of measurements in both circularity and AR, error not shown because dynamic range was calculated from the averages shown in panels (A)-(D). (E) Each bar is the mean of >10 cells per condition from 3 separate experiments with error bars representing SEM; $p \leq 0.05$ by one-way ANOVA: (*) significant difference between basal vs NE conditions of same analysis method; (@) significant difference vs threshold analysis of same condition; (#) significant difference vs WEKA analysis of same condition; ($) significant difference vs manual analysis of same condition.

CHAPTER FIVE: General Discussion

Hyperinsulinemia as an initiating factor in T2D

Type 2 diabetes is a chronic disease affecting an increasing number of people worldwide. Its financial burden on society and its patients will increase accordingly. Genome wide associated studies have implicated β-cell dysfunction in the development of diabetes. Indeed, the vast majority of genes associated with diabetes are related to β-cells and insulin secretion (Lim et al., 2011). Historically, T2D has been considered a disease of insulin resistance which is ill-compensated for and results in eventual β-cell death. However, mounting evidence suggests that hyperinsulinemia can precede insulin resistance. Resolution of hyperinsulinemia is rapid following gastric bypass surgery, and this procedure remains the only curative treatment for T2D (Lim et al., 2011; Reed et al., 2011). Because of the inherently related nature of these phenomena and their downstream effects, their exact contribution to disease progression is difficult to decipher. Islets typically secrete insulin in a pulsatile manner (Cunningham et al., 1996; Porksen et al., 2002), which mirrors Ca^{2+} oscillations (Deeney et al., 2001), which in turn mirror metabolic oscillations in glycolysis (Tornheim, 1997), all with periods of 5-10 minutes. One of the earliest hallmarks of disease is loss of the oscillatory behavior of insulin secretion. Hyperinsulinemia, loss of phase II oscillations, and increased insulin secretion in response to fatty acids are thought to contribute to the development of T2D, but the relationship between mitochondrial morphology and these phenotypes remains to be elucidated.

Investigation of non-glucose-stimulated insulin secretion revealed novel roles for mitochondrial morphology in FFA metabolism

Within this thesis, I have demonstrated that Mfn2 regulates insulin secretion in islets, particularly at substimulatory glucose concentrations and in response to FFA (Chapter 2). Other work has suggested obesity leads to increased sensitivity to FFA-induced insulin secretion, which has profound implications for the study of diabetes development (C J Nolan et al., 2006). The increased sensitivity to fatty acid induced insulin secretion could be a key progression toward T2D, because hyperlipidemia is often associated with obesity in humans. We investigated several possible mechanisms for the increased sensitivity to FFA, in addition to expanding our work to established cell lines and exhaustively investigating their suitability as a model for the reduction of Mfn2 in primary β-cells (Chapter 3). Finally, we provide novel methods to quantify high-resolution micrographs and the structure of subcellular structures in brown adipocytes (Chapter 4). Future directions include pursuit of the mechanism by which mitochondrial fragmentation induces increased nonstimulated insulin secretion and FFA-induced insulin secretion. Additionally, investigation of the lack of effects in a knockdown model of Mfn2 in INS-1 cells and significant impairment with knockout of Mfn2 in primary tissue may yield new regulatory mechanisms of metabolism and mitochondrial morphology, as well as offer a way to tease apart the role of Mfn2 in each phenomenon. Revealing the Mfn2-specific roles of fragmentation versus its metabolic regulation is a burning question in the field: does morphology govern fuel preference, or vice versa? Is

morphology a readout of the metabolic effects of Mfn2 downregulation? Future experiments should utilize recent tool peptides developed by other labs to dissect the contribution of each Mfn2 activity to the phenotype (Franco et al., 2016). These peptides are capable of manipulating mitochondrial morphology independent of other regulatory effects of Mfn2, providing an ideal manipulation to investigate the interplay of morphology and metabolic regulation.

By utilizing existing tools such as FIJI and trainable WEKA segmentation, we created a method to segment BAT that provides a previously unstudied granularity to mitochondrial measurements, which may help answer these questions, particularly in light of the recent work demonstrating ATP synthesis and respiromentric differences between these same subsets of mitochondria (Benador et al., 2018). Finally, building on the existing machine-learning classifier and applying it to additional subcellular structures will potentially provide rapid and robust image segmentation and quantification. Indeed, combining the peridroplet versus cytosolic mitochondria segmentation method with the machine learning segmentation of mitochondria could provide the most accurate, granular approach to mitochondrial quantification yet.

In chapter 2, we show that mitochondrial fragmentation is induced by excess nutrients through downregulation of Mfn2, building on previous work from our lab and others showing mitochondrial fragmentation in response to excess nutrient challenge (Molina et al., 2009). Other labs have shown a decrease in Mfn2 expression in models of obesity in muscle and adipose (Bach et al., 2003; Le Blanc

et al., 2012; Pich et al., 2005; Sorianello et al., 2012). In an effort to dissect the role of mitochondrial morphology in the obese condition, we forced the fragmentation of mitochondria by knocking out Mfn2 in primary pancreatic β-cells via the loxp-Cre system. Genetic ablation of Mfn2 in mice resulted in increased basal insulin secretion without change in insulin content. This increased insulin secretion is in part due to an increase in FFA-induced insulin secretion, mirroring previous results from other labs studying Zucker fatty rats (C J Nolan et al., 2006). At the same time, Knockout of Mfn2 resulted in increased oxygen consumption in response to FFA in the media. Taken together, the forced fragmentation of mitochondria elicited a shift at basal glucose concentrations to FFA for oxidation and insulin secretion. Not only did Mfn2-KD cells exhibit greater uptake of FFA, but they also oxidized more palmitate when provided palmitate as the primary fuel. Consistent with this observation, loss of Mfn2 resulted in increased FFA oxidation and uptake in INS-1 cells with Mfn2KD. This phenotype suggests an important role for FFA metabolism in β-cells and insulin secretion.

Mechanistic explorations of β-Mfn2KO phenotype point to fatty acids as playing a pivotal role

In an effort to determine the mechanism for insulin secretion induction by this fuel switch, we investigated several regulators of insulin secretion. We initially investigated the role of intracellular Ca^{2+} using the Fura-2 ratiometric probe because it plays an important role in triggering of insulin secretion by inducing exocytosis of insulin granules. We found that intracellular calcium was unchanged

at basal glucose in Mfn2KO islets and sought another possible explanation. ROS, specifically H_2O_2, has been demonstrated to be an insulin secretagogue (Saadeh et al., 2012), as well as the ratio of the endogenous antioxidant glutathione playing a role in insulin secretion (Ferdaoussi et al., 2015). However, H_2O_2 production was not altered by the loss of Mfn2. Other regulators of FFA metabolism remain to be investigated, such as CPT-1, the primary control point of FFA oxidation in the mitochondria.

Other processes also affect FFA-induced insulin secretion. For instance, the Prentki group has suggested a role for a futile cycle of lipolysis and reesterification which modulates intracellular concentrations of the intermediates of fatty acid metabolism, such as MAG, DAG, and LC-CoA, which have been shown to modulate insulin secretion *in vitro* (Kwan et al., 2006; Roduit et al., 2004; Saadeh et al., 2012). These intermediates can act intracellularly in the case of DAG on SNARE-mediated exocytosis of insulin granules (Kwan et al., 2006; Marc Prentki et al., 2013), or extracellularly at membrane FFA receptors, particularly GPR40, which has been implicated in insulin secretion (El-Azzouny et al., 2014; Latour et al., 2007). Taken together, the link between fatty acid metabolism and insulin secretion may play a pivotal role in the physiology of T2D, because obese subjects often have significantly elevated circulating triglyceride (Seigneur et al., 1994). However, deletion of Mfn2 in BAT increased mitochondrial FAO coupled to ATP production (Mahdaviani et al., 2017), the production of which in β-cells could also trigger the GSIS pathway via an increase in ATP/ADP ratio. While acute

exposure to FFA potentiates insulin secretion (Branstrom et al., 1997; El-Azzouny et al., 2014; Y.-P. Zhou & Grill, 1995; Y. Zhou & Grill, 1994), chronic exposure to FFA blunts GSIS (Carlsson et al., 1999), and chronic nutrient excess leads to accumulation of intracellular lipid that causes β-cells to secrete insulin at lower levels of glucose (Erion et al., 2015).

The characteristic position of the β-cell as a fuel signal integrator provides promise for novel drug targets. Inhibitors of lipolysis such as orlistat have demonstrated a role for this process in insulin secretion (Attané et al., 2016; Peyot et al., 2004; Zhao et al., 2014). FAO, likewise, is necessary for GSIS and can be inhibited via etomoxir (Rubí et al., 2002; Sako & Grill, 1990). New therapeutics such as small peptide inhibitors of the Drp1-Fis1 mitochondrial fission inducing interaction may be promising as inhibitors of mitochondrial fragmentation in pathological conditions, halting morphological changes prior to appearance of deleterious downstream effects. (Kim et al., 2015; Qi, Qvit, Su, & Mochly-Rosen, 2013).

Metabolic implications of inhibition of mitochondrial fusion

Studying the pancreatic β-cell poses unique challenges due to the low yield from isolation of islets from pancreases, and as such is amenable to use of cell lines. In chapter 3, we knocked down Mfn2 in a commonly-used β-cell line, INS-1 cells and investigated the effects of this manipulation. This adenovirally-delivered shRNA reduced the expression of Mfn2 in INS-1 cells and contributed to an increase in FFA uptake. Additionally, the Mfn2-KD cells exhibited decreased

maximal respiratory capacity and other defects not seen in primary cell models included in chapter 2 but consistent with other publications also using adenovirally-delivered shRNA for Mfn2KD in HeLa cells (Ding et al., 2015), suggesting a possible inhibition of autophagy that increased the proportion of dysfunctional mitochondria. Autophagic defects in β-cells contribute to the development of diabetes in rodents (Quan et al., 2012). Our lab previously demonstrated that rescue of autophagic flux improved insulin secretion in excess nutrient environments (Trudeau et al., 2016). However, insulin secretion was unaffected by Mfn2KD in INS-1 cells, suggesting this inhibition of autophagy was either absent or had not manifest in the time scales investigated. Because the primary functional readout of β-cells is insulin secretion, the lack of defect in this model suggested that Mfn2KD in INS-1 cells does not recapitulate the phenotype of Mfn2KO primary islets, posing a significant challenge to using this model to study the mechanisms of fuel preference switch.

B-Mfn2KO vs Mfn2-KD models may expose regulatory differences or protein half life

The differences between the INS1-KD and the primary tissue KO systems can be due to several possible mechanisms. First, cell lines and primary cells are inherently different, with cell lines being immortalized. Regardless, INS-1 cells serve as a common model of β-cells, and findings therefrom have contributed immensely to the field (Brun, Assimacopoulos-Jeannet, Corkey, & Prentki, 1997; Cerqueira et al., 2016; Erion et al., 2015; Lablanche et al., 2011; Molina et al.,

2009; Rubí et al., 2002; Skelin et al., 2010; Twig et al., 2008). One possible explanation for the mild phenotype in INS-1 Mfn2-KD cells is the timing of knockdown and knockout (72 hours). While the half-life of Mfn2 is not known, perhaps the KD of Mfn2 was assayed too early in the defect (72 hours, peak expression of shRNA from adenovirus). Additionally, truncated Mfn2 lacking fusion activity is capable of stimulating ETC activity in muscle (Pich et al., 2005), suggesting that Mfn2 may have been present at a sufficient level to maintain metabolism even in the face of overt fragmentation shown in chapter 2. Perhaps the ~60% knockdown of Mfn2 was sufficient to induce fragmentation but not metabolic defects in INS-1 cells. This hypothesis can be addressed by generating an Mfn2-KO INS-1 cell line, which is an active area of development in our lab. Yet another explanation for the difference between these two systems could stem from the AAV vector used to deliver the shRNA. While both models utilized AAV vectors to deliver the manipulation of Mfn2, the different active titers of the vectors could contribute to additional stress in the INS-1 cells, which required almost twice as many viral particles per cell for efficient transduction of KD of Mfn2.

Novel segmentation protocol of mitochondria in BAT provides granular, rapid, and robust analysis

Because of modern high-throughput data acquisition tools, such as the Operetta High Content imager, and automation of low-throughput tools like the Zeiss LSM 880, the quantity and quality of imaging data available for analysis is steadily increasing. With this proverbial firehose of data comes the need to distill it

down into its meaningful components. Less modern programming and statistical tools such as R provide ways to handle and manipulate the data once quantified, but quantification of these images is the major bridge left to be constructed in the analysis workflow.

Image analysis is a complex and growing field, providing rich opportunities for new and exciting discoveries, even from data acquired years previously. The customizable and broad program ImageJ and its plugin-rich fork FIJI (Schindelin et al., 2012) provide the basis for transparent and repeatable image analysis, while specific plugins provide the same promise to more specialized analyses. By utilizing these plugins, we are able to construct a rapid, transparent, and repeatable segmentation of mitochondria from high quality micrographs, in addition to segmentation of subcellular regions necessary for quantifying differences within a cell, such as peridroplet vs. cytosolic mitochondria and their differing H_2O_2 production (Ch. 4). Novel segmentation of images provides an opportunity to extract additional data from existing images, and can even illuminate new biology, as in the case of peridroplet and cytosolic BAT mitochondria (Benador et al., 2018), complementing more traditional biochemical approaches and isolation techniques such as mitochondrial isolation, respirometry, and western blotting.

Many other labs have provided methods for measuring mitochondrial parameters, but some bin by morphological characteristics using machine learning instead of outright quantification (Leonard et al., 2015), and some utilize traditional

segmentation methods such as filtering and thresholding (Joshi et al., 2000; Molina et al., 2009; Wiemerslage & Lee, 2016). To our knowledge, no lab has utilized a machine-learning approach to segment mitochondria to subsequently quantify. Here, we provide a machine learning classifier capable of separating and segmenting mitochondria that previously were difficult or even impossible to segment with traditional methods due to image quality, contrast, and fluorescence intensity complications. By utilizing machine learning in this new way, we have demonstrated its current and future value, though it requires an analysis computer with significant processing power and RAM. However, the input images this segmentation protocol is capable of processing is more diverse than traditional methods and includes lower-resolution (i.e. 512 x 512) images, providing a flexible tool for mitochondrial scientists.

Broader implications of the thesis and future directions

Mitochondrial dynamics may play a role in T2D and hyperlipidemia

The elucidation of mitochondrial dynamics and the lifecycle of mitochondria has had profound impacts on the study of metabolism (Liesa & Shirihai, 2013). From Alzheimer's to cancer to T2D, mitochondria play an important role in deranged metabolism and dysfunction. Single mutated proteins are capable of causing disease, such as Optic Atrophy (Opa1) and Charcot-Marie Tooth Disease Type IIa (Mfn2). Recent developments in sample throughput have increased the amount of data collected per each experiment, and the tools to analyze this large amount of data are still nascent and are actively being developed. Dissecting the

role of specific mitochondrial dynamics events, such as fusion, fission, mitophagy, and biogenesis have provided novel insights into disease mechanisms (Boutant et al., 2017; Dagda et al., 2009; Frank, 2006; Hiller & Metallo, 2013; Mahdaviani et al., 2017; Nguyen et al., 2016; Qi et al., 2013; Rocha et al., 2017). With these insights has come identification of novel regulatory mechanisms, such as autophagy (Trudeau et al., 2016), fuel preference (Mahdaviani et al., 2017), and uncoupled respiration (Ježek et al., 2014). Adding to this body of work, I have shown that mitochondrial fragmentation itself is capable of increasing insulin secretion in response to FFA while disrupting the normal pattern of insulin secretion. Not only does the increased sensitivity to palmitate reinforce the importance of hyperlipidemia in the obese patient, but also provides a potential mechanism to target for treatment. These findings may have implications in other cells types, where the regulation of mitochondrial fusion has functional consequences (Boutant et al., 2017; Mahdaviani et al., 2017). Indeed, if mitochondrial fuel preference is controlled by morphology, morphology presents an entirely new therapeutic target for a host of diseases, such as ALS (Qi et al., 2013), obesity (Mahdaviani et al., 2017), and several neurological defects (H. Chen & Chan, 2005; H. Chen et al., 2007; Wiemerslage & Lee, 2016).

One appealing hypothesis for the switch in fuel preference centers on CPT-1 and its rate-limiting control of mitochondrial FA oxidation. CPT-1 is expressed in β-cells (Assimacopoulos-Jeannet et al., 1997) and controls the entry of fatty acids conjugated to carnitine into mitochondria, and as such is tightly regulated by its

endogenous inhibitor and product of glucose metabolism, Malonyl-CoA (McGarry, Mannaerts, & Foster, 1977; Newgard & McGarry, 1995). CPT-1 sensitivity to Mal-CoA is modulated by several factors, including membrane fluidity, and mitochondrial membrane fluidity is increased in the livers of high-fat diet fed Wistar rats (Aoun et al., 2012), a condition shown to decrease CPT-1 sensitivity to inhibition by Mal-CoA (Faye et al., 2005). Conceivably, this release of inhibition on CPT-1 would increase FA oxidation in the face of excess nutrients, which would be consistent with compensatory behavior to this environment attempting to detoxify the excess lipids. However, this compensation could become pathological if it induced increased insulin secretion at a non-stimulatory glucose concentration, contributing to hyperinsulinemia prior to insulin resistance. Because mitochondrial fragmentation is observed in high-fat diet fed animals, mitochondrial membrane fluidity presents an attractive target to study the control of fuel preference.

Further investigation of the role of mitochondrial morphology on β-cell function holds promise to understand the mechanism of development of T2D. While I have not discovered the mechanism of basal hypersecretion of insulin here, I have tested several viable hypotheses and can tentatively exclude H_2O_2 and Ca^{2+} from the pathway. Indeed, the evaluation of H_2O_2 production in Mfn2KO islets presents a stronger case than previous studies due to the reversible nature of the probe used and minimum and maximum normalization every experiment (Morgan et al., 2011). This approach provides clear benefits over commonly-used ROS probes such as DHE, which is both irreversible and prone to artifacts that hamper

interpretation of the data (Fink et al., 2004; Laurindo et al., 2008; Nazarewicz et al., 2013; Tollefson et al., 2003). DHE, however, can be further analyzed using HPLC to separate its oxidation products and decode what ROS oxidized the probe (Laurindo et al., 2008). However, these findings still point to a possible phenomenon wherein mitochondrial morphology governs fuel preference. Several lines of evidence support this hypothesis, including the different specializations between cytosolic and peridroplet mitochondria in BAT (Benador et al., 2018), the increased FFA utilization in β-cells (Ch. 2), and the changes in mitochondrial morphology during overfeeding and starvation (Liesa & Shirihai, 2013). This may represent a basic eukaryotic regulatory system – one which remains to be fully investigated and manipulated. Even in cells lacking a functional outcome from forced mitochondrial fragmentation, fuel preference and FFA uptake is altered (Ch. 3). In hepatocytes, mitochondrial morphology is governed by fuel environment as well, which can be counteracted by upregulation of Mfn2 (Zhang, Jiang, Hu, Zheng, & Xiang, 2011).

New analysis methods provide data to complement other biochemical methods

Measurement of mitochondrial parameters presents unique challenges related to their size and physiological environment. Isolated mitochondria must be maintained in the proper osmotic environment and with appropriate nutrients generally found in the cytoplasm. Even then, mitochondria lose their distinct morphological characteristics when removed from the cytoplasm and cytoskeleton. Measuring mitochondria in intact cells poses challenges – primarily related to size

and nutrient availability. Not only do mitochondria require a high-resolution high-magnification microscope to visualize, but they also must be separated from one another in order to measure. Within a cell body, this is no small task. Expressly because of these challenges, I have provided novel analysis methods to extract data from high-resolution micrographs. Protocols like the novel segmentation described herein provide powerful and flexible tools to speed and assist the mitochondrial scientist with these issues. The approaches described herein are complementary and can be combined to provide extremely granular data describing mitochondria within living cells.

Not only do analysis protocols like those contained herein provide rapid and robust analysis, but they can be further developed to facilitate workflow management. Some programs exist to manage the entire workflow from data collection to analysis, such as the Harmony software from Perkin Elmer. Not only does Harmony automate image acquisition, but it facilitates construction of (albeit limited) analysis macros. Potential exists for combining disparate softwares from various manufacturers to manage workflow and expedite analysis. For this reason, analysis protocols contained in this thesis are built in an open-source platform for maximal cross-platform performance. By maximizing flexibility and transparency in the analysis workflow, these tools are made available to the widest audience.

Conclusion

The long-term goal of this research is to elucidate the role of mitochondrial morphology and function in the development of T2D and find ways to prevent or

reverse disease progression. We have provided evidence demonstrating that mitochondrial morphology is governed by the nutrient environment and may underlie compensatory or pathological changes in metabolism and have provided novel ways to quantify the role of mitochondria in these models. Multiple tissues are involved in T2D, and many show similar mitochondrial behavior in response to similar stimuli. Thus, this work explored what may be an ancient regulatory mechanism responsible for nutrient induced stress. Further research is needed to understand the nature of this regulation and its implications for β-cell function specifically and T2D more broadly.

BIBLIOGRAPHY

Abbe, E. (1873). Beiträge zur Theorie des Mikroskops und der mikroskopischen Wahrnehmung. *Archiv Für Mikroskopische Anatomie*, *9*(1), 413–418. https://doi.org/10.1007/BF02956173

Anello, M., Lupi, R., Spampinato, D., Piro, S., Masini, M., Boggi, U., … Marchetti, P. (2005). Functional and morphological alterations of mitochondria in pancreatic beta cells from type 2 diabetic patients. *Diabetologia*, *48*(2), 282–289. https://doi.org/10.1007/s00125-004-1627-9

Aoun, M., Feillet-Coudray, C., Fouret, G., Chabi, B., Crouzier, D., Ferreri, C., … Coudray, C. (2012). Rat liver mitochondrial membrane characteristics and mitochondrial functions are more profoundly altered by dietary lipid quantity than by dietary lipid quality: effect of different nutritional lipid patterns. *The British Journal of Nutrition*, *107*(5), 647–59. https://doi.org/10.1017/S000711451100331X

Arganda-Carreras, I., Kaynig, V., Rueden, C., Eliceiri, K. W., Schindelin, J., Cardona, A., & Sebastian Seung, H. (2017). Trainable Weka Segmentation: a machine learning tool for microscopy pixel classification. *Bioinformatics*, *33*(15), 2424–2426. https://doi.org/10.1093/bioinformatics/btx180

Argus, J. P., Yu, A. K., Wang, E. S., Williams, K. J., & Bensinger, S. J. (2017). An optimized method for measuring fatty acids and cholesterol in stable isotope-labeled cells. *Journal of Lipid Research*, *58*(2), 460–468. https://doi.org/10.1194/jlr.D069336

Asfari, M., Janjic, D., Meda, P., Li, G., Halban, P. A., & Wollheim, C. B. (1992). Establishment of 2-mercaptoethanol-dependent differentiated insulin-secreting cell lines. *Endocrinology*, *130*(1), 167–178. https://doi.org/10.1210/endo.130.1.1370150

Assimacopoulos-Jeannet, F., Thumelin, S., Roche, E., Esser, V., McGarry, J. D., & Prentki, M. (1997). Fatty acids rapidly induce the carnitine palmitoyltransferase I gene in the pancreatic beta-cell line INS-1. *The Journal of Biological Chemistry*, *272*(3), 1659–64. https://doi.org/10.1074/jbc.272.3.1659

Attané, C., Peyot, M.-L., Lussier, R., Poursharifi, P., Zhao, S., Zhang, D., … Prentki, M. (2016). A beta cell ATGL-lipolysis/adipose tissue axis controls energy homeostasis and body weight via insulin secretion in mice. *Diabetologia*, *59*(12), 2654–2663. https://doi.org/10.1007/s00125-016-4105-2

Bach, D., Pich, S., Soriano, F. X., Vega, N., Baumgartner, B., Oriola, J., … Zorzano, A. (2003). Mitofusin-2 determines mitochondrial network architecture and mitochondrial metabolism. A novel regulatory mechanism altered in obesity. *The Journal of Biological Chemistry*, *278*(19), 17190–17197. https://doi.org/10.1074/jbc.M212754200

Benador, I. Y., Veliova, M., Mahdaviani, K., Petcherski, A., Wikstrom, J. D., Assali, E., … Shirihai, O. S. (2018). Mitochondria Bound to Lipid Droplets Have Unique Composition, Bioenergetics, and Dynamics That Support Lipid Droplet Expansion. *Cell Metabolism (in Press)*.

Bindokas, V. P., Kuznetsov, A., Sreenan, S., Polonsky, K. S., Roe, M. W., & Philipson, L. H. (2003). Visualizing superoxide production in normal and diabetic rat islets of Langerhans. *The Journal of Biological Chemistry*, *278*(11), 9796–9801. https://doi.org/10.1074/jbc.M206913200

Bollheimer, L. C., Skelly, R. H., Chester, M. W., McGarry, J. D., & Rhodes, C. J. (1998). Chronic exposure to free fatty acid reduces pancreatic beta cell insulin content by increasing basal insulin secretion that is not compensated for by a corresponding increase in proinsulin biosynthesis translation. *The Journal of Clinical Investigation*, *101*(5), 1094–101. https://doi.org/10.1172/JCI420

Bonen, A., Jain, S. S., Snook, L. A., Han, X.-X., Yoshida, Y., Buddo, K. H., … Holloway, G. P. (2015). Extremely rapid increase in fatty acid transport and intramyocellular lipid accumulation but markedly delayed insulin resistance after high fat feeding in rats. *Diabetologia*, *58*(10), 2381–91. https://doi.org/10.1007/s00125-015-3691-8

Boutant, M., Kulkarni, S. S., Joffraud, M., Ratajczak, J., Valera-Alberni, M., Combe, R., … Cantó, C. (2017). Mfn2 is critical for brown adipose tissue thermogenic function. *The EMBO Journal*, *36*(11), 1543–1558. https://doi.org/10.15252/embj.201694914

Bradley, D. C., Steil, G. M., & Bergman, R. N. (1995). OOPSEG: a data smoothing program for quantitation and isolation of random measurement error. *Computer Methods and Programs in Biomedicine*, *46*(1), 67–77. https://doi.org/10.1016/0169-2607(94)01600-K

Branstrom, R., Corkey, B. E., Berggren, P. O., & Larsson, O. (1997). Evidence for a unique long chain acyl-CoA ester binding site on the ATP-regulated potassium channel in mouse pancreatic beta cells. *The Journal of Biological Chemistry*, *272*(28), 17390–17394.

Breiman, L. (2001). Random Forests. *Machine Learning*, *45*(1), 5–32.

https://doi.org/10.1023/A:1010933404324

Brun, T., Assimacopoulos-Jeannet, F., Corkey, B. E., & Prentki, M. (1997). Long-chain fatty acids inhibit acetyl-CoA carboxylase gene expression in the pancreatic beta-cell line INS-1. *Diabetes*, *46*(3), 393–400.

Buescher, J. M., Antoniewicz, M. R., Boros, L. G., Burgess, S. C., Brunengraber, H., Clish, C. B., … Fendt, S.-M. (2015). A roadmap for interpreting 13 C metabolite labeling patterns from cells. *Current Opinion in Biotechnology*, *34*(2), 189–201. https://doi.org/10.1016/j.copbio.2015.02.003

Butler, A. E., Janson, J., Bonner-Weir, S., Ritzel, R., Rizza, R. A., & Butler, P. C. (2003). Beta-cell deficit and increased beta-cell apoptosis in humans with type 2 diabetes. *Diabetes*, *52*(1), 102–10. https://doi.org/10.2337/diabetes.52.9.2304

Carlsson, C., Håkan Borg, L. A., & Welsh, N. (1999). Sodium Palmitate Induces Partial Mitochondrial Uncoupling and Reactive Oxygen Species in Rat Pancreatic Islets in Vitro*. *Endocrinology*, *140*(8), 3422–3428. Retrieved from http://dx.doi.org/10.1210/endo.140.8.6908

Cerqueira, F. M., Chausse, B., Baranovski, B. M., Liesa, M., Lewis, E. C., Shirihai, O. S., & Kowaltowski, A. J. (2016). Diluted serum from calorie-restricted animals promotes mitochondrial beta-cell adaptations and protect against glucolipotoxicity. *The FEBS Journal*, *283*(5), 822–833. https://doi.org/10.1111/febs.13632

Cerqueira, F. M., Cunha, F. M., Laurindo, F. R. M., & Kowaltowski, A. J. (2012). Calorie restriction increases cerebral mitochondrial respiratory capacity in a NO*-mediated mechanism: impact on neuronal survival. *Free Radical Biology & Medicine*, *52*(7), 1236–1241. https://doi.org/10.1016/j.freeradbiomed.2012.01.011

Chan, N. C., Salazar, A. M., Pham, A. H., Sweredoski, M. J., Kolawa, N. J., Graham, R. L. J., … Chan, D. C. (2011). Broad activation of the ubiquitin-proteasome system by Parkin is critical for mitophagy. *Human Molecular Genetics*, *20*(9), 1726–37. https://doi.org/10.1093/hmg/ddr048

Chance, B., & Williams, G. R. (1956). The respiratory chain and oxidative phosphorylation. *Advances in Enzymology and Related Subjects of Biochemistry*, *17*, 65–134. Retrieved from http://www.ncbi.nlm.nih.gov/pubmed/13313307

Chen, H., & Chan, D. C. (2005). Emerging functions of mammalian mitochondrial fusion and fission. *Human Molecular Genetics*, *14 Spec No*, R283-9.

https://doi.org/10.1093/hmg/ddi270

Chen, H., Chomyn, A., & Chan, D. C. (2005). Disruption of Fusion Results in Mitochondrial Heterogeneity and Dysfunction. *Journal of Biological Chemistry*, *280*(28), 26185–26192. https://doi.org/10.1074/jbc.M503062200

Chen, H., McCaffery, J. M., & Chan, D. C. (2007). Mitochondrial fusion protects against neurodegeneration in the cerebellum. *Cell*, *130*(3), 548–562. https://doi.org/10.1016/j.cell.2007.06.026

Chen, Y., & Dorn, G. W. (2013). PINK1-phosphorylated mitofusin 2 is a Parkin receptor for culling damaged mitochondria. *Science (New York, N.Y.)*, *340*(6131), 471–5. https://doi.org/10.1126/science.1231031

Corkey, B. E. (2012). Diabetes: Have We Got It All Wrong?: Insulin hypersecretion and food additives: cause of obesity and diabetes? *Diabetes Care*, *35*(12), 2432–2437. https://doi.org/10.2337/dc12-0825

Costes, S., Gurlo, T., Rivera, J. F., & Butler, P. C. (2014). UCHL1 deficiency exacerbates human islet amyloid polypeptide toxicity in B-cells. *Autophagy*, *10*(6), 1004–1014.

Costes, S., Huang, C. J., Gurlo, T., Daval, M., Matveyenko, A. V, Rizza, R. a, … Butler, P. C. (2011). β-cell dysfunctional ERAD/ubiquitin/proteasome system in type 2 diabetes mediated by islet amyloid polypeptide-induced UCH-L1 deficiency. *Diabetes*, *60*(1), 227–38. https://doi.org/10.2337/db10-0522

Cribbs, J. T., & Strack, S. (2009). Functional characterization of phosphorylation sites in dynamin-related protein 1. *Methods in Enzymology*, *457*(9), 231–53. https://doi.org/10.1016/S0076-6879(09)05013-7

Criddle, D. N., Gillies, S., Baumgartner-Wilson, H. K., Jaffar, M., Chinje, E. C., Passmore, S., … Petersen, O. H. (2006). Menadione-induced reactive oxygen species generation via redox cycling promotes apoptosis of murine pancreatic acinar cells. *Journal of Biological Chemistry*, *281*(52), 40485–40492. https://doi.org/10.1074/jbc.M607704200

Cunningham, B. A., Deeney, J. T., Bliss, C. R., Corkey, B. E., & Tornheim, K. (1996). Glucose-induced oscillatory insulin secretion in perifused rat pancreatic islets and clonal beta-cells (HIT). *The American Journal of Physiology*, *271*(4 Pt 1), E702-10. https://doi.org/10.1152/ajpendo.1996.271.4.E702

Czech, M. P. (2017). Insulin action and resistance in obesity and type 2 diabetes. *Nature Medicine*, *23*(7), 804–814. https://doi.org/10.1038/nm.4350

Dagda, R. K., Cherra, S. J., Kulich, S. M., Tandon, A., Park, D., & Chu, C. T. (2009). Loss of PINK1 function promotes mitophagy through effects on oxidative stress and mitochondrial fission. *Journal of Biological Chemistry*, *284*(20), 13843–13855. https://doi.org/10.1074/jbc.M808515200

Dalbøge, L. S., Almholt, D. L. C., Neerup, T. S. R., Vassiliadis, E., Vrang, N., Pedersen, L., … Jelsing, J. (2013). Characterisation of age-dependent beta cell dynamics in the male db/db mice. *PloS One*, *8*(12), e82813. https://doi.org/10.1371/journal.pone.0082813

Deeney, J. T., Köhler, M., Kubik, K., Brown, G., Schultz, V., Tornheim, K., … Berggren, P. O. (2001). Glucose-induced metabolic oscillations parallel those of Ca2+ and insulin release in clonal insulin-secreting cells: A multiwell approach to oscillatory cell behavior. *Journal of Biological Chemistry*, *276*(40), 36946–36950. https://doi.org/10.1074/jbc.M105056200

Del Prato, S., Leonetti, F., Simonson, D. C., Sheehan, P., Matsuda, M., & DeFronzo, R. A. (1994). Effect of sustained physiologic hyperinsulinaemia and hyperglycaemia on insulin secretion and insulin sensitivity in man. *Diabetologia*, *37*(10), 1025–1035. https://doi.org/10.1007/BF00400466

Destefano, M. B., Stern, J. S., & Castonguay, T. W. (1991). Effect of chronic insulin administration on food intake and body weight in rats. *Physiology & Behavior*, *50*(4), 801–806. https://doi.org/10.1016/0031-9384(91)90021-F

Ding, Y., Gao, H., Zhao, L., Wang, X., & Zheng, M. (2015). Mitofusin 2-deficiency suppresses cell proliferation through disturbance of autophagy. *PloS One*, *10*(3), e0121328. https://doi.org/10.1371/journal.pone.0121328

Drucker, D. J., & Nauck, M. A. (2006). The incretin system: glucagon-like peptide-1 receptor agonists and dipeptidyl peptidase-4 inhibitors in type 2 diabetes. *Lancet*, *368*(9548), 1696–1705. https://doi.org/10.1016/S0140-6736(06)69705-5

Duckworth, W. C., & Kitabchi, A. E. (1981). Insulin metabolism and degradation. *Endocrine Reviews*, *2*(2), 210–233. https://doi.org/10.1210/edrv-2-2-210

El-Azzouny, M., Evans, C. R., Treutelaar, M. K., Kennedy, R. T., & Burant, C. F. (2014). Increased glucose metabolism and glycerolipid formation by fatty acids and GPR40 receptor signaling underlies the fatty acid potentiation of insulin secretion. *The Journal of Biological Chemistry*, *289*(19), 13575–88. https://doi.org/10.1074/jbc.M113.531970

Erion, K. A., Berdan, C. A., Burritt, N. E., Corkey, B. E., & Deeney, J. T. (2015). Chronic Exposure to Excess Nutrients Left-shifts the Concentration

Dependence of Glucose-stimulated Insulin Secretion in Pancreatic β-Cells. *Journal of Biological Chemistry*, *290*(26), 16191–16201. https://doi.org/10.1074/jbc.M114.620351

Escobar, O., Mizuma, H., Sothern, M. S., Blecker, U., Udall, J. N. J., Suskind, R. M., … Vargas, A. (1999). Hepatic insulin clearance increases after weight loss in obese children and adolescents. *The American Journal of the Medical Sciences*, *317*(5), 282–286.

Faye, A., Borthwick, K., Esnous, C., Price, N. T., Gobin, S., Jackson, V. N., … Prip-Buus, C. (2005). Demonstration of N- and C-terminal domain intramolecular interactions in rat liver carnitine palmitoyltransferase 1 that determine its degree of malonyl-CoA sensitivity. *The Biochemical Journal*, *387*(Pt 1), 67–76. https://doi.org/10.1042/BJ20041533

Fendt, S.-M., Bell, E. L., Keibler, M. A., Davidson, S. M., Wirth, G. J., Fiske, B., … Stephanopoulos, G. (2013). Metformin decreases glucose oxidation and increases the dependency of prostate cancer cells on reductive glutamine metabolism. *Cancer Research*, *73*(14), 4429–38. https://doi.org/10.1158/0008-5472.CAN-13-0080

Ferdaoussi, M., Dai, X., Jensen, M. V., Wang, R., Peterson, B. S., Huang, C., … MacDonald, P. E. (2015). Isocitrate-to-SENP1 signaling amplifies insulin secretion and rescues dysfunctional β cells. *Journal of Clinical Investigation*, *125*(10), 3847–3860. https://doi.org/10.1172/JCI82498

Ferrick, D. A., Neilson, A., & Beeson, C. (2008). Advances in measuring cellular bioenergetics using extracellular flux. *Drug Discovery Today*, *13*(5–6), 268–274. https://doi.org/10.1016/j.drudis.2007.12.008

Fex, M., Nitert, M. D., Wierup, N., Sundler, F., Ling, C., & Mulder, H. (2007). Enhanced mitochondrial metabolism may account for the adaptation to insulin resistance in islets from C57BL/6J mice fed a high-fat diet. *Diabetologia*, *50*(1), 74–83. https://doi.org/10.1007/s00125-006-0464-4

Fink, B., Laude, K., McCann, L., Doughan, A., Harrison, D. G., & Dikalov, S. (2004). Detection of intracellular superoxide formation in endothelial cells and intact tissues using dihydroethidium and an HPLC-based assay. *American Journal of Physiology. Cell Physiology*, *287*(4), C895-902. https://doi.org/10.1152/ajpcell.00028.2004

Franco, A., Kitsis, R. N., Fleischer, J. A., Gavathiotis, E., Kornfeld, O. S., Gong, G., … Dorn, G. W. (2016). Correcting mitochondrial fusion by manipulating mitofusin conformations. *Nature*, *540*(7631), 74–79. https://doi.org/10.1038/nature20156

Frank, S. (2006). Dysregulation of mitochondrial fusion and fission: an emerging concept in neurodegeneration. *Acta Neuropathologica*, *111*(2), 93–100. https://doi.org/10.1007/s00401-005-0002-3

Frieden, M., James, D., Castelbou, C., Danckaert, A., Martinou, J.-C., & Demaurex, N. (2004). Ca(2+) homeostasis during mitochondrial fragmentation and perinuclear clustering induced by hFis1. *The Journal of Biological Chemistry*, *279*(21), 22704–22714. https://doi.org/10.1074/jbc.M312366200

Fu, Z., Gilbert, E. R., & Liu, D. (2013). Regulation of insulin synthesis and secretion and pancreatic Beta-cell dysfunction in diabetes. *Current Diabetes Reviews*, *9*(1), 25–53. https://doi.org/10.2174/157339913804143225

Geiss, L. S., Wang, J., Cheng, Y. J., Thompson, T. J., Barker, L., Li, Y., … Gregg, E. W. (2014). Prevalence and Incidence Trends for Diagnosed Diabetes Among Adults Aged 20 to 79 Years, United States, 1980-2012. *JAMA*, *312*(12), 1218. https://doi.org/10.1001/jama.2014.11494

Glancy, B., Hartnell, L. M., Malide, D., Yu, Z.-X., Combs, C. A., Connelly, P. S., … Balaban, R. S. (2015). Mitochondrial reticulum for cellular energy distribution in muscle. *Nature*, *523*(7562), 617–620. https://doi.org/10.1038/nature14614

Hansen, B. C., & Bodkin, N. L. (1990). Beta-cell hyperresponsiveness: earliest event in development of diabetes in monkeys. *The American Journal of Physiology*, *259*(3 Pt 2), R612-7. https://doi.org/10.1152/ajpregu.1990.259.3.R612

Harwig, M. C., Viana, M. P., Egner, J. M., Harwig, J. J., Widlansky, M. E., Rafelski, S. M., & Hill, R. B. (2018). Methods for imaging mammalian mitochondrial morphology: A prospective on MitoGraph. *Analytical Biochemistry*. https://doi.org/10.1016/j.ab.2018.02.022

Heart, E., Palo, M., Womack, T., Smith, P. J. S., & Gray, J. P. (2012). The level of menadione redox-cycling in pancreatic Beta-cells is proportional to the glucose concentration: Role of NADH and consequences for insulin secretion. *Toxicology and Applied Pharmacology*, *258*(2), 216–225. https://doi.org/10.1016/j.taap.2011.11.002

Higa, M., Zhou, Y. T., Ravazzola, M., Baetens, D., Orci, L., & Unger, R. H. (1999). Troglitazone prevents mitochondrial alterations, beta cell destruction, and diabetes in obese prediabetic rats. *Proceedings of the National Academy of Sciences of the United States of America*, *96*(20), 11513–11518.

Hiller, K., & Metallo, C. M. (2013). Profiling metabolic networks to study cancer metabolism. *Current Opinion in Biotechnology*, *24*(1), 60–68. https://doi.org/10.1016/j.copbio.2012.11.001

Imperatore, G., Boyle, J. P., Thompson, T. J., Case, D., Dabelea, D., Hamman, R. F., … SEARCH for Diabetes in Youth Study Group. (2012). Projections of type 1 and type 2 diabetes burden in the U.S. population aged 20 years through 2050: dynamic modeling of incidence, mortality, and population growth. *Diabetes Care*, *35*(12), 2515–20. https://doi.org/10.2337/dc12-0669

Itoh, Y., Kawamata, Y., Harada, M., Kobayashi, M., Fujii, R., Fukusumi, S., … Fujino, M. (2003). Free fatty acids regulate insulin secretion from pancreatic beta cells through GPR40. *Nature*, *422*(6928), 173–6. https://doi.org/10.1038/nature01478

Jensen, M. D., Caruso, M., Heiling, V., & Miles, J. M. (1989). Insulin regulation of lipolysis in nondiabetic and IDDM subjects. *Diabetes*, *38*(12), 1595–1601. https://doi.org/10.2337/diab.38.12.1595

Jetton, T. L., Lausier, J., LaRock, K., Trotman, W. E., Larmie, B., Habibovic, A., … Leahy, J. L. (2005). Mechanisms of compensatory beta-cell growth in insulin-resistant rats: roles of Akt kinase. *Diabetes*, *54*(8), 2294–304. Retrieved from http://www.ncbi.nlm.nih.gov/pubmed/16046294

Ježek, P., Olejár, T., Smolková, K., Ježek, J., Dlasková, a, Plecitá-Hlavatá, L., … Jabůrek, M. (2014). Antioxidant and regulatory role of mitochondrial uncoupling protein UCP2 in pancreatic beta-cells. *Physiological Research / Academia Scientiarum Bohemoslovaca*, *63 Suppl 1*, S73-91. Retrieved from http://www.ncbi.nlm.nih.gov/pubmed/24564667

Joshi, M. S., Crouser, E. D., Julian, M. W., Schanbacher, B. L., & Bauer, J. A. (2000). Digital imaging analysis for the study of endotoxin-induced mitochondrial ultrastructure injury. *Analytical Cellular Pathology : The Journal of the European Society for Analytical Cellular Pathology*, *21*(1), 41–8. Retrieved from http://www.ncbi.nlm.nih.gov/entrez/query.fcgi?cmd=Retrieve&db=PubMed&dopt=Citation&list_uids=11254224

Kahn, S. E. (2003). The relative contributions of insulin resistance and beta-cell dysfunction to the pathophysiology of Type 2 diabetes. *Diabetologia*, *46*(1), 3–19. https://doi.org/10.1007/s00125-002-1009-0

Karamitsos, D. T. (2011). The story of insulin discovery. *Diabetes Research and Clinical Practice*, *93 Suppl 1*(SUPPL. 1), S2-8. https://doi.org/10.1016/S0168-8227(11)70007-9

Kim, K.-Y., Perkins, G. A., Shim, M. S., Bushong, E., Alcasid, N., Ju, S., … Ju, W.-K. (2015). DRP1 inhibition rescues retinal ganglion cells and their axons by preserving mitochondrial integrity in a mouse model of glaucoma. *Cell Death & Disease*, *6*, e1839. https://doi.org/10.1038/cddis.2015.180

Koopman, W. J. H., Visch, H.-J., Smeitink, J. A. M., & Willems, P. H. G. M. (2006). Simultaneous quantitative measurement and automated analysis of mitochondrial morphology, mass, potential, and motility in living human skin fibroblasts. *Cytometry Part A*, *69A*(1), 1–12. https://doi.org/10.1002/cyto.a.20198

Kotronen, A., Vehkavaara, S., Seppälä-Lindroos, A., Bergholm, R., & Yki-Järvinen, H. (2007). Effect of liver fat on insulin clearance. *American Journal of Physiology. Endocrinology and Metabolism*, *293*(6), E1709-15. https://doi.org/10.1152/ajpendo.00444.2007

Kotronen, A., Westerbacka, J., Bergholm, R., Pietiläinen, K. H., & Yki-Järvinen, H. (2007). Liver Fat in the Metabolic Syndrome. *The Journal of Clinical Endocrinology & Metabolism*, *92*(9), 3490–3497. https://doi.org/10.1210/jc.2007-0482

Kwan, E. P., Xie, L., Sheu, L., Nolan, C. J., Prentki, M., Betz, A., … Gaisano, H. Y. (2006). Munc13-1 deficiency reduces insulin secretion and causes abnormal glucose tolerance. *Diabetes*, *55*(5), 1421–9. https://doi.org/10.2337/db05-1263

Lablanche, S., Lamarche, F., Benhamou, P., Halimi, S., Leverve, X., & Fontaine, E. (2011). Protection of pancreatic INS-1 b - cells from glucose- and fructose-induced cell death by inhibiting mitochondrial permeability transition with cyclosporin A or metformin. *Cell Death and Disease*, *2*(3), e134-6. https://doi.org/10.1038/cddis.2011.15

Latour, M. G., Alquier, T., Oseid, E., Tremblay, C., Jetton, T. L., Luo, J., … Poitout, V. (2007). GPR40 is necessary but not sufficient for fatty acid stimulation of insulin secretion in vivo. *Diabetes*, *56*(4), 1087–1094. https://doi.org/10.2337/db06-1532

Laurindo, F. R. M., Fernandes, D. C., & Santos, C. X. C. (2008). Assessment of Superoxide Production and NADPH Oxidase Activity by HPLC Analysis of Dihydroethidium Oxidation Products. In *Methods in Enzymology* (Vol. 441, pp. 237–260). https://doi.org/10.1016/S0076-6879(08)01213-5

Le Blanc, S., Villarroel, P., Candia, V., Gavilan, N., Soto, N., Perez-Bravo, F., & Arredondo, M. (2012). Type 2 diabetic patients and their offspring show altered parameters of iron status, oxidative stress and genes related to

mitochondrial activity. *Biometals : An International Journal on the Role of Metal Ions in Biology, Biochemistry, and Medicine*, *25*(4), 725–735. https://doi.org/10.1007/s10534-012-9540-z

Leboucher, G. P., Tsai, Y. C., Yang, M., Shaw, K. C., Zhou, M., Veenstra, T. D., … Weissman, A. M. (2012). Stress-induced phosphorylation and proteasomal degradation of mitofusin 2 facilitates mitochondrial fragmentation and apoptosis. *Molecular Cell*, *47*(4), 547–557. https://doi.org/10.1016/j.molcel.2012.05.041

Leonard, A. P., Cameron, R. B., Speiser, J. L., Wolf, B. J., Peterson, Y. K., Schnellmann, R. G., … Rohrer, B. (2015). Quantitative analysis of mitochondrial morphology and membrane potential in living cells using high-content imaging, machine learning, and morphological binning. *Biochimica et Biophysica Acta*, *1853*(2), 348–60. https://doi.org/10.1016/j.bbamcr.2014.11.002

Liesa, M., & Shirihai, O. S. (2013). Mitochondrial dynamics in the regulation of nutrient utilization and energy expenditure. *Cell Metabolism*, *17*(4), 491–506. https://doi.org/10.1016/j.cmet.2013.03.002

Lim, E. L., Hollingsworth, K. G., Aribisala, B. S., Chen, M. J., Mathers, J. C., & Taylor, R. (2011). Reversal of type 2 diabetes: normalisation of beta cell function in association with decreased pancreas and liver triacylglycerol. *Diabetologia*, *54*(10), 2506–14. https://doi.org/10.1007/s00125-011-2204-7

MacDonald, M. J., & Marshall, L. K. (2000). Mouse lacking NAD+-linked glycerol phosphate dehydrogenase has normal pancreatic beta cell function but abnormal metabolite pattern in skeletal muscle. *Archives of Biochemistry and Biophysics*, *384*(1), 143–153. https://doi.org/10.1006/abbi.2000.2107

Mahdaviani, K., Benador, I. Y., Su, S., Gharakhanian, R. A., Stiles, L., Trudeau, K. M., … Shirihai, O. S. (2017). Mfn2 deletion in brown adipose tissue protects from insulin resistance and impairs thermogenesis. *EMBO Reports*, e201643827. https://doi.org/10.15252/embr.201643827

McGarry, J. D., Mannaerts, G. P., & Foster, D. W. (1977). A possible role for malonyl-CoA in the regulation of hepatic fatty acid oxidation and ketogenesis. *The Journal of Clinical Investigation*, *60*(1), 265–70. https://doi.org/10.1172/JCI108764

Mehran, A. E., Templeman, N. M., Brigidi, G. S., Lim, G. E., Chu, K.-Y., Hu, X., … Johnson, J. D. (2012). Hyperinsulinemia Drives Diet-Induced Obesity Independently of Brain Insulin Production. *Cell Metabolism*, *16*(6), 723–737. https://doi.org/10.1016/j.cmet.2012.10.019

Meyer, L. E., Machado, L. B., Santiago, A. P. S. A., Da-Silva, W. S., De Felice, F. G., Holub, O., … Galina, A. (2006). Mitochondrial Creatine Kinase Activity Prevents Reactive Oxygen Species Generation. *Journal of Biological Chemistry*, *281*(49), 37361–37371. https://doi.org/10.1074/jbc.M604123200

Mezza, T., Muscogiuri, G., Sorice, G. P., Clemente, G., Hu, J., Pontecorvi, A., … Kulkarni, R. N. (2014). Insulin resistance alters islet morphology in nondiabetic humans. *Diabetes*, *63*(3), 994–1007. https://doi.org/10.2337/db13-1013

Molina, A. J. a, Wikstrom, J. D., Stiles, L., Las, G., Mohamed, H., Elorza, A., … Shirihai, O. S. (2009). Mitochondrial networking protects beta-cells from nutrient-induced apoptosis. *Diabetes*, *58*(10), 2303–15. https://doi.org/10.2337/db07-1781

Morgan, B., Sobotta, M. C., & Dick, T. P. (2011). Measuring E GSH and H 2O 2 with roGFP2-based redox probes. *Free Radical Biology and Medicine*, *51*(11), 1943–1951. https://doi.org/10.1016/j.freeradbiomed.2011.08.035

Moseley, H. N. B. (2010). Correcting for the effects of natural abundance in stable isotope resolved metabolomics experiments involving ultra-high resolution mass spectrometry. *BMC Bioinformatics*, *11*, 139. https://doi.org/10.1186/1471-2105-11-139

Mourier, A., Motori, E., Brandt, T., Lagouge, M., Atanassov, I., Galinier, A., … Larsson, N.-G. (2015). Mitofusin 2 is required to maintain mitochondrial coenzyme Q levels. *The Journal of Cell Biology*, *208*(4), 429–442. https://doi.org/10.1083/jcb.201411100

Mutterer, J., & Rasband, W. (2012). ImageJ Macro Language Programmer's Reference Guide v1.46d. *RSB Homepage*, 1–45.

Nannipieri, M., Baldi, S., Mari, A., Colligiani, D., Guarino, D., Camastra, S., … Ferrannini, E. (2013). Roux-en-Y gastric bypass and sleeve gastrectomy: mechanisms of diabetes remission and role of gut+ hormones. *The Journal of Clinical Endocrinology and Metabolism*, *98*(11), 4391–9. https://doi.org/10.1210/jc.2013-2538

Nannipieri, M., Mari, A., Anselmino, M., Baldi, S., Barsotti, E., Guarino, D., … Ferrannini, E. (2011). The role of beta-cell function and insulin sensitivity in the remission of type 2 diabetes after gastric bypass surgery. *The Journal of Clinical Endocrinology and Metabolism*, *96*(9), E1372-9. https://doi.org/10.1210/jc.2011-0446

Narendra, D. P., Jin, S. M., Tanaka, A., Suen, D.-F., Gautier, C. A., Shen, J., …

Youle, R. J. (2010). PINK1 is selectively stabilized on impaired mitochondria to activate Parkin. *PLoS Biology*, *8*(1), e1000298. https://doi.org/10.1371/journal.pbio.1000298

Nazarewicz, R. R., Bikineyeva, A., & Dikalov, S. I. (2013). Rapid and specific measurements of superoxide using fluorescence spectroscopy. *Journal of Biomolecular Screening*, *18*(4), 498–503. https://doi.org/10.1177/1087057112468765

Newgard, C. B., & McGarry, J. D. (1995). Metabolic coupling factors in pancreatic beta-cell signal transduction. *Annual Review of Biochemistry*, *64*, 689–719. https://doi.org/10.1146/annurev.biochem.64.1.689

Nguyen, A., Beyersdorf, J., Riethoven, J.-J., & Pannier, A. K. (2016). High-throughput screening of clinically approved drugs that prime polyethylenimine transfection reveals modulation of mitochondria dysfunction response improves gene transfer efficiencies. *Bioengineering & Translational Medicine*, *1*(2), 123–135. https://doi.org/10.1002/btm2.10017

Nicholls, D. G., Darley-Usmar, V. M., Wu, M., Jensen, P. B., Rogers, G. W., & Ferrick, D. A. (2010). Bioenergetic profile experiment using C2C12 myoblast cells. *Journal of Visualized Experiments : JoVE*, (46), 3–7. https://doi.org/10.3791/2511

Nolan, C. J., Leahy, J. L., Delghingaro-Augusto, V., Moibi, J., Soni, K., Peyot, M.-L., … Prentki, M. (2006). Beta cell compensation for insulin resistance in Zucker fatty rats: increased lipolysis and fatty acid signalling. *Diabetologia*, *49*(9), 2120–2130. https://doi.org/10.1007/s00125-006-0305-5

Nolan, C. J., Madiraju, M. S. R., Delghingaro-augusto, V., Peyot, M., & Prentki, M. (2006). Fatty Acid Signaling in the Beta-Cell and Insulin Secretion. *Diabetes*, *55*(December), S16-23. https://doi.org/10.2337/diabetes

Nolan, C. J., & Prentki, M. (2008). The islet Beta-cell: fuel responsive and vulnerable. *Trends in Endocrinology and Metabolism*, *19*(8), 285–291. https://doi.org/10.1016/j.tem.2008.07.006

Olefsky, J., Crapo, P. a, Ginsberg, H., & Reaven, G. M. (1975). Metabolic effects of increased caloric intake in man. *Metabolism*, *24*(4), 495–503. https://doi.org/10.1016/0026-0495(75)90074-8

Opie, L. H., & Walfish, P. G. (1963). Plasma free fatty acid concentrations in obesity. *The New England Journal of Medicine*, *268*, 757–60. https://doi.org/10.1056/NEJM196304042681404

Pallett, A. L., Morton, N. M., Cawthorne, M. A., & Emilsson, V. (1997). Leptin Inhibits Insulin Secretion and Reduces Insulin mRNA Levels in Rat Isolated Pancreatic Islets. *Biochemical and Biophysical Research Communications*, *238*(1), 267–270. https://doi.org/10.1006/bbrc.1997.7274

Patterson, J. N., Cousteils, K., Lou, J. W., Manning Fox, J. E., MacDonald, P. E., & Joseph, J. W. (2014). Mitochondrial Metabolism of Pyruvate Is Essential for Regulating Glucose-stimulated Insulin Secretion. *Journal of Biological Chemistry*, *289*(19), 13335–13346. https://doi.org/10.1074/jbc.M113.521666

Perley, M. J., & Kipnis, D. M. (1967). Plasma Insulin Responses to Oral and Intravenous Glucose: Studies in Normal and Diabetic Subjects*. *Journal of Clinical Investigation*, *46*(12), 1954–1962. https://doi.org/10.1172/JCI105685

Perry, R. J., Camporez, J. G., Kursawe, R., Titchenell, P. M., Zhang, D., Perry, C. J., … Shulman, G. I. (2015). Hepatic acetyl CoA links adipose tissue inflammation to hepatic insulin resistance and type 2 diabetes. *Cell*, *160*(4), 745–58. https://doi.org/10.1016/j.cell.2015.01.012

Peyot, M.-L., Nolan, C. J., Soni, K., Joly, E., Lussier, R., Corkey, B. E., … Prentki, M. (2004). Hormone-Sensitive Lipase Has a Role in Lipid Signaling for Insulin Secretion but Is Nonessential for the Incretin Action of Glucagon-Like Peptide 1. *Diabetes*, *53*(7), 1733–1742. https://doi.org/10.2337/diabetes.53.7.1733

Pi, J., Bai, Y., Zhang, Q., Wong, V., Floering, L. M., Daniel, K., … Collins, S. (2007). Reactive Oxygen Species as a Signal in Glucose- Stimulated Insulin Secretion. *Diabetes*, *56*(July), 1783–1791. https://doi.org/10.2337/db06-1601.Additional

Pich, S., Bach, D., Briones, P., Liesa, M., Camps, M., Testar, X., … Zorzano, A. (2005). The Charcot-Marie-Tooth type 2A gene product, Mfn2, up-regulates fuel oxidation through expression of OXPHOS system. *Human Molecular Genetics*, *14*(11), 1405–15. https://doi.org/10.1093/hmg/ddi149

Pickrell, A. M., & Youle, R. J. (2015). The roles of PINK1, parkin, and mitochondrial fidelity in Parkinson's disease. *Neuron*, *85*(2), 257–73. https://doi.org/10.1016/j.neuron.2014.12.007

Poitout, V., Amyot, J., & Semache, M. (2010). Glucolipotoxicity of the pancreatic beta cell. *… BBA)-Molecular and Cell …*, *1801*(3), 289–98. https://doi.org/10.1016/j.bbalip.2009.08.006

Poitout, V., Olson, L. K., & Robertson, R. P. (1996). Insulin-secreting cell lines: classification, characteristics and potential applications. *Diabetes &*

Metabolism, *22*(1), 7–14.

Poitout, V., & Robertson, R. P. (1996). An integrated view of beta-cell dysfunction in type-II diabetes. *Annual Review of Medicine*, *47*, 69–83. https://doi.org/10.1146/annurev.med.47.1.69

Polonsky, K. S., Given, B. D., Hirsch, L., Shapiro, E. T., Tillil, H., Beebe, C., … Van Cauter, E. (1988). Quantitative study of insulin secretion and clearance in normal and obese subjects. *The Journal of Clinical Investigation*, *81*(2), 435–41. https://doi.org/10.1172/JCI113338

Polonsky, K. S., Given, B. D., & Van Cauter, E. (1988). Twenty-four-hour profiles and pulsatile patterns of insulin secretion in normal and obese subjects. *The Journal of Clinical Investigation*, *81*(2), 442–8. https://doi.org/10.1172/JCI113339

Porksen, N., Hollingdal, M., Juhl, C., Butler, P., Veldhuis, J. D., & Schmitz, O. (2002). Pulsatile Insulin Secretion: Detection, Regulation, and Role in Diabetes. *Diabetes*, *51*(Supplement 1), S245–S254. https://doi.org/10.2337/diabetes.51.2007.S245

Prentki, M., & Corkey, B. E. (1996). Are the beta-cell signaling molecules malonyl-CoA and cystolic long-chain acyl-CoA implicated in multiple tissue defects of obesity and NIDDM? *Diabetes*, *45*(3), 273–283. https://doi.org/10.2337/diabetes.45.3.273

Prentki, M., Matschinsky, F. M., & Madiraju, S. R. M. (2013). Metabolic signaling in fuel-induced insulin secretion. *Cell Metabolism*. Elsevier Inc. https://doi.org/10.1016/j.cmet.2013.05.018

Qi, X., Qvit, N., Su, Y.-C., & Mochly-Rosen, D. (2013). A novel Drp1 inhibitor diminishes aberrant mitochondrial fission and neurotoxicity. *Journal of Cell Science*, *126*(Pt 3), 789–802. https://doi.org/10.1242/jcs.114439

Quan, W., Hur, K. Y., Lim, Y., Oh, S. H., Lee, J.-C., Kim, K. H., … Lee, M.-S. (2012). Autophagy deficiency in beta cells leads to compromised unfolded protein response and progression from obesity to diabetes in mice. *Diabetologia*, *55*(2), 392–403. https://doi.org/10.1007/s00125-011-2350-y

Rambold, A. S., Cohen, S., & Lippincott-Schwartz, J. (2015). Fatty acid trafficking in starved cells: regulation by lipid droplet lipolysis, autophagy, and mitochondrial fusion dynamics. *Developmental Cell*, *32*(6), 678–92. https://doi.org/10.1016/j.devcel.2015.01.029

Reed, M. A., Pories, W. J., Chapman, W., Pender, J., Bowden, R., Barakat, H.,

… Dohm, G. L. (2011). Roux-en-Y gastric bypass corrects hyperinsulinemia implications for the remission of type 2 diabetes. *The Journal of Clinical Endocrinology and Metabolism*, *96*(8), 2525–31. https://doi.org/10.1210/jc.2011-0165

Rocha, N., Bulger, D. A., Frontini, A., Titheradge, H., Gribsholt, S. B., Knox, R., … Semple, R. K. (2017). Human biallelic MFN2 mutations induce mitochondrial dysfunction, upper body adipose hyperplasia, and suppression of leptin expression. *eLife*, *6*, 1–27. https://doi.org/10.7554/eLife.23813

Roduit, R., Nolan, C., Alarcon, C., Moore, P., Barbeau, A., Delghingaro-Augusto, V., … Prentki, M. (2004). A role for the malonyl-CoA/long-chain acyl-CoA pathway of lipid signaling in the regulation of insulin secretion in response to both fuel and nonfuel stimuli. *Diabetes*, *53*(4), 1007–19. Retrieved from http://www.ncbi.nlm.nih.gov/pubmed/15047616

Rubí, B., Antinozzi, P. A., Herrero, L., Ishihara, H., Asins, G., Serra, D., … Hegardt, F. G. (2002). Adenovirus-mediated overexpression of liver carnitine palmitoyltransferase I in INS1E cells: effects on cell metabolism and insulin secretion. *The Biochemical Journal*, *364*(Pt 1), 219–26. https://doi.org/10.1042/bj3640219

Saadeh, M., Ferrante, T. C., Kane, A., Shirihai, O., Corkey, B. E., & Deeney, J. T. (2012). Reactive oxygen species stimulate insulin secretion in rat pancreatic islets: Studies using mono-oleoyl-glycerol. *PLoS ONE*, *7*(1). https://doi.org/10.1371/journal.pone.0030200

Sako, Y., & Grill, V. E. (1990). A 48-hour lipid infusion in the rat time-dependently inhibits glucose-induced insulin secretion and B cell oxidation through a process likely coupled to fatty acid oxidation. *Endocrinology*, *127*(4), 1580–1589. https://doi.org/10.1210/endo-127-4-1580

Sauer, U. (2006). Metabolic networks in motion: 13C-based flux analysis. *Molecular Systems Biology*, *2*, 1–10. https://doi.org/10.1038/msb4100109

Scherer, T., Lindtner, C., Zielinski, E., O'Hare, J., Filatova, N., & Buettner, C. (2012). Short Term Voluntary Overfeeding Disrupts Brain Insulin Control of Adipose Tissue Lipolysis. *Journal of Biological Chemistry*, *287*(39), 33061–33069. https://doi.org/10.1074/jbc.M111.307348

Schindelin, J., Arganda-Carreras, I., Frise, E., Kaynig, V., Longair, M., Pietzsch, T., … Cardona, A. (2012). Fiji: an open-source platform for biological-image analysis. *Nature Methods*, *9*(7), 676–82. https://doi.org/10.1038/nmeth.2019

Schrepfer, E., & Scorrano, L. (2016). Mitofusins , from Mitochondria to

Metabolism. *Molecular Cell*, *61*(5), 683–694. https://doi.org/10.1016/j.molcel.2016.02.022

Schuit, F., De Vos, A., Farfari, S., Moens, K., Pipeleers, D., Brun, T., & Prentki, M. (1997). Metabolic Fate of Glucose in Purified Islet Cells. *Journal of Biological Chemistry*, *272*(30), 18572–18579. https://doi.org/10.1074/jbc.272.30.18572

Seahorse. (2017). Mito Stress Test. *Agilent*.

Seigneur, M., Freyburger, G., Gin, H., Claverie, M., Lardeau, D., Lacape, G., … Boisseau, M. R. (1994). Serum fatty acid profiles in type I and type II diabetes: metabolic alterations of fatty acids of the main serum lipids. *Diabetes Research and Clinical Practice*, *23*(3), 169–177.

Sesaki, H., & Jensen, R. E. (1999). Division versus fusion: Dnm1p and Fzo1p antagonistically regulate mitochondrial shape. *The Journal of Cell Biology*, *147*(4), 699–706. https://doi.org/10.1083/jcb.147.4.699

Seufert, J., Kieffer, T. J., Leech, C. A., Holz, G. G., Moritz, W., Ricordi, C., & Habener, J. F. (1999). Leptin suppression of insulin secretion and gene expression in human pancreatic islets: implications for the development of adipogenic diabetes mellitus. *The Journal of Clinical Endocrinology and Metabolism*, *84*(2), 670–6. https://doi.org/10.1210/jcem.84.2.5460

Shaw, J. M., & Nunnari, J. (2002). Mitochondrial dynamics and division in budding yeast. *Trends in Cell Biology*, *12*(4), 178–84. https://doi.org/10.3174/ajnr.A1256.Functional

Skelin, M., Rupnik, M., & Cencic, A. (2010). Pancreatic beta cell lines and their applications in diabetes mellitus research. *ALTEX*, *27*(2), 105–13. https://doi.org/20686743

Skulachev, V. P. (2001). Mitochondrial filaments and clusters as intracellular power-transmitting cables. *Trends in Biochemical Sciences*, *26*(1), 23–29.

Smith, D. D., Kovats, S., Lee, T. D., & Cano, L. (2006). Median filter algorithm for estimating the threshold of detection on custom protein arrays. *BioTechniques*, *41*(1), 74–8. https://doi.org/10.2144/000112204

Song, M., Mihara, K., Chen, Y., Scorrano, L., & Ii, G. W. D. (2015). Mitochondrial Fission and Fusion Factors Reciprocally Orchestrate Mitophagic Culling in Mouse Hearts and Cultured Fibroblasts. *Cell Metabolism*, *21*(2), 273–285. https://doi.org/10.1016/j.cmet.2014.12.011

Sorianello, E., Soriano, F. X., Fernandez-Pascual, S., Sancho, A., Naon, D., Vila-Caballer, M., … Zorzano, A. (2012). The promoter activity of human Mfn2 depends on Sp1 in vascular smooth muscle cells. *Cardiovascular Research*, *94*(1), 38–47. https://doi.org/10.1093/cvr/cvs006

Steil, G. M., Trivedi, N., Jonas, J. C., Hasenkamp, W. M., Sharma, A., Bonner-Weir, S., & Weir, G. C. (2001). Adaptation of beta-cell mass to substrate oversupply: enhanced function with normal gene expression. *American Journal of Physiology. Endocrinology and Metabolism*, *280*(5), E788-96. https://doi.org/10.1152/ajpendo.2001.280.5.E788

Stiles, L., & Shirihai, O. S. (2012). Mitochondrial dynamics and morphology in beta-cells. *Best Practice and Research: Clinical Endocrinology and Metabolism*. https://doi.org/10.1016/j.beem.2012.05.004

Svedberg, J., Strömblad, G., Wirth, A., Smith, U., & Björntorp, P. (1991). Fatty acids in the portal vein of the rat regulate hepatic insulin clearance. *The Journal of Clinical Investigation*, *88*(6), 2054–8. https://doi.org/10.1172/JCI115534

Szabadkai, G., Simoni, A. M., Chami, M., Wieckowski, M. R., Youle, R. J., & Rizzuto, R. (2004). Drp-1-dependent division of the mitochondrial network blocks intraorganellar Ca2+ waves and protects against Ca2+-mediated apoptosis. *Molecular Cell*, *16*(1), 59–68. https://doi.org/10.1016/j.molcel.2004.09.026

Thai, M., Graham, N. A., Braas, D., Nehil, M., Komisopoulou, E., Kurdistani, S. K., … Christofk, H. R. (2014). Adenovirus E4ORF1-induced MYC activation promotes host cell anabolic glucose metabolism and virus replication. *Cell Metabolism*, *19*(4), 694–701. https://doi.org/10.1016/j.cmet.2014.03.009

Thorens, B. (2015). GLUT2, glucose sensing and glucose homeostasis. *Diabetologia*, *58*(2), 221–32. https://doi.org/10.1007/s00125-014-3451-1

Titchenell, P. M., Lazar, M. A., & Birnbaum, M. J. (2017). Unraveling the Regulation of Hepatic Metabolism by Insulin. *Trends in Endocrinology and Metabolism: TEM*, *28*(7), 497–505. https://doi.org/10.1016/j.tem.2017.03.003

Tollefson, K. E., Kroczynski, J., & Cutaia, M. V. (2003). Time-dependent interactions of oxidant-sensitive fluoroprobes with inhibitors of cellular metabolism. *Laboratory Investigation; a Journal of Technical Methods and Pathology*, *83*(3), 367–375.

Tornheim, K. (1997). Are metabolic oscillations responsible for normal oscillatory insulin secretion? *Diabetes*, *46*(9), 1375–80.

https://doi.org/10.2337/diab.46.9.1375

Trudeau, K. M., Colby, A. H., Zeng, J., Las, G., Feng, J. H., Grinstaff, M. W., & Shirihai, O. S. (2016). Lysosome acidification by photoactivated nanoparticles restores autophagy under lipotoxicity. *Journal of Cell Biology*, *214*(1), 25–34. https://doi.org/10.1083/jcb.201511042

Twig, G., Elorza, A., Molina, A. J. A., Mohamed, H., Wikstrom, J. D., Walzer, G., … Shirihai, O. S. (2008). Fission and selective fusion govern mitochondrial segregation and elimination by autophagy. *The EMBO Journal*, *27*(January), 433–446. https://doi.org/10.1038/sj.emboj.7601963

Twig, G., Graf, S. A., Wikstrom, J. D., Mohamed, H., Haigh, S. E., Elorza, A., … Shirihai, O. S. (2006). Tagging and tracking individual networks within a complex mitochondrial web with photoactivatable GFP. *American Journal of Physiology. Cell Physiology*, *291*(1), C176-84. https://doi.org/10.1152/ajpcell.00348.2005

Valente, A. J., Maddalena, L. A., Robb, E. L., Moradi, F., & Stuart, J. A. (2017). A simple ImageJ macro tool for analyzing mitochondrial network morphology in mammalian cell culture. *Acta Histochemica*, *119*(3), 315–326. https://doi.org/10.1016/j.acthis.2017.03.001

Vijayaraghavan, K. (2010). Treatment of dyslipidemia in patients with type 2 diabetes. *Lipids in Health and Disease*, *9*(1), 144. https://doi.org/10.1186/1476-511X-9-144

Wasserman, D. H. (2009). Four grams of glucose. *American Journal of Physiology. Endocrinology and Metabolism*, *296*(1), E11-21. https://doi.org/10.1152/ajpendo.90563.2008

Weisshart, K. (2014). The Basic Principle of Airyscanning The Basic Principle of Airyscanning. *Zeiss Microscopy*, 22.

Wiemerslage, L., & Lee, D. (2016). Quantification of mitochondrial morphology in neurites of dopaminergic neurons using multiple parameters. *Journal of Neuroscience Methods*, *262*, 56–65. https://doi.org/10.1016/j.jneumeth.2016.01.008

Wikstrom, J. D., Katzman, S. M., Mohamed, H., Twig, G., Graf, S. a., Heart, E., … Shirihai, O. S. (2007). Beta-Cell mitochondria exhibit membrane potential heterogeneity that can be altered by stimulatory or toxic fuel levels. *Diabetes*, *56*(10), 2569–2578. https://doi.org/10.2337/db06-0757

Wikstrom, J. D., Mahdaviani, K., Liesa, M., Sereda, S. B., Si, Y., Las, G., …

Shirihai, O. S. (2014). Hormone-induced mitochondrial fission is utilized by brown adipocytes as an amplification pathway for energy expenditure. *EMBO Journal*, *33*(5), 418–436. https://doi.org/10.1002/embj.201385014

Yaffe, M. P. (1999). The machinery of mitochondrial inheritance and behavior. *Science (New York, N.Y.)*, *283*(5407), 1493–7. Retrieved from http://www.ncbi.nlm.nih.gov/pubmed/10066164

Yoshii, H., Lam, T. K. T., Gupta, N., Goh, T., Haber, C. A., Uchino, H., … Giacca, A. (2006). Effects of portal free fatty acid elevation on insulin clearance and hepatic glucose flux. *American Journal of Physiology-Endocrinology and Metabolism*, *290*(6), E1089–E1097. https://doi.org/10.1152/ajpendo.00306.2005

Young, J. (2013). Metabolic flux rewiring in mammalian cell cultures. *Current Opinion in Biotechnology*, *24*(6), 1–16. https://doi.org/10.1016/j.copbio.2013.04.016.Metabolic

Yun, J., Puri, R., Yang, H., Lizzio, M. A., Wu, C., Sheng, Z.-H., & Guo, M. (2014). MUL1 acts in parallel to the PINK1/parkin pathway in regulating mitofusin and compensates for loss of PINK1/parkin. *eLife*, *3*, e01958. https://doi.org/10.7554/eLife.01958

Zhang, Y., Jiang, L., Hu, W., Zheng, Q., & Xiang, W. (2011). Mitochondrial dysfunction during in vitro hepatocyte steatosis is reversed by omega-3 fatty acid-induced up-regulation of mitofusin 2. *Metabolism: Clinical and Experimental*, *60*(6), 767–775. https://doi.org/10.1016/j.metabol.2010.07.026

Zhao, S., Mugabo, Y., Iglesias, J., Xie, L., Delghingaro-Augusto, V., Lussier, R., … Prentki, M. (2014). α/β-Hydrolase domain-6-accessible monoacylglycerol controls glucose-stimulated insulin secretion. *Cell Metabolism*, *19*(6), 993–1007. https://doi.org/10.1016/j.cmet.2014.04.003

Zhou, Y.-P., & Grill, V. E. (1995). Palmitate-Induced β-Cell Insensitivity to Glucose is Coupled to Decreased Pyruvate Dehydrogenase Activity and Enhanced Kinase Activity in Rat Pancreatic Islets. *Diabetes*, *44*(4), 394 LP-399. Retrieved from http://diabetes.diabetesjournals.org/content/44/4/394.abstract

Zhou, Y., & Grill, V. E. (1994). Long-Term Exposure of Rat Pancreatic Islets to Fatty Acids Inhibits Glucose- induced Insulin Secretion and Biosynthesis through a Glucose Fatty Acid Cycle, *93*(February), 870–876.

Zingaretti, M. C., Crosta, F., Vitali, A., Guerrieri, M., Frontini, A., Cannon, B., … Cinti, S. (2009). The presence of UCP1 demonstrates that metabolically

active adipose tissue in the neck of adult humans truly represents brown adipose tissue. *FASEB Journal : Official Publication of the Federation of American Societies for Experimental Biology*, *23*(9), 3113–20. https://doi.org/10.1096/fj.09-133546

Ziviani, E., Tao, R. N., & Whitworth, A. J. (2010). Drosophila parkin requires PINK1 for mitochondrial translocation and ubiquitinates mitofusin. *Proceedings of the National Academy of Sciences of the United States of America*, *107*(11), 5018–23. https://doi.org/10.1073/pnas.0913485107

CURRICULUM VITAE